Exploring Hydrodynamics of a Vertically Oriented Oscillating Surge Wave Energy Converter using BEM and System Identification Wave Tank Testing

A THESIS

SUBMITTED TO THE FACULTY OF THE

UNIVERSITY OF MINNESOTA

BY

Gracie M. Bahr

IN PARTIAL FULFILLMENT OF THE REQUIREMENTS

FOR THE DEGREE OF MASTER OF SCIENCE

Advisor:

CRAIG S. HILL, Ph.D.

Committee Members:

RUIHANG ZHANG, Ph.D.

HARISH R. PALNITKAR, Ph.D.

August 2025

Acknowledgements

I am immensely grateful to my advisor, Dr. Craig Hill, for being the best mentor I could have hoped for. From the very beginning, you listened to the things I said once, the ideas and interests I shared, what I was passionate about, and created every opportunity for me to pursue them. Thank you for dreaming with me about the possibilities we have to save the world and working to transform those possibilities into blueprints and then reality. Thank you for taking action, for creating space for me to explore, and for encouraging me to step into all the challenges. You pushed me to try the scary things, supported me through every step, and made the journey so much fun. I am deeply grateful for your support, guidance, and your belief in me (and my jokes). Thank you.

I would like to sincerely thank my thesis committee members for their willingness to serve on my committee, for their openness throughout this process, and for generously sharing their expertise to guide and strengthen my work. It has been a privilege to learn from you, both through your classes and your outside encouragement. Your support and commitment has been extremely meaningful, and I am sincerely thankful for the opportunity to work with you.

Finally, I would like to say “Hallo Family”. I am endlessly thankful to my family for their unending love, support, and encouragement throughout this journey. Your genuine excitement for what I am doing, your willingness to listen to me talk at length about my work, and your constant presence at every presentation, concert, ceremony, and the million other milestones have meant more than I can express. You have celebrated every step with me as if it were your own, and that has made all the difference. To my mom and sister, thank you for always, always, always giving the best advice and the biggest laughs, and reminding me that joy (and sleep) is just as important as hard work. I couldn’t have done this without you, and I wouldn’t have wanted to.

Abstract

Marine renewable energy (MRE) offers a promising pathway toward sustainable, low-carbon power generation by harnessing the predictable and abundant energy of ocean waves. This study investigates the hydrodynamic performance and optimization of a vertically oriented oscillating surge wave energy converter (VOSWEC) designed for integration into coastal protection structures. Using linear wave theory as a foundation, boundary element method (BEM) simulations were conducted in Capytaine to evaluate excitation torque, radiation damping, and added mass for 24 plate configurations varying in length, thickness, and submergence depth, targeting an approximately 1:30 scaled model of the original WEC-Sim OSWEC geometry. Results revealed that increased submergence depth consistently enhanced all three hydrodynamic coefficients, while intermediate plate widths often produced the highest added mass and damping values—indicating nonlinear geometry–hydrodynamic interactions. The BEM results informed geometry selection for scaled physical testing at Michigan Technological University's wave tank, enabling targeted evaluation of frequency response and system identification under controlled regular, irregular, and multisine wave conditions. These experimental findings will support the integration of the BEM-informed VOSWEC models into WEC-Sim for time-domain performance analysis in both scaled and realistic Lake Superior wave conditions. The outcomes of this research aim to advance understanding of geometry-dependent performance in coastal-integrated WECs, providing a hydrodynamic basis for design optimization and contributing to the broader deployment of MRE technologies for both power generation and shoreline protection.

Table of Contents

List of Tables

List of Figures

1. Introduction

Marine renewable energy (MRE) presents a transformative solution for sustainable power generation (Shields, 2014). Leveraging the vast and untapped kinetic energy of waves, tides, and currents to enhance energy security, reduce reliance on fossil fuels, and provide reliable electricity for coastal and remote communities, MRE has the potential to revolutionize renewable energy globally.

Marine renewable energy is a crucial component of a sustainable energy future, offering a clean, sustainable, predictable, and emissions-free power source (Weiss et al., 2018). By harnessing the highly predictable motion of waves, tides, and currents, it provides a continuous and reliable supply of electricity, making it an ideal energy source for coastal and island communities that often rely on costly and environmentally harmful imported fossil fuels. Marine energy benefits from the consistent and cyclical nature of oceanic movements, ensuring grid stability and energy security (Iglesias, Abanades, 2015). Expanding MRE technologies can help mitigate climate change through the significant reduction of greenhouse gas emissions (Rusu, 2024), supporting national and international commitments to decarbonization. With over 70% of the Earth's surface covered by water and more than a third of the global population living near coastlines, marine energy has the potential to play a crucial role in diversifying energy sources, driving economic growth in coastal regions, and strengthening energy independence.

Wave energy converters (WECs) are devices designed to harness the kinetic and potential energy of ocean waves and transform them into usable electrical power. By capturing the natural motion of waves, WECs convert with movement into mechanical energy that is transformed into electricity through the use of mechanical systems such as pistons, spinning shafts, pumped air, or

turbines that drive generators, thus producing electrical power. There are many types of WECs, with the most common including point absorbers, attenuators, oscillating wave surge converts (OSWECs), oscillating water columns, overtopping devices, submerged pressure differentials, bulge wave converters, rotating masses, and more (Figure 1).

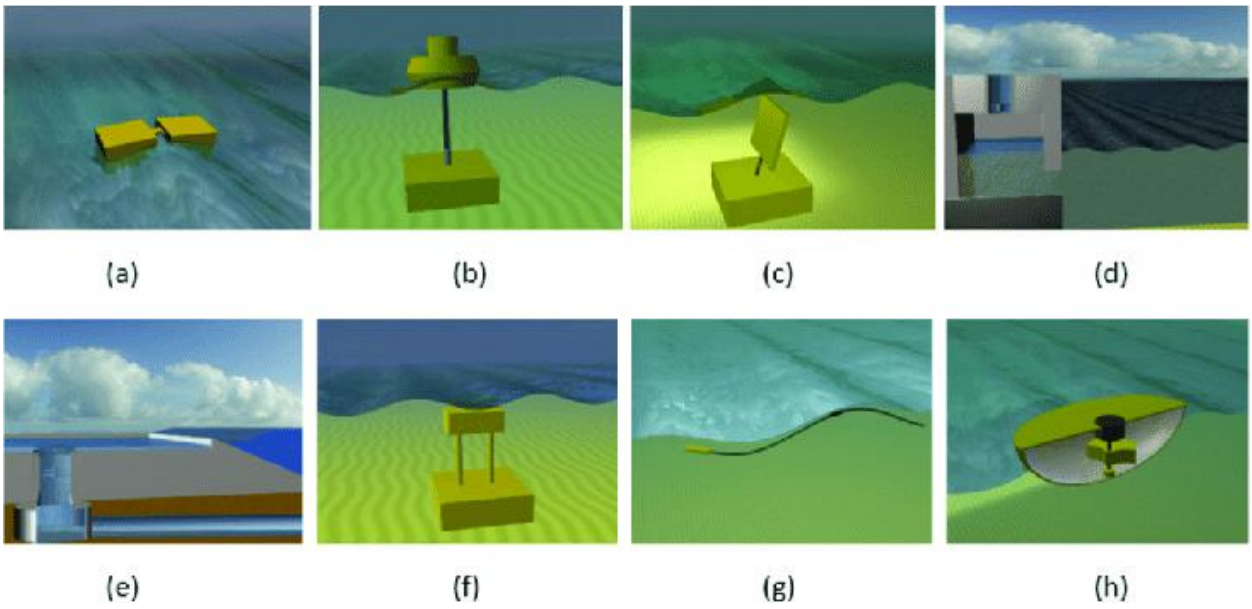

Figure 1. Example of WECs, including attenuators (a), point absorbers (b), oscillating surge wave energy converter (c), oscillating water column (d), overtopping device (e), submerged pressure differential (f), bulge wave (g), and rotating mass (h) (Wang, Kolios, 2018).

Currently, wave energy technology is still in the developmental and demonstration phases, with limited commercial deployment. The global installed capacity of wave energy remains relatively low compared to other renewable sources like wind and solar. While wave energy's predictability and high energy density make it an attractive renewable resource, significant technological and financial hurdles must be addressed before large-scale commercialization can

occur. However, advancements continue, with several companies and research institutions actively working to overcome technical and economic challenges. Research efforts are focused on improving the efficiency, reliability, and cost-effectiveness of WECs.

Oscillating Surge Wave Energy Converters (OSWECs) are a type of wave energy technology that harnesses the horizontal motion of ocean waves, known as surge, to generate electricity. Typically, these devices consist of a buoyant flap or paddle, hinged at the seabed or attached to a substructure, which oscillates back and forth as waves pass, converting mechanical energy into electrical power. These devices are predominantly deployed in nearshore environments, typically at depths ranging from 10 to 25 meters, where wave surge forces are most pronounced. Despite their potential, OSWECs are not yet widely commercialized. OSWEC technology remains in the research and development phase, with ongoing studies focusing on improving efficiency, durability, and cost-effectiveness. For instance, researchers have been testing models of new floating OSWEC designs (Golbaz et al., 2021; Mi et al., 2024; Ruehl et al., 2020) to enable deployment in deeper waters without the need for seabed anchoring, thereby minimizing environmental impact.

Coastal Structure Integrated Wave Energy Converters (CSI-WECs) are innovative systems that combine traditional coastal defense structures, such as breakwaters and seawalls, with wave energy harvesting technologies. This integration serves the dual purpose of protecting shorelines from erosion and storm surges while generating renewable energy from ocean waves (Zhang et al., 2019). CSI-WECs are not yet widespread but are gaining attention in regions with existing or planned coastal defenses. In the United States alone, over 13,000 miles of breakwaters and similar structures have been constructed to protect against coastal erosion and storms, and are

increasing in numbers (“Coastal Structure Integrated Wave Energy Converters”, NREL). Integrating wave energy converters into these structures presents an opportunity to enhance their functionality by adding renewable energy generation capabilities while utilizing the existing structures to reduce construction costs and environmental impact, while protecting these infrastructures and natural resources by absorbing more of the wave impact and preventing erosion. Research on CSI-WECs is ongoing, focusing on optimizing site selection, design, and performance. For example, studies have utilized Geographic Information System (GIS) tools to identify optimal locations for these systems, considering factors like wave energy flux and the capacity of existing coastal structures (Hall, 2024). Additionally, numerical models have been developed to assess the potential of integrating specific wave energy converters into coastal protection schemes. While not widely explored yet, CSI-WECs provide an opportunity to increase protection on natural and built shoreline environments and accessibility, improving overall longevity, while reducing construction costs and open water deployment risks.

The foundation of all WEC development lies in the understanding of wave dynamics. Linear Wave Theory (LWT) is a fundamental mathematical framework used to describe the behavior of ocean waves under the assumption that wave amplitudes are small relative to their wavelengths. This theory simplifies wave motion by assuming sinusoidal waveforms and negligible nonlinear interactions, allowing researchers and engineers to predict wave propagation, velocity, pressure distribution, and energy potential with high accuracy (Penalba et al., 2017). This framework is crucial for understanding ocean dynamics and plays a central role in designing WECs, providing equations for calculating wave forces on structures, optimizing energy extraction, and assessing the feasibility of WEC deployments in different marine environments. Additionally, it is widely

applied in coastal engineering, offshore structure stability analysis, and environmental impact assessments. As waves transition from deep to shallow water, their behavior changes significantly due to interactions with the seabed. In deep water, waves maintain their speed and energy, but as they enter shallower regions, they slow down, shorten in wavelength, increase in height, and eventually break. This transformation impacts WEC design, as devices placed in shallow waters must account for increased wave steepness and breaking forces, whereas deep-water WECs must be designed for stable operation in long-period swells.

Once wave dynamics are well understood, WEC development typically progresses through a variety of numerical modeling, experimental, and design for manufacturing iterations enroute to field deployments and validating system performance to reach high technology readiness levels (TRLs). Among those tasks, performing tank testing is a critical experimental method to validate wave energy converter designs before full-scale deployment. By simulating ocean wave conditions in controlled environments, engineers can analyze WEC performance, efficiency, and structural resilience. This helps refine device configurations, reduce risks, and improve energy capture potential.

One early-stage systematic approach in tank testing includes system identification (SID), which plays an important role in the design process through the development of mathematical models that characterize how WECs respond to different wave conditions. By analyzing the input against the output, controls can be optimized, improving energy conversion efficiency, and enhancing the reliability of WEC systems. Combining numerical modeling with experimental testing allows for more accurate predictions of real-world performance and aids in adjusting devices for optimal performance without incurring the upfront costs associated with multiple

field deployments. LWT provides the foundation for understanding ocean wave behavior, guiding the design and optimization of wave energy converters. Through the analysis of wave transformations, tank tests, and refinement of modeled systems, development and deployment of WECs can be streamlined in performance and efficiency improvement without compromising the integrity of these technologies. This project seeks to employ some of those early design processes to explore the feasibility of a new CSI-WEC, a vertically oriented OSWEC device. Specifically, this project explores wave kinematics through LWT, WEC dynamic response through numerical modeling, and system identification testing in a scaled laboratory wave tank facility.

The progression of this research followed a structured sequence beginning with numerical modeling and physical testing to build a comprehensive understanding of the VOSWEC's hydrodynamic performance. The study began with the application of linear wave theory, which established the fundamental framework for characterizing incident wave conditions and their interaction with floating bodies. Building on this foundation, a Boundary Element Method (BEM) approach was implemented using Capytaine to numerically evaluate the hydrodynamic coefficients governing VOSWEC dynamics, including excitation torque, radiation damping, and added mass across a range of plate geometries and submergence depths. These simulations provided critical insight into the frequency-dependent behavior of the device and revealed trends that informed design decisions prior to fabrication and testing.

With this hydrodynamic basis established, the project advanced to physical testing at the Michigan Technological University (MTU) wave facility. The BEM results served as a predictive benchmark against which experimental outcomes could be compared, while also narrowing the

scope of conditions to be explored in the laboratory. Tank testing introduced additional complexities not captured in the frequency-domain simulations, such as nonlinearities, viscous effects, and mechanical dynamics of the test apparatus. Using this structure, the numerical and experimental stages complemented one another: Capytaine simulations provided confidence and direction for the experimental campaign, and the MTU tests supplied the opportunity for validation and refinement of the numerical models.

This iterative process established a coherent progression from theoretical analysis to numerical modeling to physical validation. This process not only strengthens the reliability of the findings presented here but also highlights the importance of coupling BEM-based hydrodynamic modeling with experimental testing to develop wave energy technologies that are both physically realizable and scalable to ocean environments.

2. Background

Wave energy resource characterization involves assessing the potential of wave energy at specific locations to inform the development and deployment of WECs. Accurate characterization is necessary for optimizing WEC design, minimizing financial risks, and guiding site selection to achieve energy production goals. Currently, there are a variety of tools used to understand the wave energy resources. Wave measurement instruments such as buoys and sensors collect data on wave height, period, and direction, providing real-time information on wave conditions (e.g., Spotter buoys, NDBC buoys, among others). Numerical modeling and computational models are used to simulate and understand wave behavior under various environmental conditions (e.g., WaveWatch III, SWAN, among others). Geographical Information Systems (GIS) are also helpful to integrate spatial data to visualize and analyze wave energy resources across different regions.

The North American Great Lakes are slowly gaining attention in the potential wave energy that could provide otherwise landlocked areas with MRE that can compare to ocean coastlines globally. While these studies highlight the potential of wave energy in the Great Lakes (e.g., Sogut et. al, 2018; Sogut et. al 2019; Li et al., 2024; Pheifer and Hill, 2024), several gaps remain, including comprehensive year-round resource assessments that detail evaluations of wave energy potential across all Great Lakes and adequate high-resolution prediction models (Ahn et al., 2022), environmental impact studies (Shields et al., 2011) to understanding the ecological effects of deploying WECs in freshwater environments (Bergstrom et al., 2022), and technological adaptation in developing WECs tailored to the unique conditions of the Great Lakes, such as ice cover and variable wave climates (Jabbari et al., 2021), is essential. For example, the University

of Michigan's Beaver Island project exemplifies ongoing efforts to develop community-focused WEC prototypes in the Great Lakes, providing insight into practical deployment and local energy integration (University of Michigan, 2024). Addressing these gaps necessitates interdisciplinary collaboration, long-term monitoring, and the development of technologies suited to freshwater wave energy extraction.

Wave energy converters vary in design and operating principles to suit different marine environments and wave conditions. The most commonly found wave energy converters include multiple varieties (Figure 1). Attenuators are positioned parallel to the wave direction and typically consists of multiple segments connected by joints. As waves pass, the segments flex and generate energy through hydraulic or mechanical means. Point Absorbers utilize a floating device that moves up and down with the motion of waves. This movement drives a mechanical system, often a linear generator or hydraulic piston, that converts buoyant motion into electrical power. Oscillating Surge Wave Energy Converters use a large pivoting arm or flap attached to a fixed structure. As waves pass, the arm swings back and forth, driving a hydraulic or mechanical power take-off (PTO) system. Oscillating Water Columns have a partially submerged chamber where incoming waves force air through a turbine. The rise and fall of the water column compress and decompress the air, driving a bidirectional turbine to generate power. Overtopping / Terminator Devices collect wave water in an elevated reservoir. The stored water then flows back into the ocean through a turbine, converting potential energy into electricity. Submerged Pressure Differentials use a device placed underwater that capitalizes on the pressure changes caused by wave-induced sea level fluctuations. These pressure variations drive a hydraulic system to generate power. A Bulge Wave Converter uses a flexible rubber tube filled with water

stretches along the wave direction. As waves pass, they create bulges that travel along the tube, pushing water through a turbine at the opposite end.

Rotating Mass converters utilize the heave (vertical) and sway (horizontal) motion of waves to drive a rotating mass, either an eccentric weight or a gyroscope, that powers an electric generator. While these technologies remain in the early stages compared to wind and solar energy, various research efforts are underway. Companies such as CorPower Ocean, Carnegie Clean Energy, and AW-Energy are developing innovative WECs to improve efficiency and durability. Research institutions, including the European Marine Energy Centre (EMEC) and the Pacific Northwest National Laboratory (PNNL), are working to refine resource characterization and enhance wave energy harvesting technologies.

3. Motivation

The integration of WECs into coastal infrastructure presents a promising avenue for renewable energy generation. However, the development of cost-effective, efficient, and environmentally sustainable WECs for nearshore deployment remains limited. Existing research on coastal infrastructure-integrated WECs primarily focuses on marine environments, leaving a significant knowledge gap regarding their feasibility in freshwater systems such as Lake Superior. Developing WECs for nearshore environments and utilizing substantial freshwater sources such as Lake Superior could prove to be course-changing for the field of MRE technologies. The Great Lakes region experiences substantial wave activity, offering an untapped renewable energy resource. Second, integrating WECs into existing coastal structures—such as breakwaters and piers—can reduce costs and environmental impact compared to standalone offshore installations. Third, freshwater systems present unique challenges, including seasonal ice cover, lower salinity, and distinct ecological conditions, necessitating site-specific WEC designs. By exploring new designs that are adaptable to multiple locations, this research seeks to contribute to a broader understanding of sustainable wave energy utilization beyond oceanic applications.

While there has been significant progress in offshore wave energy research, coastal infrastructure-integrated WECs remain relatively underexplored. Existing studies, such as those conducted at the European Marine Energy Centre (EMEC) and the Pacific Northwest National Laboratory (PNNL), have demonstrated the feasibility of WECs integrated into breakwaters and seawalls. However, few studies focus specifically on freshwater environments.

Existing and future coastal structures provide unique opportunities for deploying coastal structure-integrated WECs. Advantages include easier access than open-water test locations, opportunities for designs where power take-off equipment remains outside of the water, and other design aspects that can potentially lower the cost of energy for WECs. Projects have explored integrating overtopping WECs and hinged point absorbers (e.g. Eco Wave Power), among other technologies, yet previously unexplored vertical OSWECs could provide new options for powering coastal communities or offshore structures, or other blue economic industries (desalination plants, nearshore or onshore aquaculture, etc.). To realize this potential, WEC dynamic models for vertical OSWECs are needed to explore power harnessing potential. This begins with system identification tank test methods that pave the way for addressing this problem in detail through future device modeling (WEC-Sim, CFD) and larger-scale tank testing.

Coastal infrastructure presents a compelling opportunity for the integration of wave energy systems, offering benefits such as reduced accessibility constraints, simplified maintenance, and lower deployment costs. Previous efforts have demonstrated success with technologies such as overtopping devices and hinged point absorbers, yet VOSWEC concepts remain underexplored. Realizing their potential for powering coastal communities and blue economy industries, such as desalination and aquaculture, requires development of validated dynamic models. Tank-based system identification is a critical early step toward this end, informing subsequent model development and scaled prototyping.

By addressing these key challenges, this project aims to contribute to the advancement of coastal wave energy technology. In the near term, it seeks to generate foundational knowledge on nearshore wave dynamics and WEC feasibility in Lake Superior. In the long term, it aims to

develop a well-rounded, adaptable WEC design that can be implemented in other coastal environments, supporting the broader adoption of wave energy as a sustainable power source.

4. Methods

4.1 Linear Wave Theory

Linear Wave Theory, also known as Airy wave theory, provides a mathematical framework for describing the behavior of small-amplitude surface waves in an idealized fluid environment. This theory assumes that wave motion follows a sinusoidal pattern, meaning that wave height is small compared to both the wavelength and water depth. It relies on potential flow assumptions, treating the fluid as incompressible and irrotational while neglecting viscosity and turbulence. These simplifications allow for the derivation of analytical solutions that describe wave kinematics and dynamics, making it a foundational tool in wave modeling.

To determine how waves propagate in different depth regimes, distinguishing between deep, intermediate, and shallow water waves, LWT relies on the dispersion relation relating wave frequency, wavenumber, wavelength, and depth, defined as:

$$\omega^2 = (gk)tanh(kh)$$

where $\omega = \frac{2\pi}{T}$ is the angular frequency (rad/sec), g is the gravitational acceleration (m/s^2), $k = \frac{2\pi}{L}$ is the wave number (m^{-1}), h is the water depth (m), T is the wave period (s), and L is the wavelength (m). This equation determines how waves propagate in different depth regimes, distinguishing between deep (h > L/2), intermediate (L/20 < h < L/2), and shallow water waves (h < L/20) (Karageorgis, 2012).

In the context of wave energy converters (WECs), LWT plays a crucial role in understanding the forces acting on floating or submerged structures. The time-resolved equation of motion for WECs can be expressed as:

$$m\ddot{X} = F_{Total} = F_{exc} + F_{md} + F_{rad} + F_{PTO} + F_v + F_{ME} + F_B + F_m$$

where F_{exc} is the wave excitation force and torque vector with six degrees of freedom (DOF), F_{md} represents the mean drift force, F_{rad} is the wave radiation force, F_{PTO} corresponds to the power take-off (PTO) force, F_v is the viscous damping force, F_{ME} accounts for Morison elements force, F_B represents the buoyancy force, and F_m accounts for mooring connections (Forbush et al., 2022). The excitation, radiation, and buoyancy forces are typically sourced from boundary element method (BEM) solvers (e.g., Nemoh, Capytaine, WAMIT, among others), which often are solved in the frequency domain. Since LWT assumes small wave heights, uniform depth, and an inviscid, incompressible fluid, non-linear effects such as viscous forces and turbulent stresses are neglected. In some cases, mean drift, buoyancy, mooring, and radiation forces may also be ignored in the time-domain WEC of motion to simplify calculations further.

Linear Wave Theory is essential in ocean and coastal engineering because it provides a fundamental analytical basis for understanding wave behavior. Despite its simplifying assumptions, it accurately predicts wave characteristics in most practical scenarios where wave steepness is low. One of its key applications is estimating wave forces on structures, which is critical for designing offshore platforms, breakwaters, and WECs. Additionally, the theory helps describe wave kinematics by determining velocity and acceleration fields, which play a crucial role in sediment transport and coastal erosion studies (Le Roux, 2008). LWT also serves as the foundation for more advanced models, such as nonlinear and spectral wave theories, which

account for higher-order effects, such as wave-wave interactions, small wave steepness, etc. Furthermore, it explains wave transformation processes such as refraction, diffraction, and shoaling, which are essential for understanding how waves behave as they travel from deep to shallow waters.

In practical applications, LWT is widely used across various ocean and coastal engineering disciplines, playing a significant role in wave energy conversion by modeling the hydrodynamic response of WECs. In offshore structure design, the theory provides essential force estimations necessary for stability analysis. Coastal management also relies on LWT to assess wave-driven sediment transport and shoreline evolution. Additionally, numerical wave modeling tools such as WEC-Sim and SWAN (Simulating Waves Nearshore) incorporate LWT to simulate wave propagation and interactions with structures (Booij, 1999; Flanagan et all., 2022).

Although LWT does not account for large wave amplitudes, breaking waves, or wave-wave interactions, it remains the first step in wave analysis due to its simplicity and accuracy in most engineering applications. When higher precision is required, more complex models such as second-order Stokes waves or Boussinesq equations are used to capture nonlinear effects. Nonetheless, LWT remains an indispensable tool for engineers and researchers studying ocean wave dynamics.

4.2 BEM and WEC-Sim

Following the theoretical framework provided by LWT, it was necessary to conduct numerical hydrodynamic analysis to quantify the wave-structure interactions for the VOSWEC geometry prior to time-domain simulations. This step bridges the gap between analytical predictions and dynamic modeling, providing an insight regarding what to expect by providing frequency-domain hydrodynamic coefficients that accurately represent the physical response of the device. For this work, the open-source (BEM) solver Capytaine was used to simulate the hydrodynamic behavior of the VOSWEC under a range of wave frequencies and geometric configurations. Capytaine was selected for its ability to handle complex floating body geometries, integrate directly with WEC-Sim through standardized output formats, and provide high-resolution hydrodynamic data critical for early-stage design optimization.

Capytaine uses a panelized mesh of the device geometry, solving the linearized potential flow equations under the assumptions of inviscid, incompressible, and irrotational flow. For the VOSWEC analysis, the model was discretized into a high-fidelity STL mesh exported from CAD, which was then used to compute hydrodynamic coefficients over a range of wave frequencies and incident wave headings. The primary degree of freedom (DOF) of interest was yaw rotation about the vertical axis, as this motion directly corresponds to the energy capture mechanism of the vertically oriented surge flap. Other DOFs were constrained in the BEM runs to isolate the hydrodynamic response in yaw and reduce computational cost. The main outputs from Capytaine included frequency-dependent excitation torque, added mass, and radiation damping coefficients. These parameters define how the WEC interacts with the surrounding wave field. Excitation torque quantifies the wave-induced forcing, added mass reflects the

additional inertia due to accelerated fluid, and radiation damping represents the wave energy radiated away due to device motion. The resulting hydrodynamic coefficient curves provided insight into the influence of plate geometry and draught on device performance.

Once the hydrodynamic coefficients were obtained from Capytaine, they were exported in .h5 format compatible with WEC-Sim. WEC-Sim is an open-source simulation tool funded by the U.S. Department of Energy's Water Power Technologies Office (WPTO) (Ogden et all., 2022). It is designed to model WECs by solving the governing equations of motion for these devices. Built on MATLAB/SIMULINK with Simscape Multibody, WEC-Sim provides a comprehensive platform for simulating the dynamic behavior of WECs, incorporating components such as bodies, joints, PTO systems, and moorings. The software supports both rigid and flexible body modeling, and operates in the time domain, solving the equations of motion across six Cartesian DOF: surge, sway, heave, roll, pitch, and yaw (Figure 2). While Capytaine operates in the frequency domain, WEC-Sim uses the hydrodynamic data as input to solve the coupled equations of motion for the device in the time domain. This approach allowed for the inclusion of nonlinearities, control strategies, and realistic wave inputs that cannot be captured in frequency-domain BEM alone. By linking the two tools, the project leveraged the strengths of both: Capytaine provided the accurate hydrodynamic foundation, and WEC-Sim extended this into dynamic performance predictions under realistic operating conditions.

This integrated workflow, beginning with LWT for foundational understanding, progressing through Capytaine for frequency-domain hydrodynamic characterization, and culminating in WEC-Sim for time-domain device simulation ensured that the VOSWEC design was grounded in sound hydrodynamic principles while enabling robust performance assessment

before physical testing. This process also informed design iterations prior to the MTU wave tank experiments, reducing the risk of costly redesigns during experimental validation.

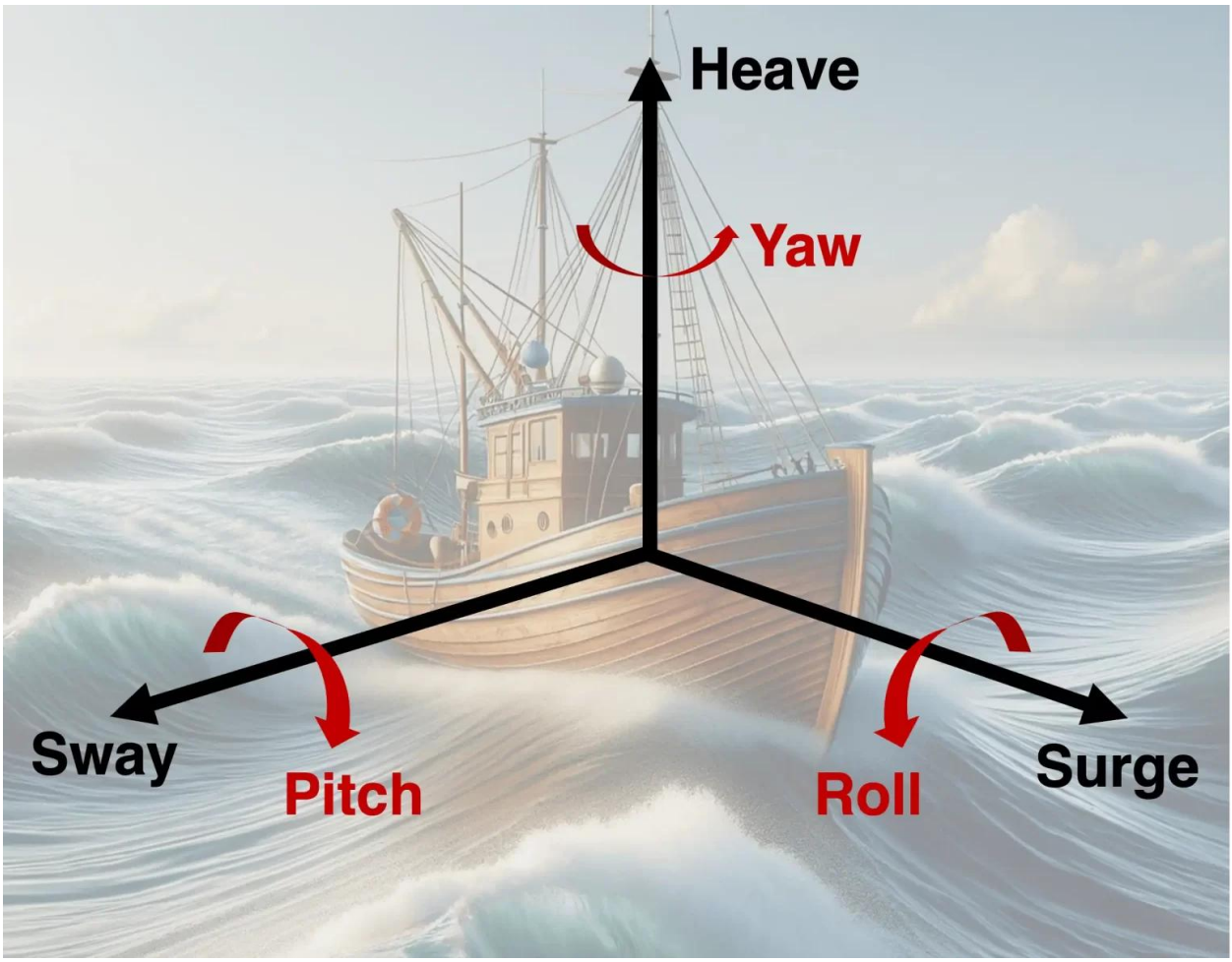

Figure 2. Illustration of 6 Degrees of Freedom (DOF) in marine settings.

The operating principles of WEC-Sim are centered around multi-body dynamics simulation, where it models the interaction of interconnected bodies, such as floating structures, using numerical methods in MATLAB/Simulink and Simscape Multibody. It captures the real-

time dynamic response of WECs through time-domain analysis by solving the equations of motion, incorporating hydrodynamic forcing, and simulating all six DOF of motion. The tool includes wave excitation forces, radiation forces, and added mass effects, which are derived from hydrodynamic coefficients precomputed using boundary element method (BEM) solvers as discussed above. Additionally, WEC-Sim allows users to model PTO systems, including linear dampers and hydraulic systems, to convert mechanical energy from wave motion into usable power. It also supports the integration of mooring system dynamics, either through simplified quasi-static models or external dynamic solvers. The flexibility and customizability of WEC-Sim make it suitable for numerous engineering applications, and its open-source framework allows users to extend or modify the software as needed.

In the context of physical testing, WEC-Sim supports pre-test planning and design optimization. It enables virtual prototyping, allowing users to simulate and refine a device's design, mass properties, and PTO configurations before conducting expensive physical tests. The tool also facilitates parameter sensitivity analysis, enabling users to study the impact of different parameters, such as wave height, period, and PTO damping, on WEC performance. Additionally, WEC-Sim can be used to validate model scaling based on Froude scaling laws, ensuring that experimental designs accurately represent full-scale behavior. In system identification and model calibration, WEC-Sim allows for hydrodynamic coefficient validation by comparing simulated results with experimental data from tests like decay or forced oscillations. It also helps estimate system parameters such as added mass, damping, and stiffness by fitting simulation results to experimental data.

The use of WEC-Sim is instrumental in testing real-time control strategies. It supports hardware-in-the-loop (HIL) testing, enabling the validation of control algorithms before physical implementation (Guerrero-Fernandez, 2022). The tool can simulate wave conditions used in physical wave tanks and real sea states, ensuring that the experimental wave spectra align with real ocean conditions. WEC-Sim aids in data comparison and validation by matching time-domain responses and analyzing force and motion tracking, which helps ensure that the simulated and experimental results align with expected performance. This combination of virtual and physical testing capabilities enhances the accuracy and efficiency of WEC design and testing, ultimately contributing to the successful development of wave energy technology.

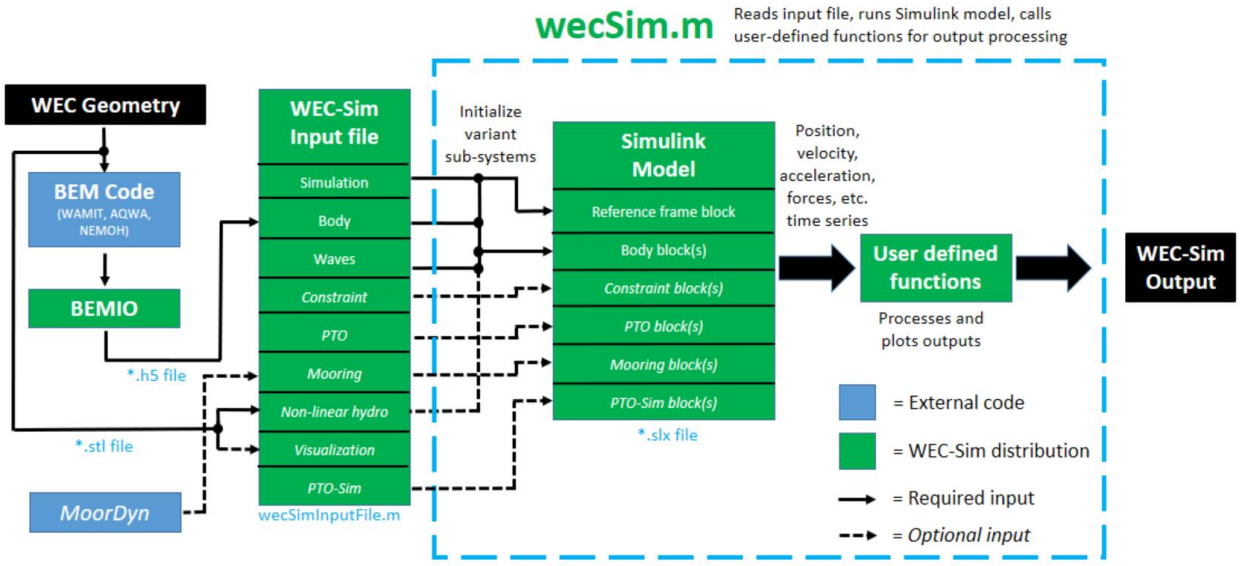

Figure 3. High level WEC-Sim functionality workflow diagram.

4.3 Michigan Technological University Wave Tank Testing

4.3.1 System Setup for MTU Wave Tank Testing

System Identification (SID) is a widely used tool across many engineering industries. This process measures input forcing and output response signals of a system in the time domain, and when converted to the frequency domain, provides critical information for understanding the system's dynamics. Ultimately SID proved to be a crucial step in the early design of mathematical models along the path towards more complex system design and control strategies. For WECs, SID allows developers to focus on accurately modeling system dynamics, validating system parameters, and refining control strategies. The process begins with the development of a WEC model. In the first step, prior to testing, the WEC design is created using CAD software (e.g., SolidWorks), ensuring that mass distribution, buoyancy, and hydrodynamic surfaces are accurately represented. The next part of this phase involves setting up the WEC-Sim simulation environment, where initial estimates for hydrodynamic coefficients (obtained from BEM solvers like WAMIT, NEMOH, or Capytaine), PTO properties, and mooring dynamics are defined (Figure 3). Preliminary simulations are then run in WEC-Sim, using theoretical or estimated parameters, to identify key parameters that may need refinement based on expected wave conditions and control objectives.

Next, and often simultaneously, the experiments for conducting wave tank experiments for model testing are designed. Test conditions are selected, which include both regular and irregular waves for controlled input-output analysis, as well as decay tests to estimate natural frequencies and damping. Forced oscillation tests are performed to determine hydrodynamic coefficients, and PTO characterization tests assess power conversion efficiency and dynamic

response at small-scale. Instrumentation and data collection are crucial in this phase. Wave elevation, WEC motions (across six DOF), PTO forces, mooring loads, and output power are measured using high-resolution sensors, ensuring proper synchronization between wave gauges, motion tracking, and force sensors.

Following this, the experimental data is processed and system parameters are extracted. Time-domain analysis is used to fit equations of motion to the observed responses, employing system identification techniques such as least squares estimation or Kalman filtering. The comparison between simulated and experimental time series responses is essential for parameter estimation. Additionally, frequency-domain analysis is conducted to compute frequency response functions (FRF), which help extract hydrodynamic parameters such as added mass, damping, and excitation forces. Optimization methods are then used to refine the model parameters, including hydrodynamic coefficients, PTO damping, and mooring stiffness, before updating the WEC-Sim model with calibrated parameters to improve predictive accuracy.

Taking in the initial experimental information, the model is validated and further refinement occurs as necessary. Simulation results are compared to experimental data to validate responses, ensuring that simulated motions match those observed in various wave conditions. Energy capture efficiency and PTO performance are also assessed, comparing numerical and physical models. If discrepancies are found, numerical models are adjusted to account for nonlinear effects or improve PTO dynamics. If necessary, modifications are made to the prototype to better align with the simulation results.

A validated model is used for developing control strategies, optimizing PTO settings based on refined system parameters, and implementing advanced control algorithms such as

reactive control or latching. Scaling considerations are also addressed using Froude scaling principles to extrapolate the results from tank testing to full-scale deployment. The information gained from SID processes are applied to refine the full-scale hydrodynamic models, ensuring more accurate performance predictions for real-world applications.

4.3.2 Project Objectives

The wave tank testing campaign is designed to evaluate a small-scale, wall-mounted, vertically oriented oscillating surge wave energy converter (VOSWEC) to establish system identification (SID) parameters for future numerical model validation and device optimization. Establishing baseline experimental data is foundational to enabling SID methods to drive future WEC dynamic model development for this type of technology, with the ultimate goal of informing the design and control of full-scale energy harvesting devices. The specific assistant objectives include (1) performing forced VOSWEC oscillation tests to model device impedance, (2) performing diffraction tests using a locked VOSWEC to establish excitation transfer functions, and (3) exploring multiple VOSWEC plate aspect ratios to understand variations in device impedance and excitation transfer functions. Developing these transfer functions assists in providing clear routes for modeling WEC dynamics and designing device controllers that enable maximum power transfer from waves. Throughout all experiments, key metrics will be measured including OSWEC angular position, shaft torque, forces, and wave characteristics. Following prescribed and proven SID methods using wave tank experiments will allow assistance objectives to be met and establish new information to advance the state of marine energy technology development. Specifically, vertical OSWECs provide potential advantages, including

out-of-water power take-off systems, integration into existing or new coastal infrastructure, attachment to existing or new offshore platforms or coastal pier foundations, relatively simple in-water geometric configurations, and adoption of other OSWEC advancements, among other advantages. Through these SID approaches, validating models (WEC-Sim, CFD, etc.) will be utilized for further advancing the technology concept, while also producing publicly available information that can integrate into graduate-level course design and workforce development for the marine energy sector.

The planned MTU experiments comprise a comprehensive system identification (SID) methodology for a VOSWEC deployed in the MTU Wave Tank. The testing campaign includes six experiments, each targeting specific hydrodynamic and control-related characteristics of the system.

- *Experiment 1* begins with baseline wave field characterization. This includes deploying wave gauges throughout the tank, with one temporarily positioned at the VOSWEC location, to establish the spatial variation of wave elevation and ensure accurate interpretation of wave-structure interactions during later tests.
- *Experiments 2 and 3* focus on quantifying the intrinsic hydrodynamic impedance of the VOSWEC through forced oscillation tests in calm water. Experiment 2 uses sinusoidal inputs to evaluate the frequency-dependent torque response at discrete amplitudes, while Experiment 3 applies a multisine (white noise) input to excite a broad range of frequencies, enabling system identification in the frequency domain. These tests measure torque, angular velocity, and motion response to construct the device's impedance characteristics (Figure 4).

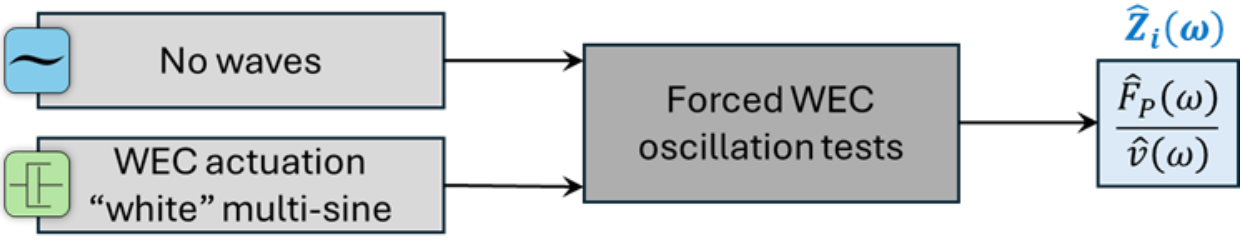

Figure 4. System identification workflow used from *Experiments 2 and 3* to determine the intrinsic impedance for the VOSWEC.

- *Experiments 4 and 5* transition to diffraction-based testing. The VOSWEC is locked in place while exposed to both regular and multisine wave conditions. These tests measure the unactuated system's response, specifically wave-induced excitation forces, captured via torque sensors and load cells. (Figure 5) illustrates the procedure for deriving the excitation frequency response function by correlating the locked-body force measurements with baseline wave probe data collected in Experiment 1.

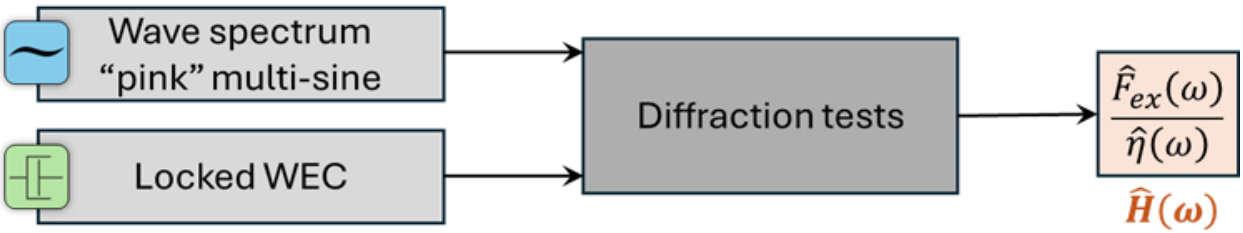

Figure 5. System identification workflow used from *Experiments 4 and 5* to determine the wave excitation frequency response function for the VOSWEC.

- *Experiment 6* repeats the prior experimental sequence for multiple plate geometries to assess how changes in aspect ratio influence both impedance and excitation response. The

combined outcomes from *Experiments 2–6* provide the two essential components of the WEC's dynamic behavior: the intrinsic impedance and the wave excitation transfer function. These are ultimately integrated (Figure 6) to establish a system-level model that supports dynamic simulation, control design, and full-scale scaling assessments for vertical OSWEC deployment.

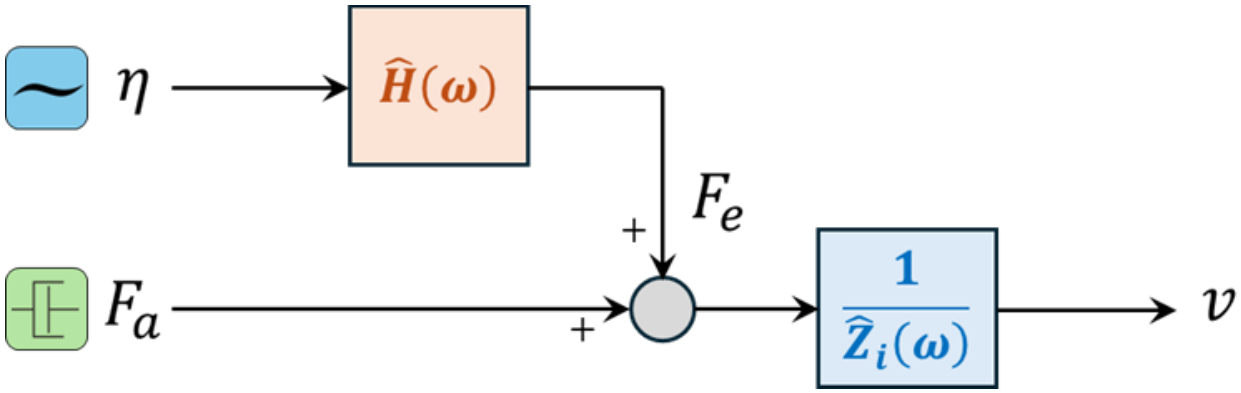

Figure 6. System identification workflow resulting from determining the wave excitation frequency response function and the intrinsic impedance frequency response from these experiments to develop and understand VOSWEC dynamics for use in developing control strategies in the future.

Overall, these are designed to enable frequency-domain modeling, enhance understanding of geometry-dependent performance characteristics, and support future simulation and control validation work using tools such as WEC-Sim and CFD.

4.3.3 System Identification Pre-MTU Investigation

4.3.3.1 Boundary Element Method Modeling Using Capytaine

To evaluate the hydrodynamic performance of various VOSWEC plate configurations under wave excitation in yaw, a boundary element method (BEM) approach was implemented

using the open-source solver Capytaine written in Python. Capytaine computes these coefficients by solving the linearized potential flow equations under the assumption of an incompressible, inviscid, and irrotational fluid. These assumptions are consistent with LWT and enable the decomposition of hydrodynamic forces into components that can be readily incorporated into time-domain models such as WEC-Sim.

Two cases of three WEC plates were designed in SolidWorks, to produce three-dimensional STL files, with a constant height h = 0.6 m and varying thicknesses of b = 0.02 m, 0.04 m, and 0.06 m. Case A of these plates had a length of L = 0.3 m and Case B plates were given a length of L = 0.4 m. Each of these plates were tested at varying draughts of d = 0.3 m, 0.4 m, 0.5 m, and 0.6 m, for a total of 12 plate configurations for each case (making 24 configurations tested in total). Each plate geometry corresponds to a unique configuration labeled as Plate 1a through 12a for Case A and Plate 1b through 12b for Case B, as shown in Table 1 with the supporting diagram in Figure 7

Table 1. Naming Convention for Plate Configurations for both Case A and Case B

Plate Naming Conventions			
Draught (d) [m]	**Width (b) [m]**		
	0.02	**0.04**	**0.06**
0.3	**1**	**5**	**9**
0.4	**2**	**6**	**10**
0.5	**3**	**7**	**11**
0.6	**4**	**8**	**12**

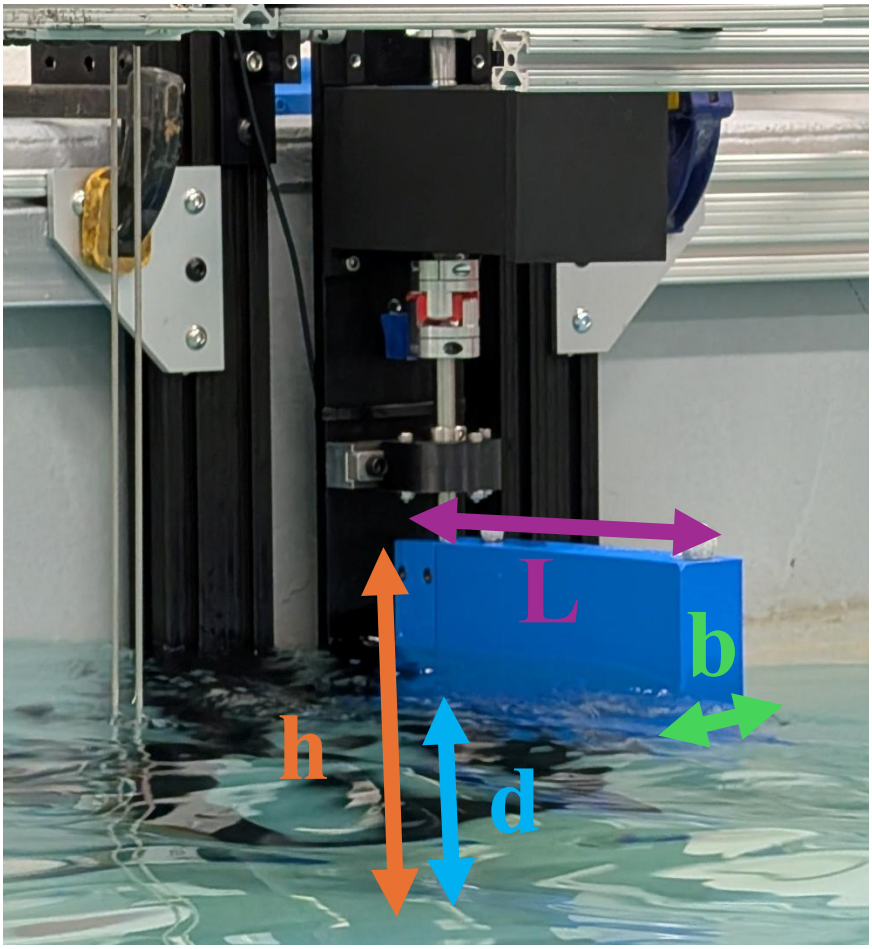

Figure 7. WEC Plate Prototype where b is the width of the plate, d is the draught, h is the height, and L is the length.

Using Capytaine's Python API, automated simulation scripts were developed to batch-process all STL geometries and compute their frequency-domain hydrodynamic coefficients. The simulations were configured to solve for motion in the yaw degree of freedom, chosen based on the device's design for oscillation about the vertical axis. Frequency sweeps ranged from 0.5 to 3.0 rad/s (corresponding to wave periods of ~2.1–12.5 s), encompassing the range of dominant ocean wave frequencies observed in many nearshore and coastal environments. A refined frequency resolution of 0.05 rad/s steps was used to capture a more detailed resonance behavior. For each geometry, Capytaine calculated the excitation torque, added mass, and radiation damping. These outputs characterize the linear hydrodynamic response of the structure under harmonic wave loading. All simulations assumed incompressible, inviscid, and irrotational flow conditions, consistent with the assumptions of potential flow theory.

4.6.3.2 Data Post-Processing and MATLAB Analysis

The hydrodynamic coefficients computed in Capytaine were exported as .csv files for each plate and condition. In MATLAB, a post-processing script was written to import, organize, and visualize this data across the full matrix of design variations. For each configuration, data columns corresponding to frequency, excitation torque magnitude, excitation phase, added mass, and radiation damping were extracted.

MATLAB scripts generated overlay plots for each hydrodynamic quantity as a function of frequency. These plots were grouped by draught, with each subplot comparing three plates of varying width at a constant immersion depth. Consistent color-coding and line styles were used to clearly distinguish plates, and separate figures were created for Case A and Case B to assess

the influence of plate length. These visualizations allowed for side-by-side comparisons of the resonance characteristics, damping behavior, and inertial response across the plate geometries. This system identification process allowed for visualization and understanding of possible optimal VOSWEC configurations prior to prototyping and wave tank testing.

4.3.4 MTU Wave Tank Experimental Setup

4.3.4.1 MTU Wave Tank Facility Overview

The MTU Wave facility is equipped to support advanced marine energy and offshore engineering research and development through its state-of-the-art wave tank and associated instrumentation. These systems include:

- ***Physical Equipment*:** The MTU wave tank facility includes an 8-paddle Edinburgh Designs wave generator and customizable resistance wave gauges, 11-camera Qualisys motion tracking system, and various hardware for mooring configurations. A dSPACE Microlab Box data acquisition (DAQ) system is used to integrate and synchronize the facility instrumentation with WEC hardware or other instrumentation and controls necessary to accomplish experimental tests.
- ***Software*:** DAQ applications are designed and deployed using ControlDesk with MATLAB/Simulink. The application developed for the VOSWEC testing included analog output control for sinusoidal motion of the WEC plate, analog input DAQ for four S-type load cells and an inline rotary torque transducer, two encoders, as well as other tasks necessary to synchronize and control multiple signals.

- ***Test Site Conditions*:** Testing uses Froude scaling to match wave conditions to the WEC scale. Waves are designed in Wave Synthesizer software and deployed through the wave generator to replicate precise ocean conditions. These can include a range of regular, irregular, and multi-sine wave conditions.

4.3.4.2 Experimental Setup, Data Acquisition System, and Instrumentation

The experiments (completed and future) are conducted in the MTU Wave Tank facility, a 10 m x 3 m wide x 1 m deep wave tank (Figure 8). A 1:30 and 1:40 scale wall-mounted vertically oriented OSWEC (VOSWEC) was designed for laboratory data collection (Figure 9), consisting of the necessary controls and sensors to perform open and closed-loop system identification (SID) tests. A structural low-profile extruded aluminum frame secures all components to the concrete wall of the MTU Wave Tank while transferring vertical loads of the mounting structure to the bottom of the tank. To isolate forces and torques experienced by the WEC during experiments, a central vertical plate is mounted to the structural low-profile frame only through four S-Type load cells (two near the top, two near the bottom, measuring either tension or compression). All control and sensing components are mounted to this central plate. A detailed description of the components used for the experimental setup is included below.

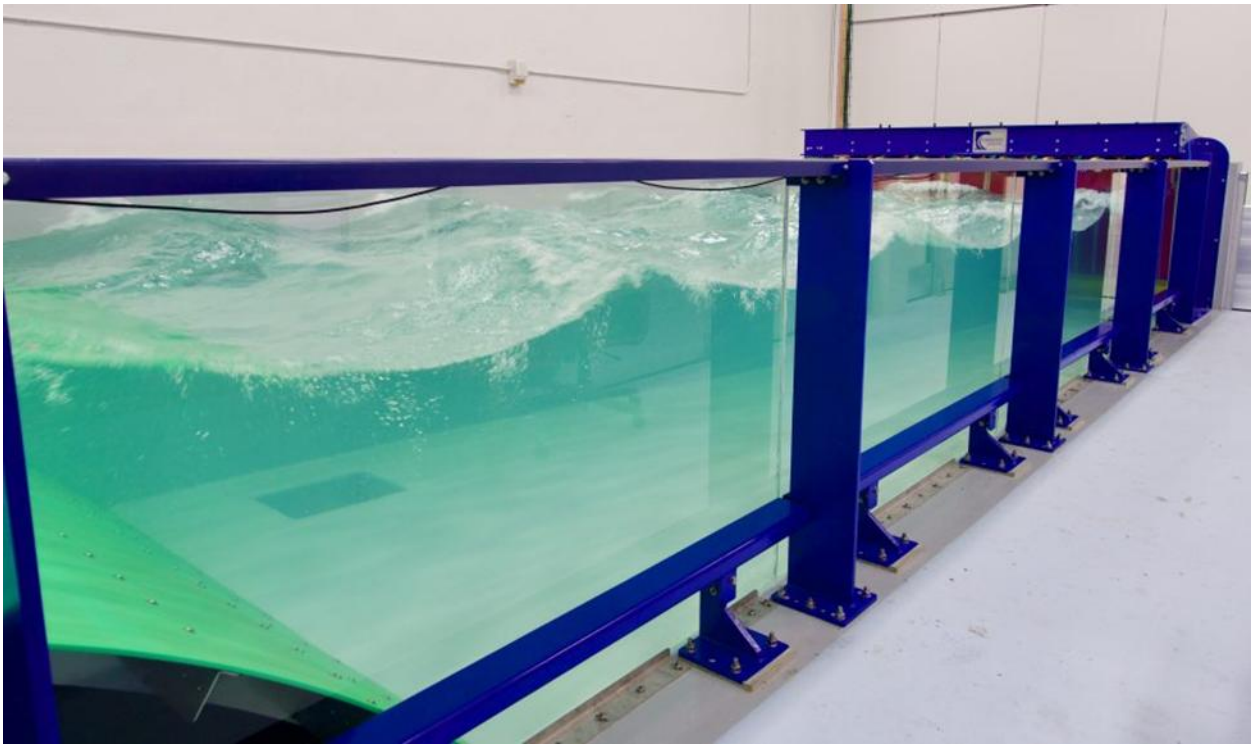

Figure 8. MTU Wave tank facility, a 10m x 3m x 1m concrete and glass basin with 8 independently controlled wave paddles with force feedback, capable of generating regular and irregular waves across a range of frequencies and wave heights.

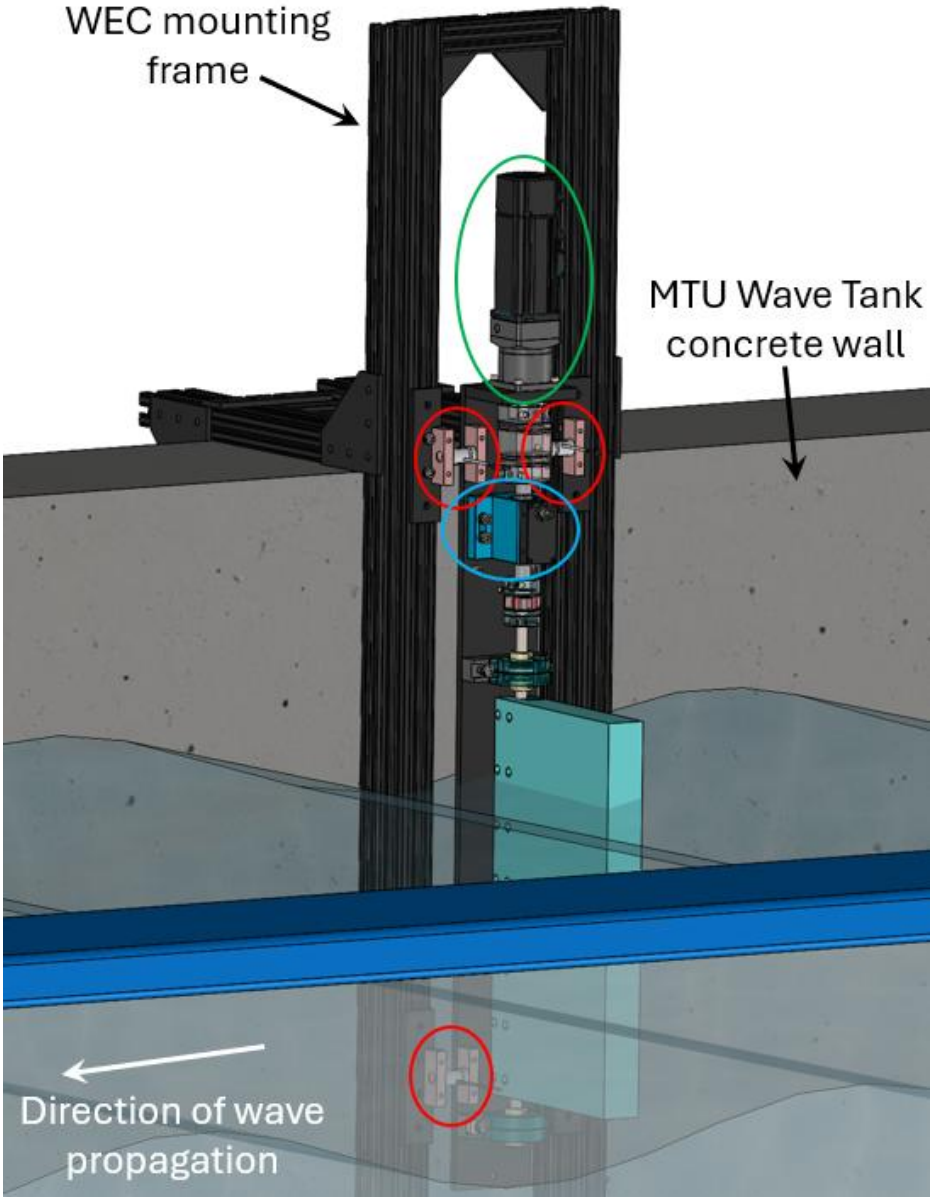

Figure 9. CAD schematic of the VOSWEC test setup for the MTU wave tank tests. Circled in red are 3 of the 4 S-type load cells measuring forces in the direction of wave propagation (the 4th load cell is hidden by the light-blue colored VOSWEC plate). The inline rotary torque transducer is circled in blue. The servo motor and 1:10 gearbox is circled in green.

- ***WEC Oscillation Control*:** Angular rotation of the VOSWEC plate is controlled by a servo motor (Applied Motion Products J0400-351). Due to the frequency and amplitude of oscillations, a speed-reducing gearbox (Automation Direct high-precision planetary gearbox, 10:1 ratio, Part 96200005) is used in line with the servo motor to allow the servo to operate at higher RPMs while driving the WEC oscillations at more acceptable speeds. The servo motor is equipped with an internal electromagnetic brake which locks the WEC in place during experiments when only wave forcing is applied. Precise control and angular positioning are enabled through an integrated encoder. The servo motor unit allows for precise torque and/or position control modes from a servo drive unit (Applied Motion Products SV2A5-Q-AE). The dSpace wave tank software application outputs user-defined sinusoidal analog voltage signals at 1000Hz, allowing for easily configured oscillatory controls of the WEC. A precision servo motor shaft coupling connects the gearbox output shaft to one side of the rotary torque transducer. Additional VOSWEC plate motion is captured using the overhead precision motion tracking system at the MTU Wave facility (11-camera Qualisys motion capture system). A minimum of three reflective markers will be attached to the top surface of the VOSWEC, allowing the plate to be defined as a rigid body within the Qualisys Track Manager software. The software will then automatically track and determine the plate's full six-degree-of-freedom (6DOF) trajectory.
- ***Shaft Torque and Angular Speed Measurements*:** An Interface Force Model T5 Pedestal Rotary Torque Transducer with integrated speed/angle measurements (encoder) (Model

T5-50-A6A) is mounted in line with the driving servo motor and primary drive shaft (i.e. the VOSWEC plate hinge). This rotary sensor measures shaft torque and angular speed/location during operations. Output signals in the +/- 5 VDC range are measured by the DAQ system and converted to engineering units during post-processing.

- ***Force Measurements*:** Four environmentally sealed submersible SSC S-Type load cells (Interface Force model SSC-50) are used to mount the VOSWEC assembly (and motion control components). Tension and compression forces aligned with the direction of wave propagation are measured from these four load cells, which are positioned at the upper and lower ends of the mounting bracket to attempt to fully isolate and measure loads experienced by the VOSWEC plate from the tank mounting structure. Interface Force SGA signal amplifier boxes are used for each load cell to boost mV signals to acceptable +/- 5 VDC signals measured by the DAQ system and converted to engineering units during post-processing.
- ***Data Acquisition System*:** The MTU Wave facility (Figure 10) has a dSPACE MicroLabBox Gen 1 data acquisition system with many analog inputs (14-bit, 10 MHz max and 16 bit 1 MHz). It also has six encoder input channels and several additional digital I/O channels for synchronization, etc. (i.e., sending TTL pulses to external systems). Alligator Technology anti-alias filters are used in line with the signals from the four load cells and the rotary torque sensor, each set to a 500Hz filter. The MTU Wave facility data acquisition application logs all data simultaneously (and synchronized) with the MTU Wave tank data including paddle commands/motion, wave gauges, and Qualisys motion tracking, among other operational characteristics.

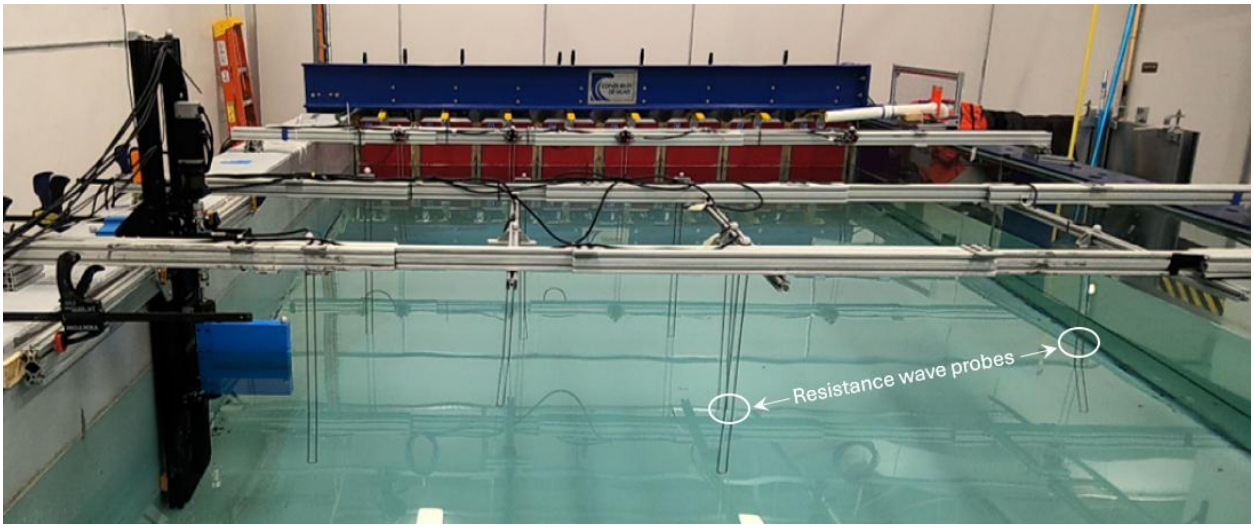

Figure 10. Photo from the VOSWEC experiments in the MTU wave tank facility. The WEC mounting frame and plate are seen in the left-hand portion of the photograph (corresponding to the CAD schematic in Figure 9). Eleven resistance wave probes were used and positioned at strategic locations around the wave basin (two are circled in white circles). The wave tank control station and DAQ computers are out of frame to the right of the photograph.

4.4 Froude Scaling Methods

Froude scaling is a principle used in hydrodynamics to model the behavior of floating and submerged bodies at different scales while maintaining dynamic similarity. It is based on the Froude number (Fr), a dimensionless quantity that compares inertial forces to gravitational forces in a fluid system. The Froude number is expressed as $Fr = \frac{v}{\sqrt{gL}}$, where v is velocity, g is gravitational acceleration, and L is a characteristic length, such as the hull length or wavelength (and oftentimes indicated as the flow depth, h, in open-channel flow scenarios). This principle is essential in marine and coastal engineering for designing and testing scaled models of structures to predict their behavior at full scale (Schmitt and Elsäßer, 2017).

Froude scaling has numerous applications across fields. In wave energy converter (WEC) testing, it is used to predict how a full-scale WEC will perform based on wave tank experiments with smaller models. Similarly, it is applied in ship hydrodynamics to assess resistance, propulsion, and maneuverability by testing small-scale ship models. In coastal engineering, it is utilized to model breakwaters, harbor designs, and coastal erosion studies. Additionally, Froude scaling plays a role in offshore structures, such as designing floating wind turbines, oil platforms, and mooring systems.

The scaling method involves several key components, shown in Table 2. The Length Scale **(λ_L)** defines the ratio of the model's length to that of the full-scale prototype, the time scale **(λ_T)** accounts for the fact that larger models experience slower characteristic timescales for motion, the velocity scale **(λ_V)** ensures that flow speeds in the model correctly represent full-scale conditions, the acceleration scale **(**λremains constant between the model and prototype systems because gravity is unchanged, the force scale **(λ_F)** accounts for forces like buoyancy and hydrodynamic loads, and the power scale **(λ_P)** is used to extrapolate energy conversion predictions from model tests to real-world applications.

Table 2. Froude Scale Factors and corresponding relationships.

Parameter	Scale Factor	Relationship
Length (L)	λ_L	$\frac{L_{full-scale}}{L_{model}}$
Time Scale (T)	λ_T	$\sqrt{\lambda_L}$
Velocity Scale (V)	λ_V	$\sqrt{\lambda_L}$
Acceleration Scale (A)	λ_A	1
Force Scale (F)	λ_F	λ_L^3
Power Scale (P)	λ_P	$\lambda_L^{3.5}$

Despite the usefulness, Froude scaling has limitations. It does not capture viscous effects, as it does not account for Reynolds number similarity. For flows dominated by viscosity, Reynolds scaling may be necessary. Additionally, material properties such as elasticity and stiffness do not always scale directly, requiring corrections for flexible structures. Furthermore,

wave tank effects and imperfections in scale models can introduce deviations, which must be considered when extrapolating results to full-scale applications.

4.4.1 Comparison of Scaling Methods

Froude scaling is the primary method used in hydrodynamic applications where gravitational and inertial forces dominate, ensuring dynamic similarity between model and full-scale systems by maintaining a constant Froude number. It is widely applied in wave energy converter testing, ship hydrodynamics, and offshore structure modeling. However, Froude scaling does not account for viscosity, elasticity, or surface tension, which can introduce inaccuracies in some fluid–structure interactions. *Reynolds scaling* preserves the balance between inertial and viscous forces and is essential for applications where viscosity significantly influences flow behavior, such as in aerodynamics or turbulent drag studies. Since it excludes gravitational effects, Reynolds scaling is not appropriate for wave-dominated systems. *Cauchy scaling* addresses elastic force similarity and is important for flexible structures like mooring lines, deformable WEC components, and floating platforms. It compensates for material stiffness differences not captured by Froude laws. *Weber scaling* focuses on inertial and surface tension forces and is mainly relevant for microscale phenomena like droplet formation or capillary waves, with limited applicability in large-scale marine systems.

In wave energy research, Froude scaling remains the dominant approach due to gravity-driven wave dynamics. However, in systems where viscous or elastic effects are non-negligible, supplemental consideration of Reynolds or Cauchy scaling may be necessary to ensure accurate model-to-prototype extrapolation.

4.5 Nearshore Wave Resource Assessment

Accurate characterization of nearshore wave energy resources is essential for advancing the development of wave energy converters (WECs) from small-scale laboratory experiments to full-scale deployment. While this project emphasizes scaled tank design, hydrodynamic testing, and early-stage system identification, the long-term objective involves understanding and harnessing real-world sea states for practical energy generation. A critical step in this progression is the estimation of available wave power in nearshore environments, particularly under shallow-water conditions where many WECs, including the VOSWEC, are likely to be deployed. The methodologies used to quantify wave energy potential, such as comparing deep and shallow water formulations of wave power, play a significant role in determining both the feasibility and optimal design parameters for scaled-up systems.

Nearshore wave resource assessment involves understanding how wave power changes with varying water depths, as the wave power equations differ between deep, intermediate, and shallow water due to the depth-related effects on wave kinematics. In deep water, where the depth is greater than half the wavelength ($d > \frac{1}{2}L$), the wave power density is primarily determined by significant wave height and energy period, as the depth does not significantly affect wave dynamics. The wave power per unit wave crest width in deep water is given by the equation:

$$P = \frac{\rho g^2}{64\pi} H_s^2 T_e$$

where P is the wave power per unit width (W/m), g is the gravitational acceleration (9.81 m/s²), H_s is the significant wave height (m), and T_e is the energy period (s). In deep water, the wave

power is directly proportional to the square of the wave height and the period, with the depth having little impact on the calculation.

However, in shallow and intermediate water, wave power becomes more complex due to the interaction between waves and the seabed. As the water depth decreases, the wave behavior changes, and the group velocity becomes depth dependent. The wave power equation remains similar to that in deep water:

$$P = \frac{1}{16} g H_s^2 C_g$$

but now, the group velocity C_g is modified to account for the depth by the equation:

$$C_g = \frac{1}{2} C (1 + \frac{2kh}{sinh(2kh)})$$

where *C* is the phase velocity, *k* is the wave number, and *h* is the water depth. In shallow water ($d < \frac{1}{20} L$), the approximation $tanh(kh) \approx kh$ can be used along with additional equation reductions and relationships, thereby simplifying the group velocity to $C_g \approx \sqrt{gh}$. As a result, wave power in shallow water is calculated as:

$$P = \frac{1}{8} \rho g H_s^2 \sqrt{gh}$$

The classification of water depth plays a significant role in wave power calculations. In deep water, wave power is influenced primarily by wave height and period, with minimal impact from depth. In intermediate water, wave power depends on both wave height and the depth, as the waves begin to interact with the seabed. In shallow water, the wave power is highly dependent on depth due to the seabed's influence on wave behavior. The transition from deep to shallow

water is governed by the wavelength-to-depth ratio, with the power equations adjusting to reflect these changes.

5. Results

A comprehensive boundary element method (BEM) analysis was conducted using the Python-based program Capytaine to explore the hydrodynamic behavior of a vertically-oriented oscillating surge wave energy converter (VOSWEC) with varying plate geometries. The influence on the excitation torque ($M_{exc}(\omega)$), added mass ($A(\omega)$), and radiation damping ($B(\omega)$) by various geometric configurations was observed, aiming to understand the dynamics of the WEC geometries studies across a range of wave angular frequencies. The simulation campaign was divided into two cases based on plate length, L, the spanwise dimension from the yaw axis perpendicular to the wall (or coastal infrastructure) and perpendicular to the direction of wave propagation. The two cases studied include Case A, with a plate length L = 0.3 m, and Case B, with L = 0.4 m. Within each case, twelve unique plate scenarios were examined. These scenarios were defined by three distinct plate thicknesses: b = 0.02 m, b = 0.04 m, and 0.06 m, with each being tested at four submergence depths (draughts) of d = 0.3 m, 0.4m, 0.5 m, and 0.6 m. This approach allowed for a systematic investigation of the effects of the VOSWEC plate geometry on key hydrodynamic coefficients over a representative range of wave frequencies. In the end, a total of 24 scenarios were investigated, corresponding to Table 1 and discussed below and in the following section.

5.1 Excitation Torque

Excitation torque, $M_{exc}(\omega)$, is a fundamental metric in the performance assessment of wave energy converters. It represents the torque induced by incident wave pressure differentials acting on the submerged surface of the device. For this VOSWEC concept, this torque drives the rotational motion of the plate, this motion is then harnessed by a power take-off (PTO) system to

generate electricity. The magnitude of the excitation torque is directly influenced by wave amplitude and frequency, as well as the geometry and placement of the converter. Therefore, understanding excitation torque variation across a range of wave angular frequencies and different WEC geometric configurations is essential for both design optimization and the development of control strategies that maximize energy yield.

The simulations showed the frequency-dependent behavior of excitation torque for each plate geometry. The goal was to identify designs that exhibit a peak excitation response near the dominant wave frequencies. Geometries that showed higher excitation torque in this frequency band are considered more favorable, as they suggest a greater capacity for wave-induced rotational energy input. This information informs system tuning of the WEC to local sea states and helps maximize the overall energy conversion efficiency.

For Case A, there was a wide range of variations in excitation torque across the tested geometries (Figures 10-13). Plate 12a, which combines the largest width (b = 0.06 m) and deepest draught (d = 0.6 m) tested, produced the highest excitation torque, reaching M_{exc} = 145.42 Nm at a frequency of $\omega = 5.68$ rad/s. In contrast, the smallest excitation torque of M_{exc} = 28.30 Nm was observed at Plate 7a (b = 0.04 m and d = 0.5 m), occurring at a higher frequency of $\omega = 12.57$ rad/s. In general, excitation torque magnitude increased as the VOSWEC plate draught depth increased, and the wave angular frequency of the peak excitation torque decreased as draught depth increased. These results emphasize the importance of geometric tuning to ensure that peak excitation torque occurs within the target operational frequency band for a given deployment site. Ideally the peak of the excitation torque also aligns with, or near, the peak of the radiation damping for the WEC geometry.

For Case B, the configuration that produced the highest excitation torque was Plate 8b, with the thick plate width (b = 0.06 m) and the deepest submergence depth tested (d = 0.6 m), generating an excitation torque of M_{exc} = 335.40 Nm at a frequency of $\omega = 5.55$ rad/s, (Figure 15-17). Conversely, the lowest excitation torque observed in Case B occurred with Plate 7b, which, like Case A, is characterized by the intermediate plate width (b = 0.04 m) and a draught of d = 0.5 m. This configuration yielded a maximum excitation torque of only M_{exc} = 51.44 Nm, peaking at a frequency of $\omega = 12.57$ rad/s.

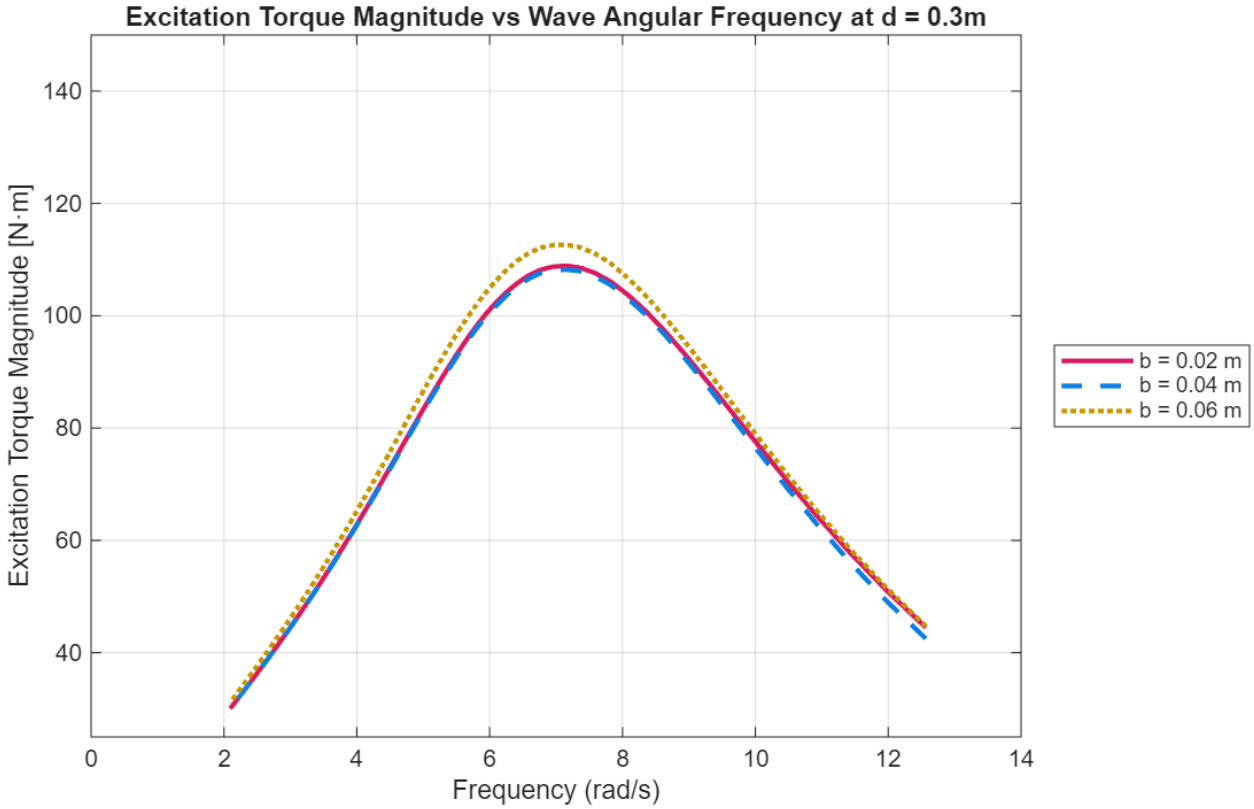

Figure 11. Case A: Excitation Torque comparison of three WEC plate thicknesses (b = 0.02 m (-), 0.04 m (--), and 0.06 m (:)) at draught condition d = 0.3 m and plate length L = 0.3 m.

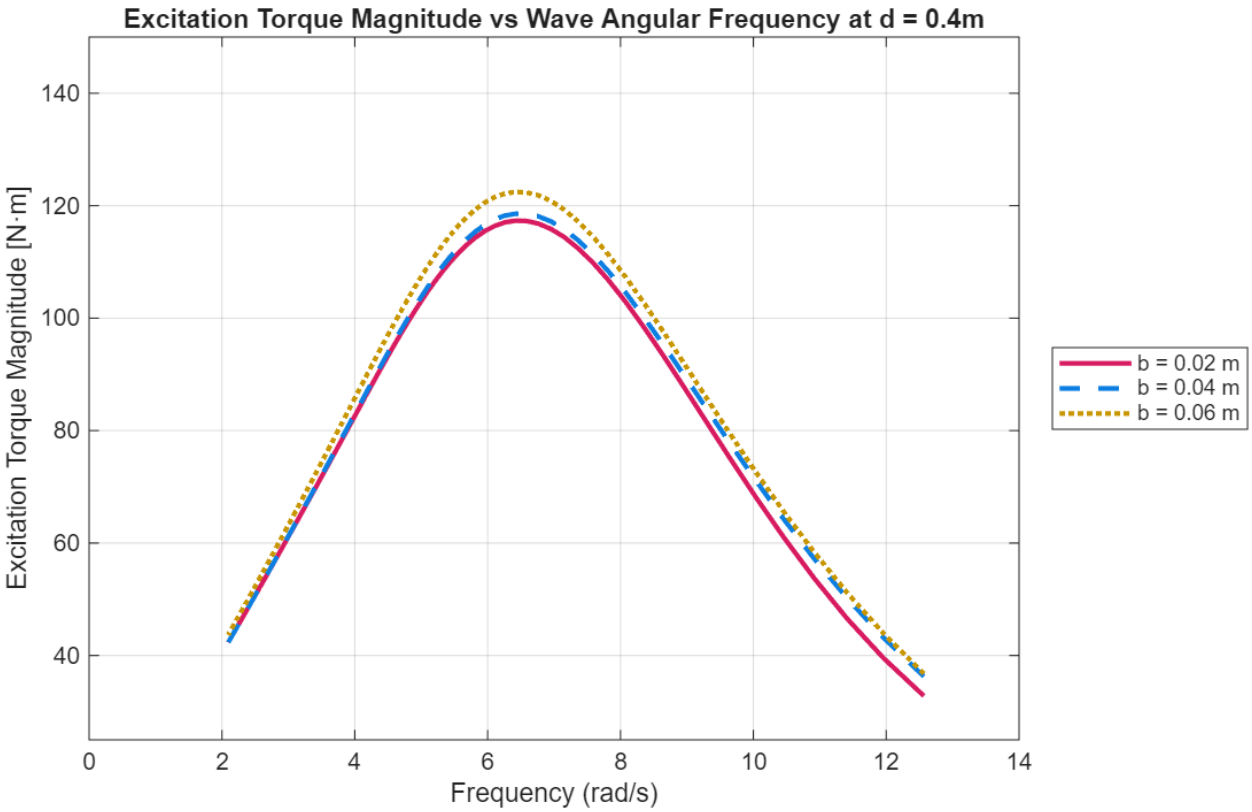

Figure 12. Case A: Excitation Torque comparison of three WEC plate thicknesses (b = 0.02 m (-), 0.04 m (--), and 0.06 m (:)) at draught condition d = 0.4 m and plate length L = 0.3 m.

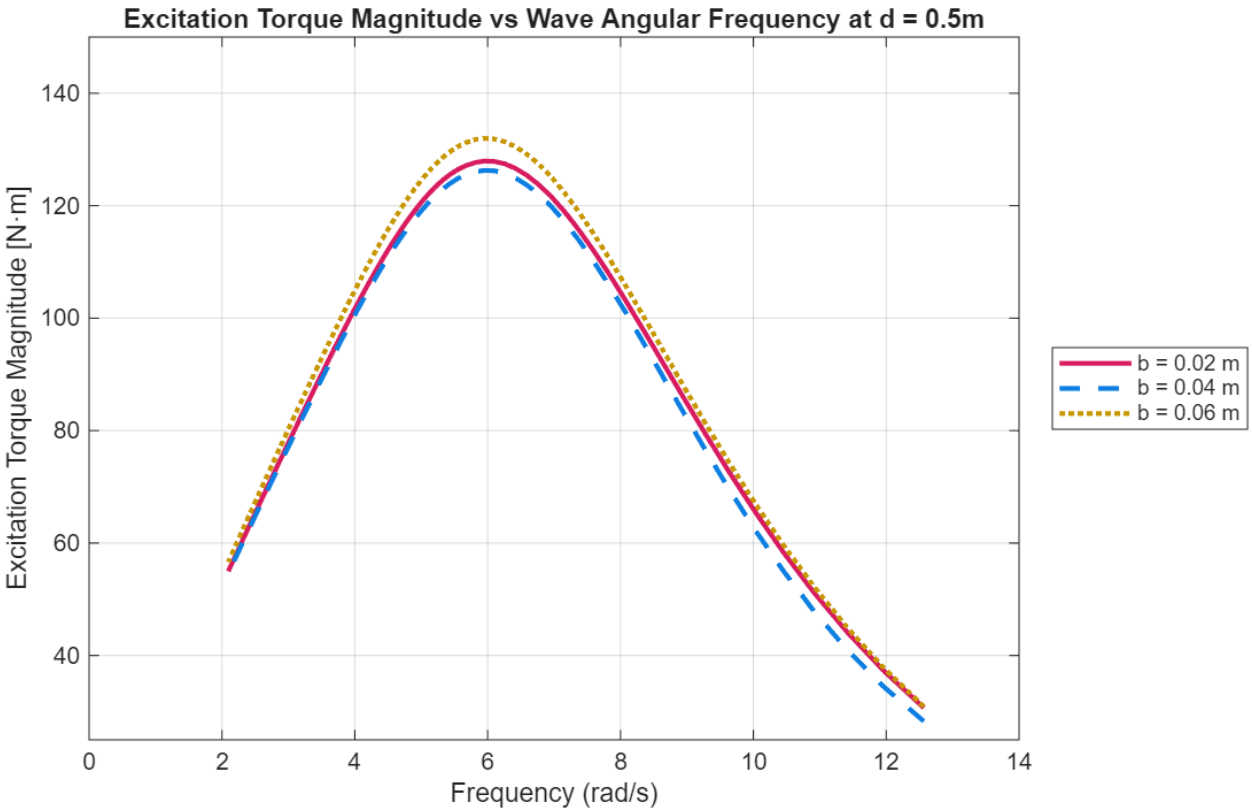

Figure 13. Case A: Excitation Torque comparison of three WEC plate thicknesses (b = 0.02 m (-), 0.04 m (--), and 0.06 m (:)) at draught condition d = 0.5 m and plate length L = 0.3 m.

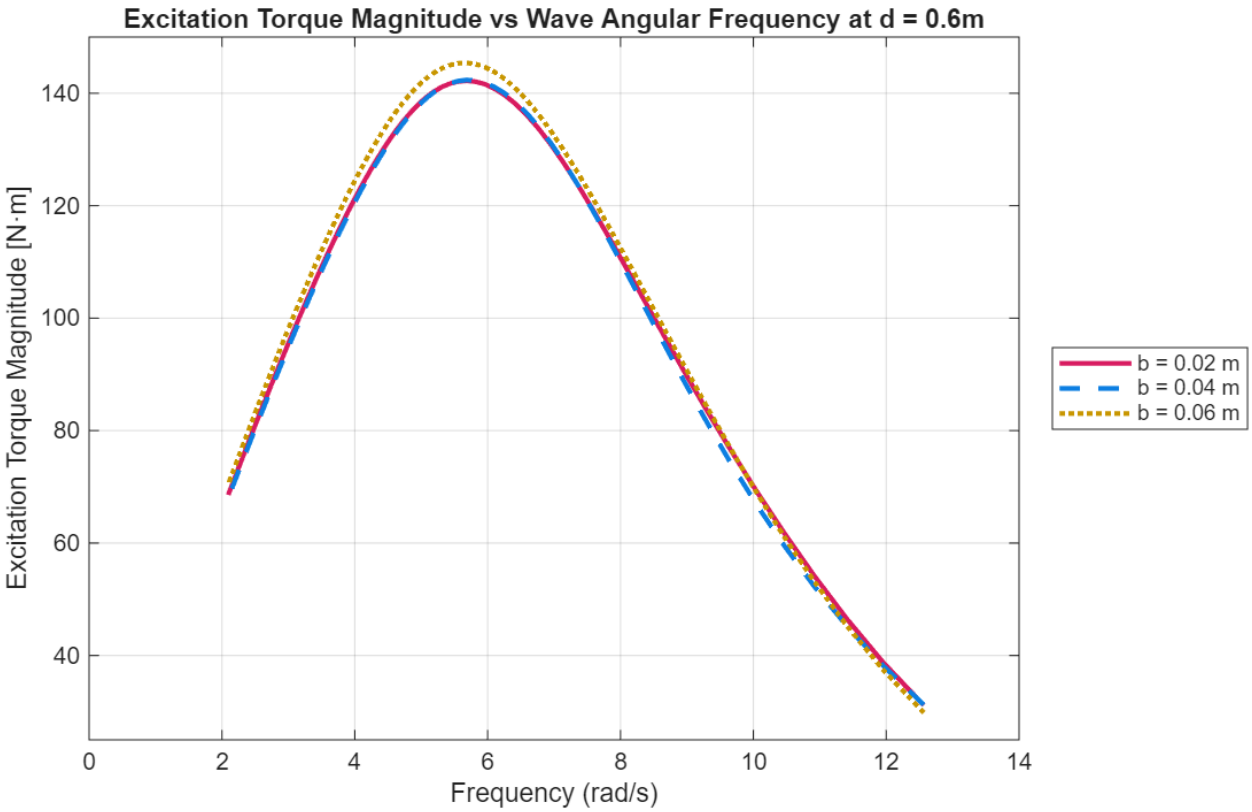

Figure 14. Case A: Excitation Torque comparison of three WEC plate thicknesses (b = 0.02 m (-), 0.04 m (--), and 0.06 m (:)) at draught condition d = 0.6 m and plate length L = 0.3 m.

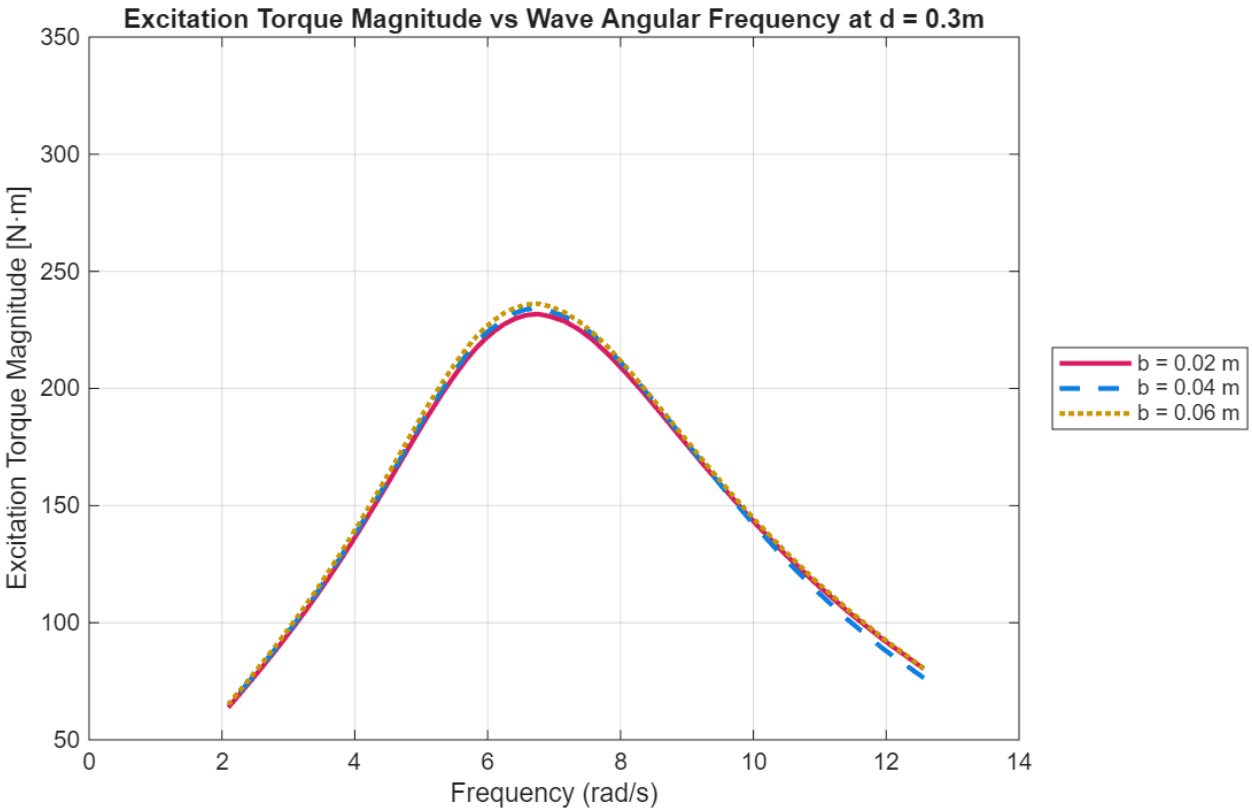

Figure 15. Case B: Excitation Torque comparison of three WEC plate thicknesses (b = 0.02 m (-), 0.04 m (--), and 0.06 m (:)) at draught condition d = 0.3 m and plate length L = 0.4 m.

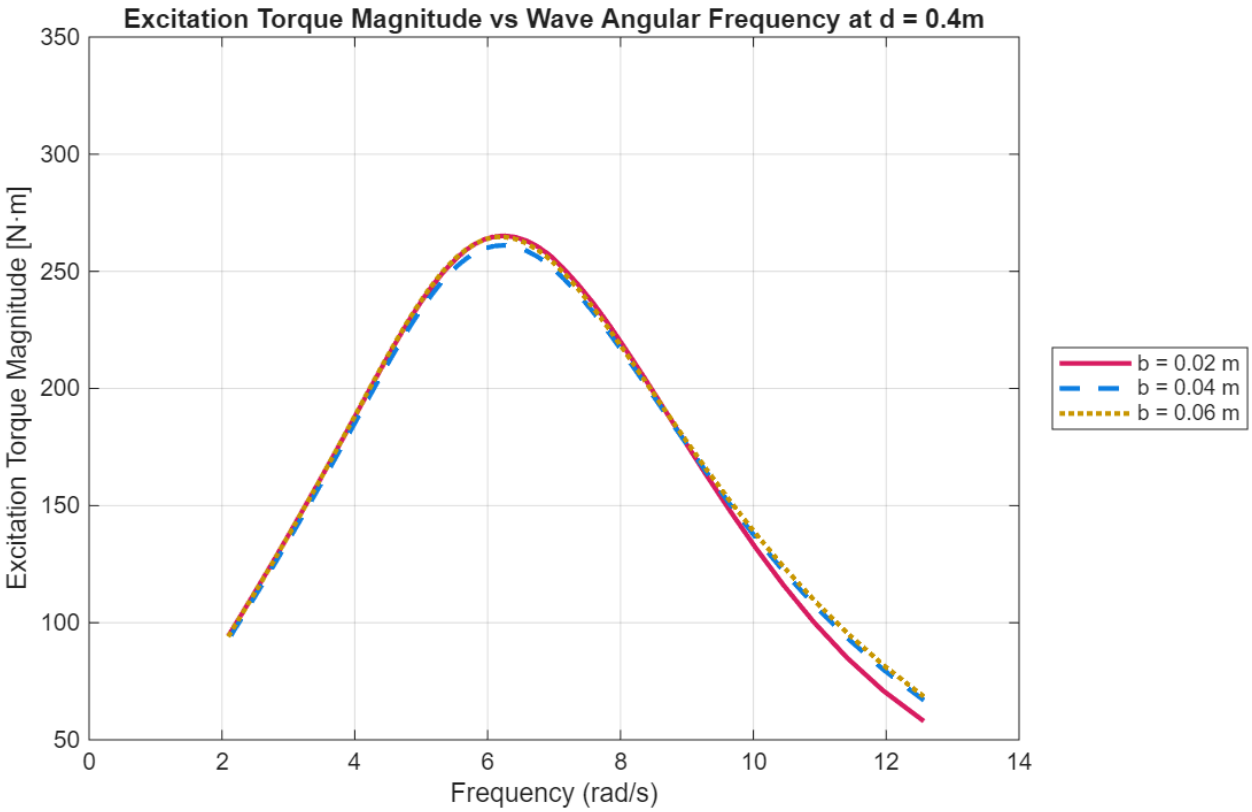

Figure 16. Case B: Excitation Torque comparison of three WEC plate thicknesses (b = 0.02 m (-), 0.04 m (--), and 0.06 m (:)) at draught condition d = 0.4 m and plate length L = 0.4 m.

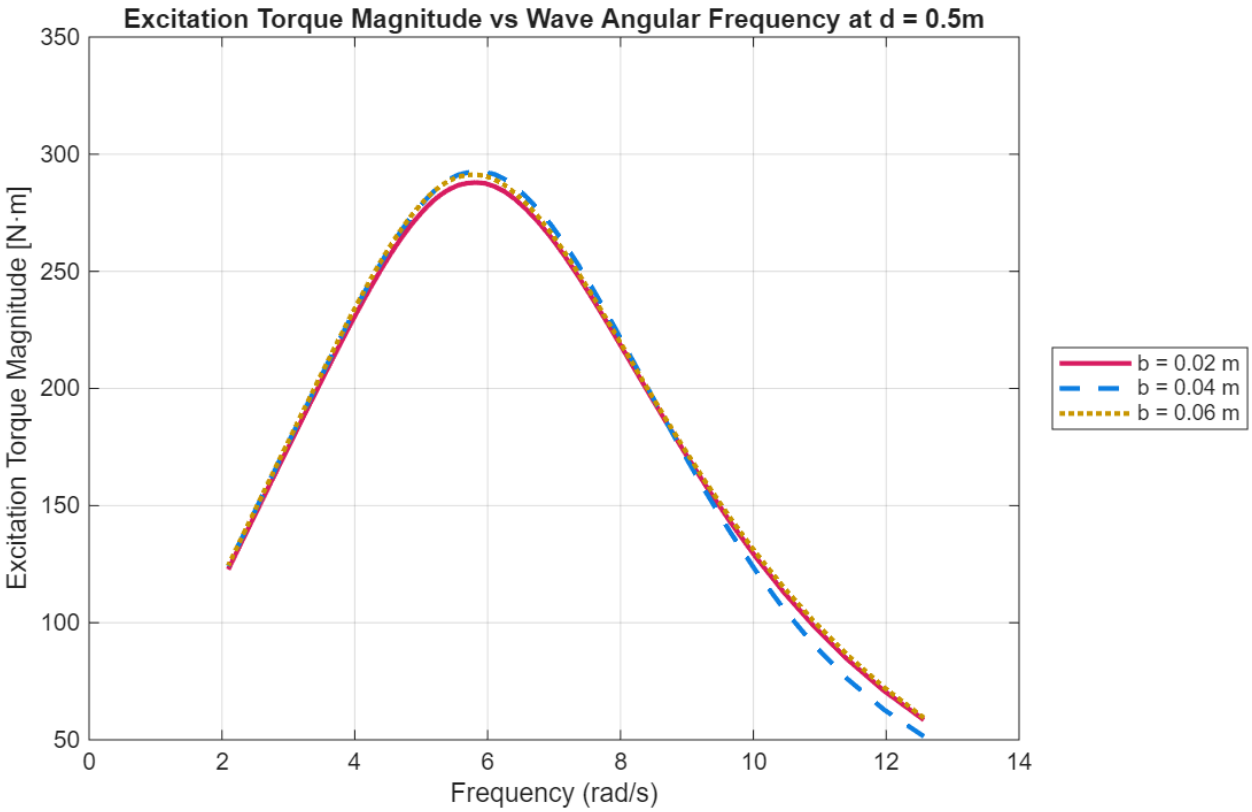

Figure 17. Case B: Excitation Torque comparison of three WEC plate thicknesses (b = 0.02 m (-), 0.04 m (--), and 0.06 m (:)) at draught condition d = 0.5 m and plate length L = 0.4 m.

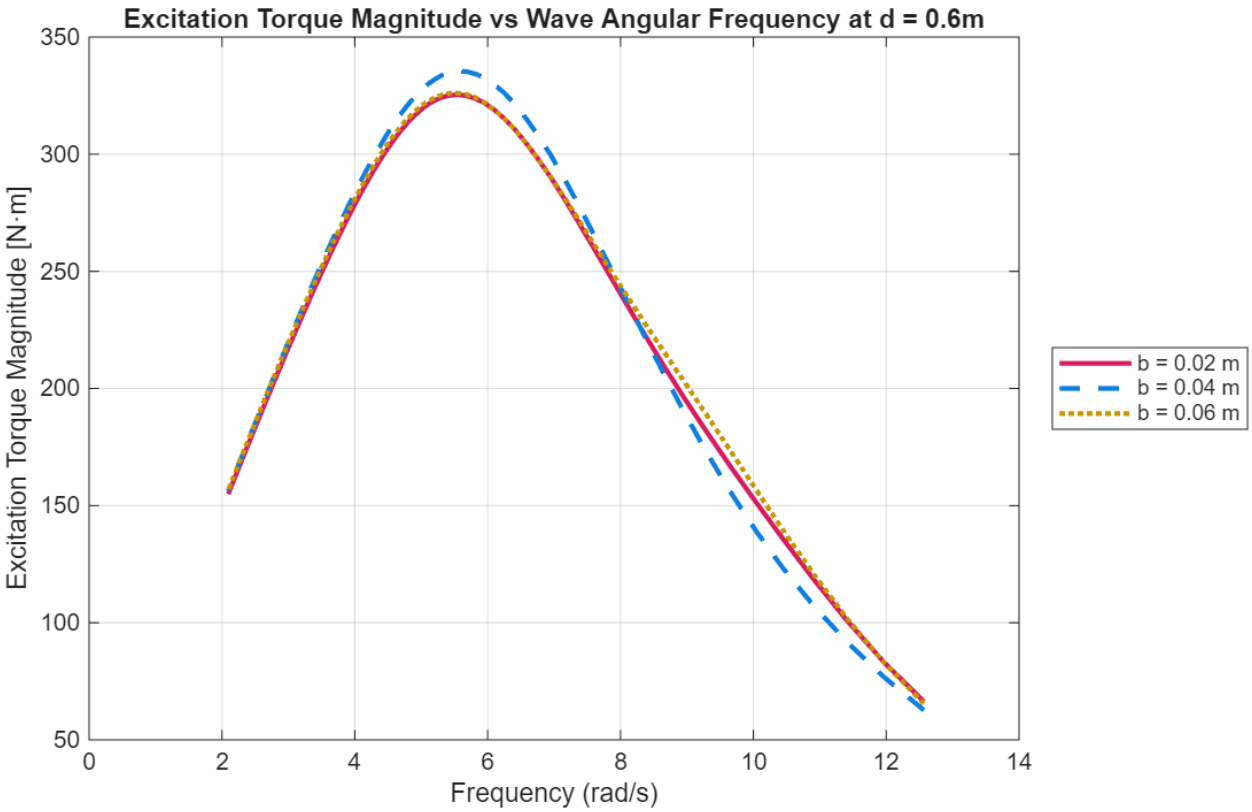

Figure 18. Case B: Excitation Torque comparison of three WEC plate thicknesses (b = 0.02 m (-), 0.04 m (--), and 0.06 m (:)) at draught condition d = 0.6 m and plate length L = 0.4 m.

5.2 Added Mass

Added mass is an additional critical hydrodynamic parameter that significantly affects the dynamic response of a wave energy converter. When a structure accelerates through water, it must move not only its own mass but also a portion of the surrounding fluid. This effectively increases the inertia of the system, a phenomenon known as added mass. In the context of the VOSWEC, added mass influences the system's natural frequency, damping characteristics, and phase response to incoming wave excitation. In Case A, the plate configuration with the highest added mass was Plate 8a, tested at the intermediate plate width (b = 0.04 m) and deep submergence (d = 0.6 m), produced an added mass of $A(\omega) = 1.70$ kg·m² at a frequency of $\omega =$ 4.9 rad/s (Figure 22). The minimum added mass was found to be $A(\omega) = 0.42$ kg·m² at Plate 9a, with b = 0.06 m and at the shallow draught (d = 0.3 m) at $\omega = 12.57$ rad/s (Figure 19). In Case B, the highest added mass exhibited was at Plate 8b, reaching $A(\omega) = 5.39$ kg·m² at $\omega = 4.8$ rad/s (Figure 26). Conversely, the lowest added mass was measured at Plate 9b, with the thick plate (b = 0.06 m) with shallow submergence (d = 0.3 m) (Figure 23). This configuration yielded an added mass of only $A(\omega) = 1.05$ kg·m² at $\omega = 12.57$ rad/s. In general, added mass magnitude increased as the VOSWEC plate draught depth increased, and the wave angular frequency of the peak added mass decreased as draught depth increased for both cases.

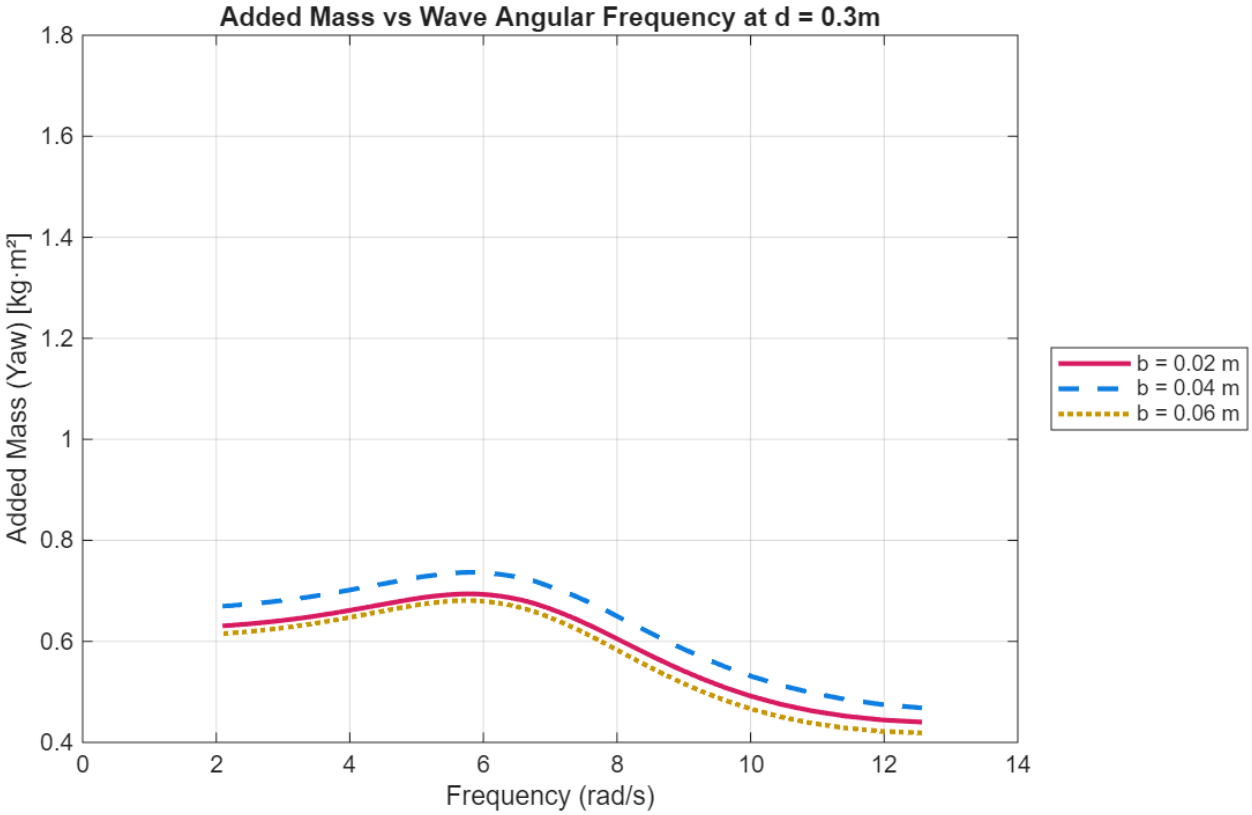

Figure 19. Case A: Added Mass comparison of three WEC plate thicknesses (b = 0.02 m (-), 0.04 m (--), and 0.06 m (:)) at draught condition d = 0.3 m and plate length L = 0.3 m.

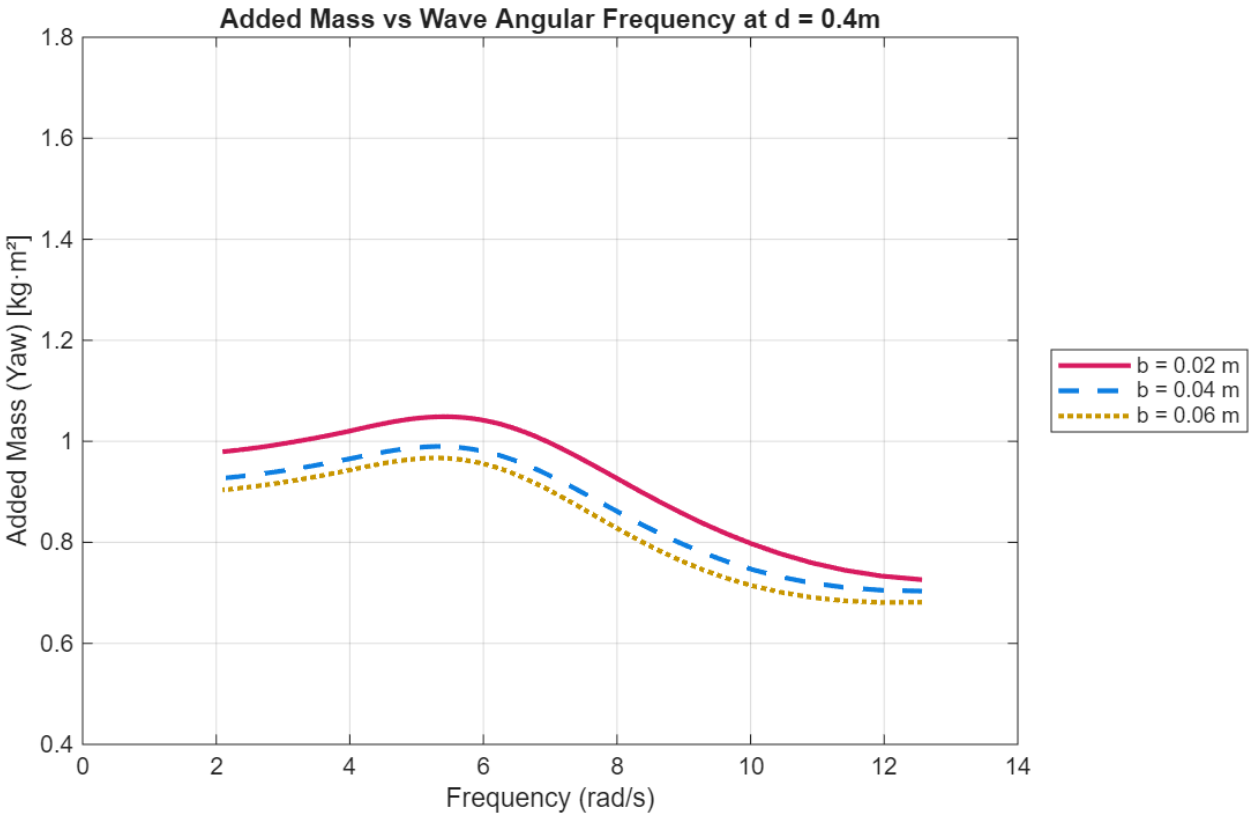

Figure 20. Case A: Added Mass comparison of three WEC plate thicknesses (b = 0.02 m (-), 0.04 m (--), and 0.06 m (:)) at draught condition d = 0.4 m and plate length L = 0.3 m.

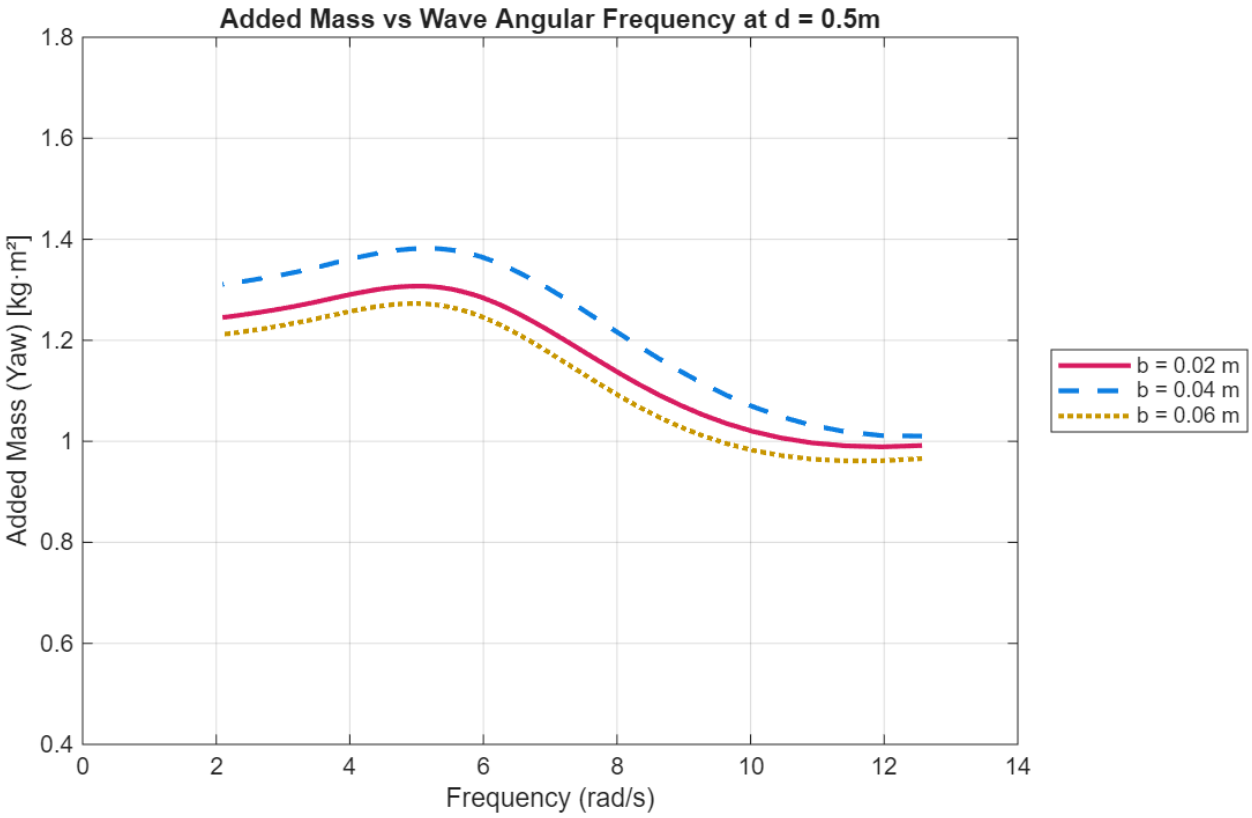

Figure 21. Case A: Added Mass comparison of three WEC plate thicknesses (b = 0.02 m (-), 0.04 m (--), and 0.06 m (:)) at draught condition d = 0.5 m and plate length L = 0.3 m.

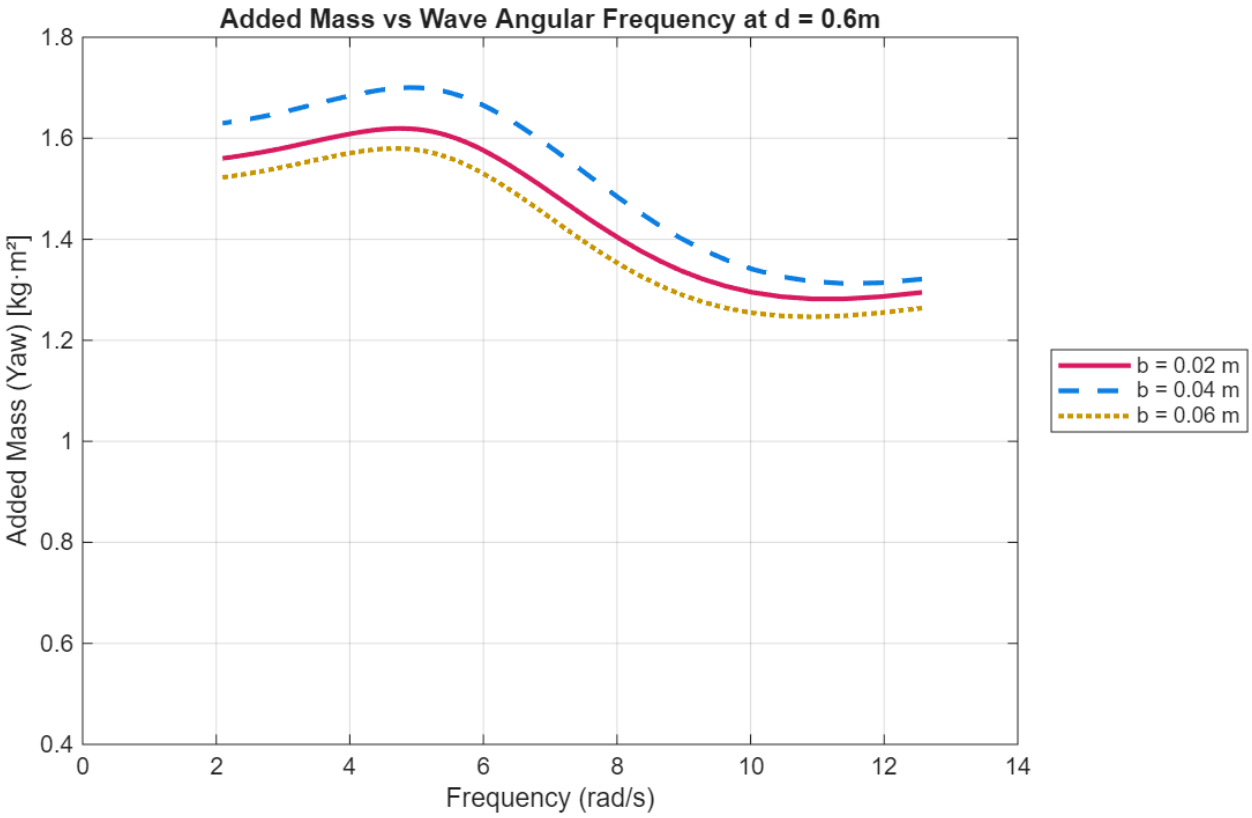

Figure 22. Case A: Added Mass comparison of three WEC plate thicknesses (b = 0.02 m (-), 0.04 m (--), and 0.06 m (:)) at draught condition d = 0.6 m and plate length L = 0.3 m.

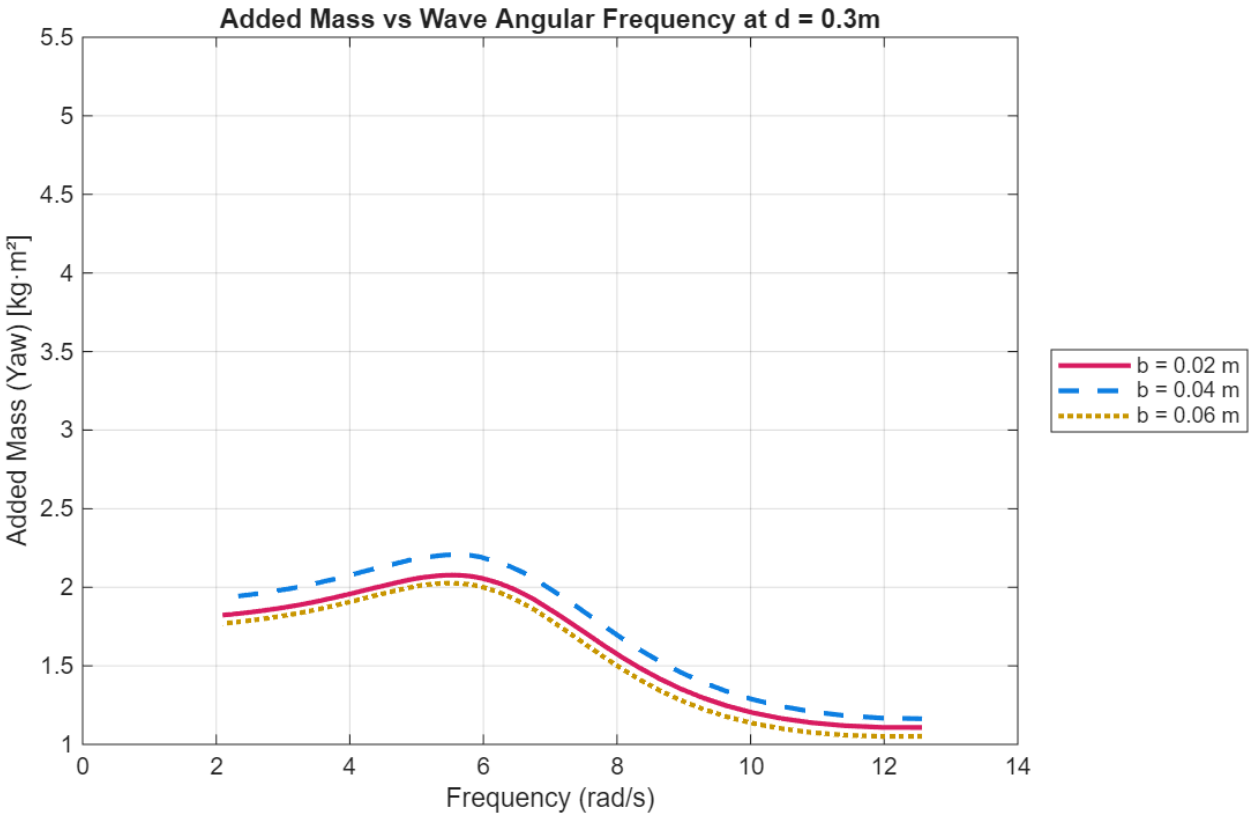

Figure 23. Case B: Added Mass comparison of three WEC plate thicknesses (b = 0.02 m (-), 0.04 m (--), and 0.06 m (:)) at draught condition d = 0.3 m and plate length L = 0.4 m.

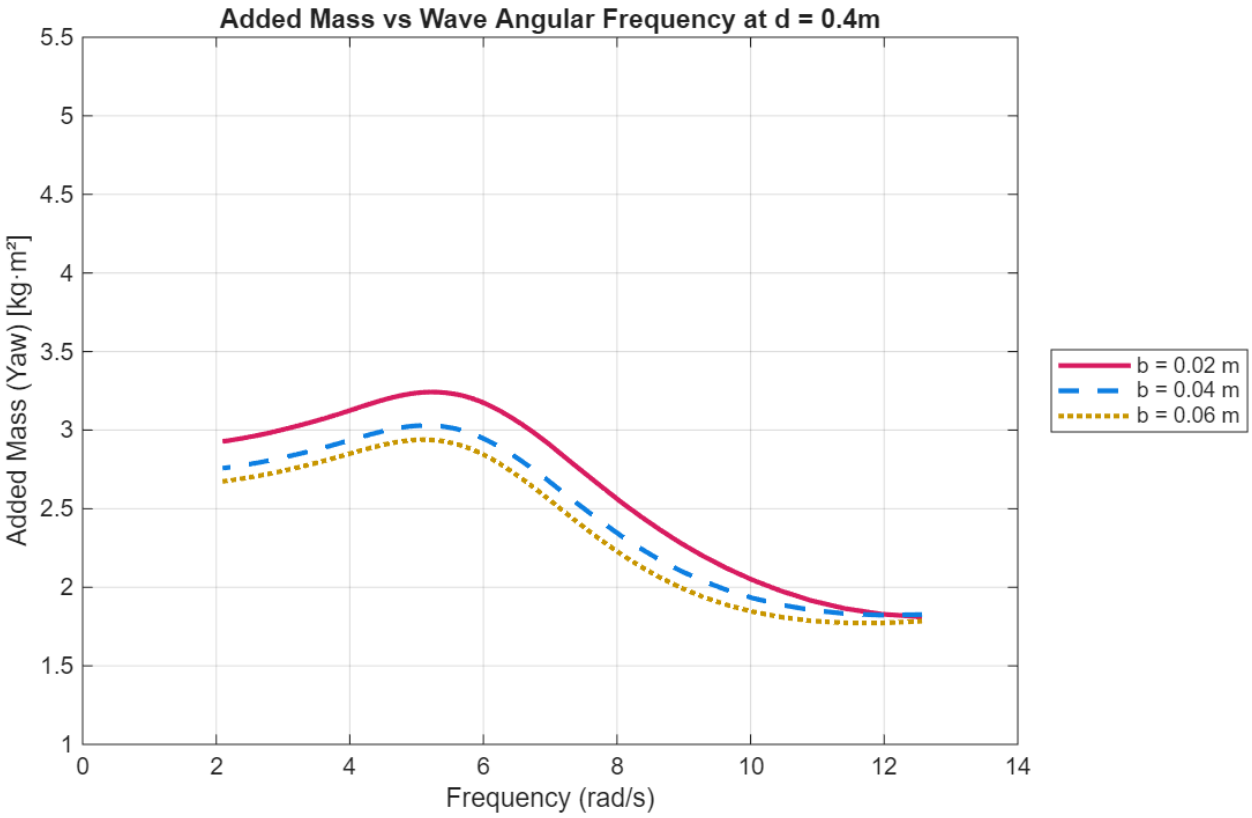

Figure 24. Case B: Added Mass comparison of three WEC plate thicknesses (b = 0.02 m (-), 0.04 m (--), and 0.06 m (:)) at draught condition d = 0.4 m and plate length L = 0.4 m.

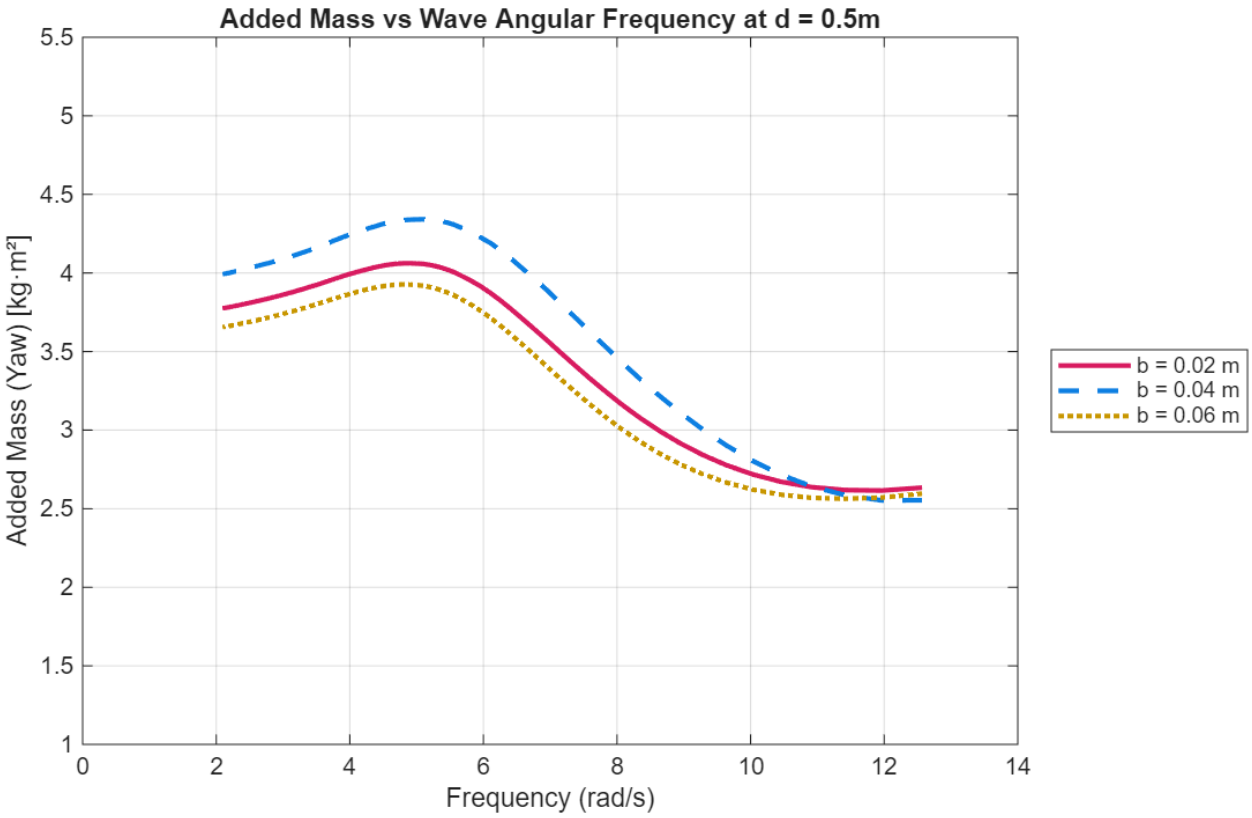

Figure 25. Case B: Added Mass comparison of three WEC plate thicknesses (b = 0.02 m (-), 0.04 m (--), and 0.06 m (:)) at draught condition d = 0.5 m and plate length L = 0.4 m.

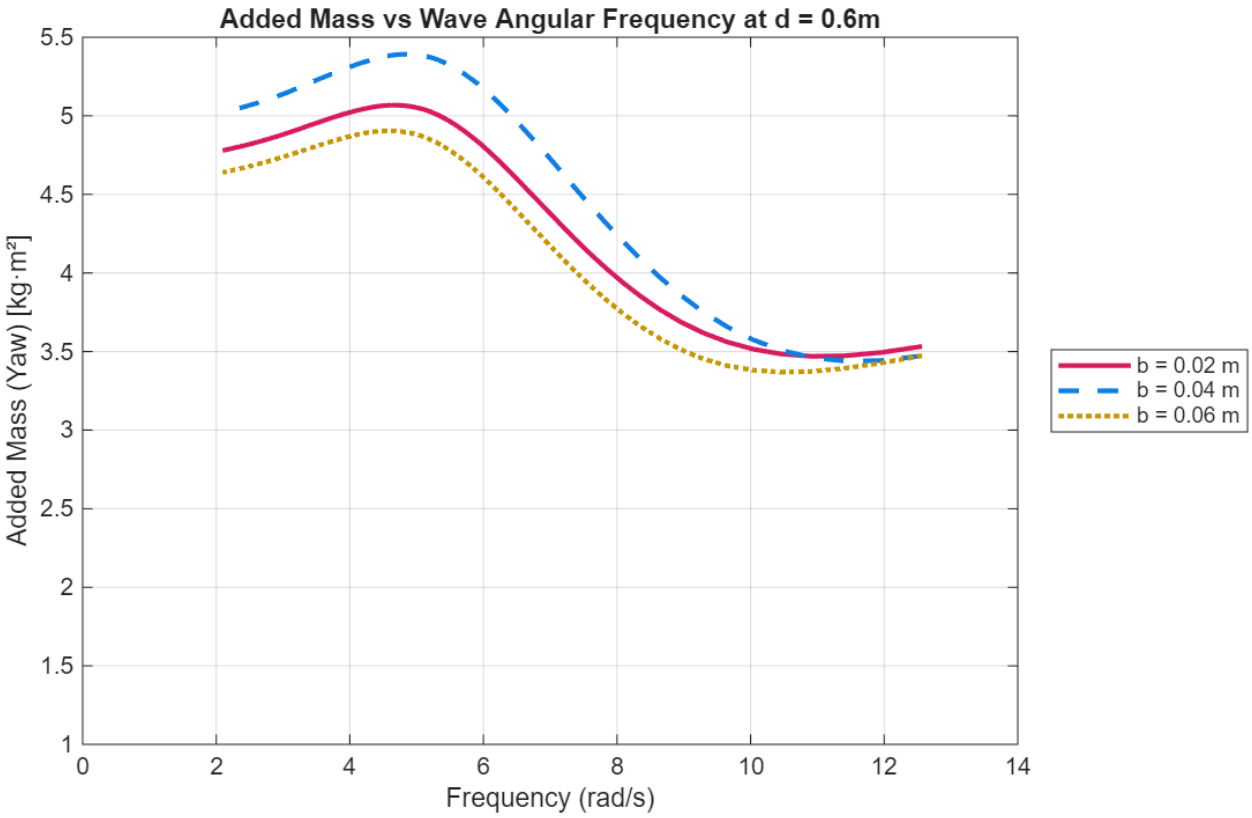

Figure 26. Case B: Added Mass comparison of three WEC plate thicknesses (b = 0.02 m (-), 0.04 m (--), and 0.06 m (:)) at draught condition d = 0.6 m and plate length L = 0.4 m.

5.3 Radiation Damping

Radiation damping describes the energy dissipated by the WEC as it radiates waves away from itself in response to its motion. When a flap-type WEC moves under wave excitation, it displaces water, generating secondary waves that propagate outward. The energy carried by these waves represents a loss from the system's mechanical motion, effectively acting as a damping force. While some degree of radiation damping is necessary to enable wave-structure interaction, excessive damping can reduce the amplitude of motion and, consequently, limit energy extraction.

The yaw radiation damping, $B_{66}(\omega)$, was evaluated as a function of wave frequency for each of the 24 plate configurations. Ideally, peak radiation damping should coincide with peak excitation torque to maximize power capture. Too little radiation damping results in poor wave coupling and inefficient energy transfer, while excessive radiation damping can overly suppress motion. The goal for these experiments was to identify geometries in which radiation damping was sufficiently strong to facilitate dynamic interaction, but not so dominant that it suppressed relative motion to the point of energy loss.

For Case A, the highest radiation damping occurred with Plate 7a, yielding a peak damping of $B_{66}(\omega) = 2.45$ kg·m²/s at a frequency of $\omega = 9.28$ rad/s (Figure 29). In contrast, the lowest radiation damping of $B_{66}(\omega) = 0.003$ kg·m²/s in Case A was observed in Plate 1a (b = 0.02 m and d = 0.3 m) at $\omega = 2.09$ rad/s. For Case B, Plate 8b exhibited the maximum radiation damping across all test conditions, reaching $B_{66}(\omega) = 12.23$ kg·m²/s at a frequency of $\omega =$ 8.64 rad/s (Figure 34). In contrast, Plate 1b (b = 0.02 m, d = 0.3 m) produced the smallest radiation damping of $B_{66}(\omega) = 0.01537$ kg·m²/s at $\omega = 2.09$ rad/s (Figure 31). In general, radiation damping magnitude increased as the VOSWEC plate draught depth increased up until a depth of about d = 0.5 m, at which point it remained similar to the d = 0.6 m case. The peak stayed at a relatively consistent wave angular frequency across all depths ($\omega = 8 - 9$ rads/s) for both cases.

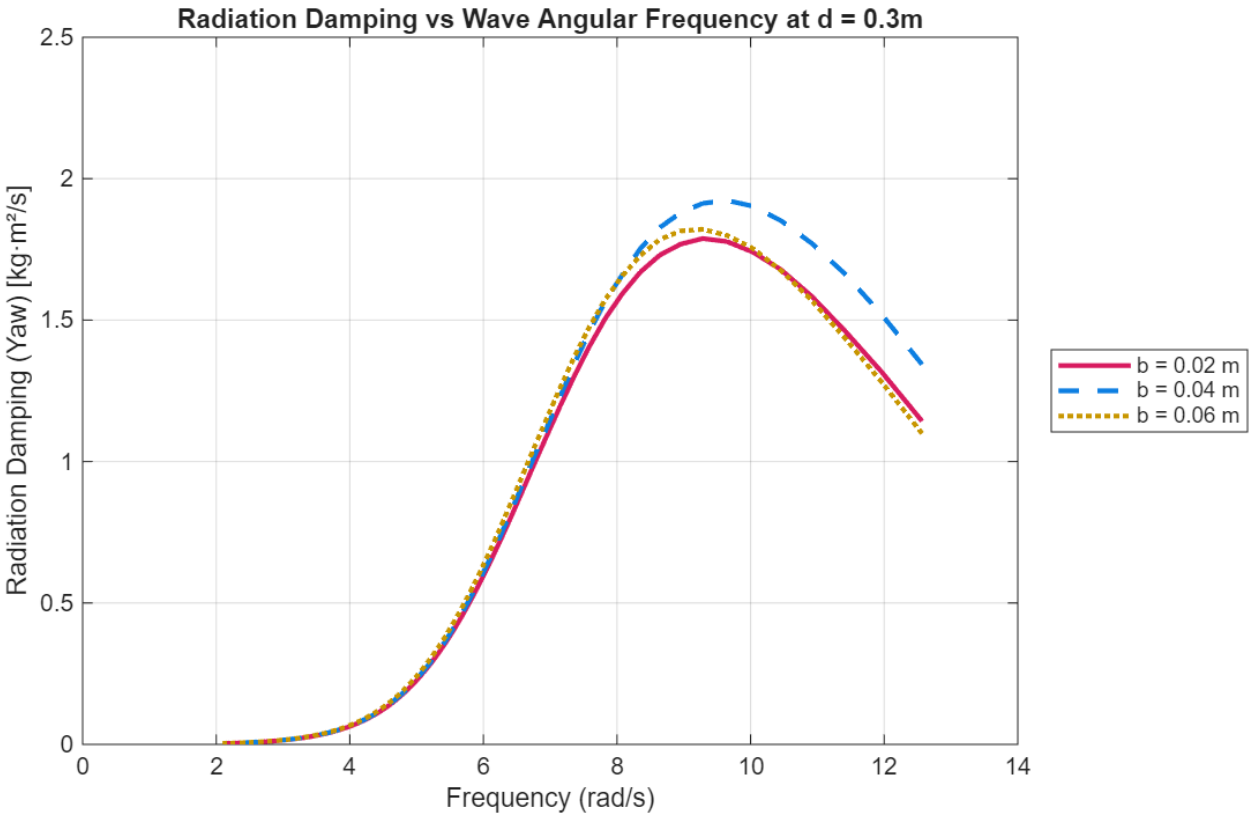

Figure 27. Case A: Radiation Damping comparison of three WEC plate thicknesses (b = 0.02 m (-), 0.04 m (--), and 0.06 m (:)) at draught condition d = 0.3 m and plate length L = 0.3 m.

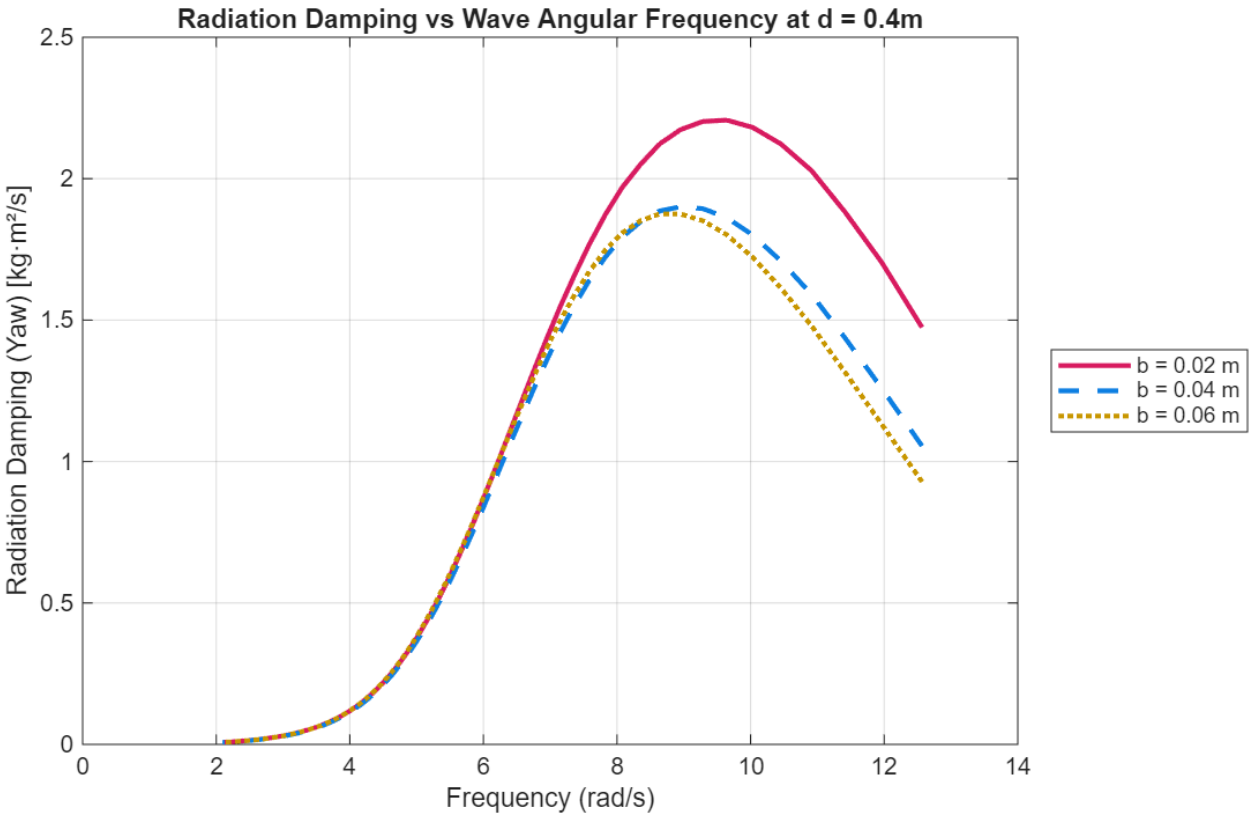

Figure 28. Case A: Radiation Damping comparison of three WEC plate thicknesses (b = 0.02 m (-), 0.04 m (--), and 0.06 m (:)) at draught condition d = 0.4 m and plate length L = 0.3 m.

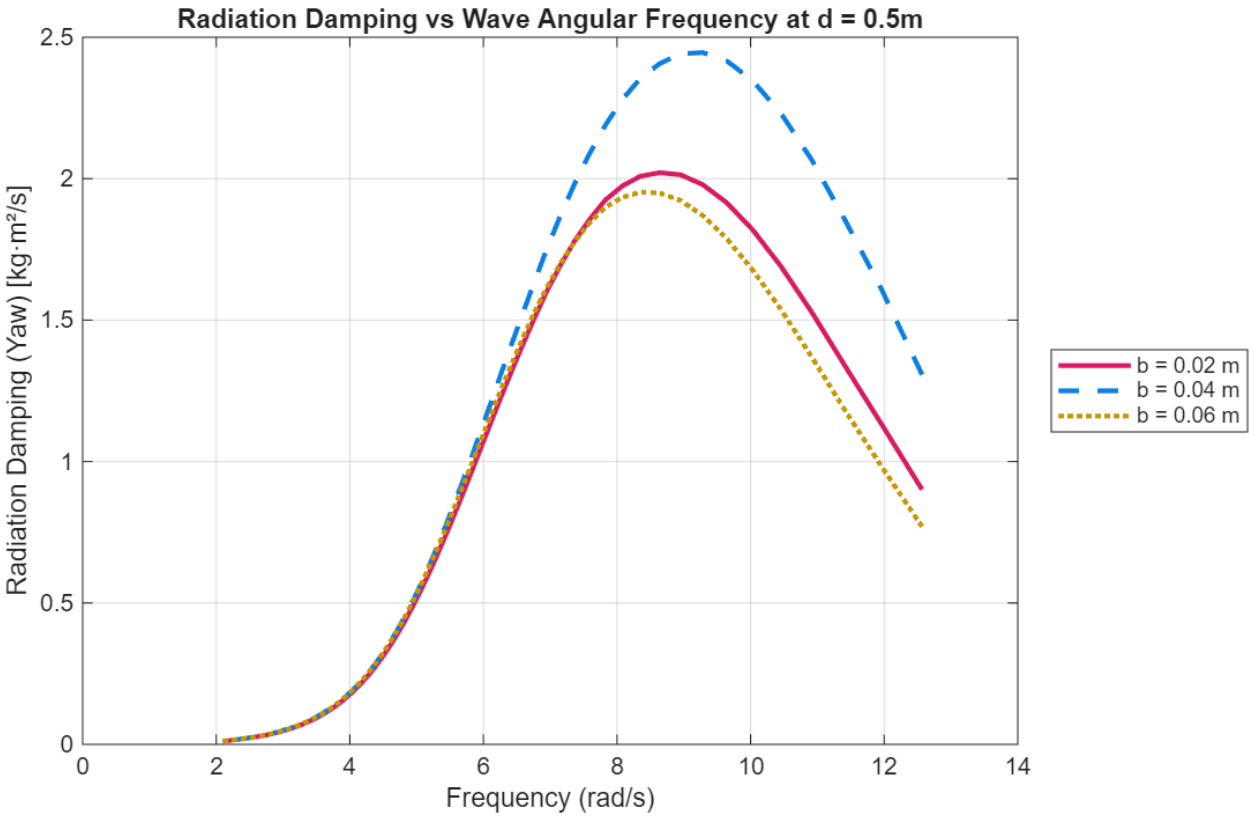

Figure 29. Case A: Radiation Damping comparison of three WEC plate thicknesses (b = 0.02 m (-), 0.04 m (--), and 0.06 m (:)) at draught condition d = 0.5 m and plate length L = 0.3 m.

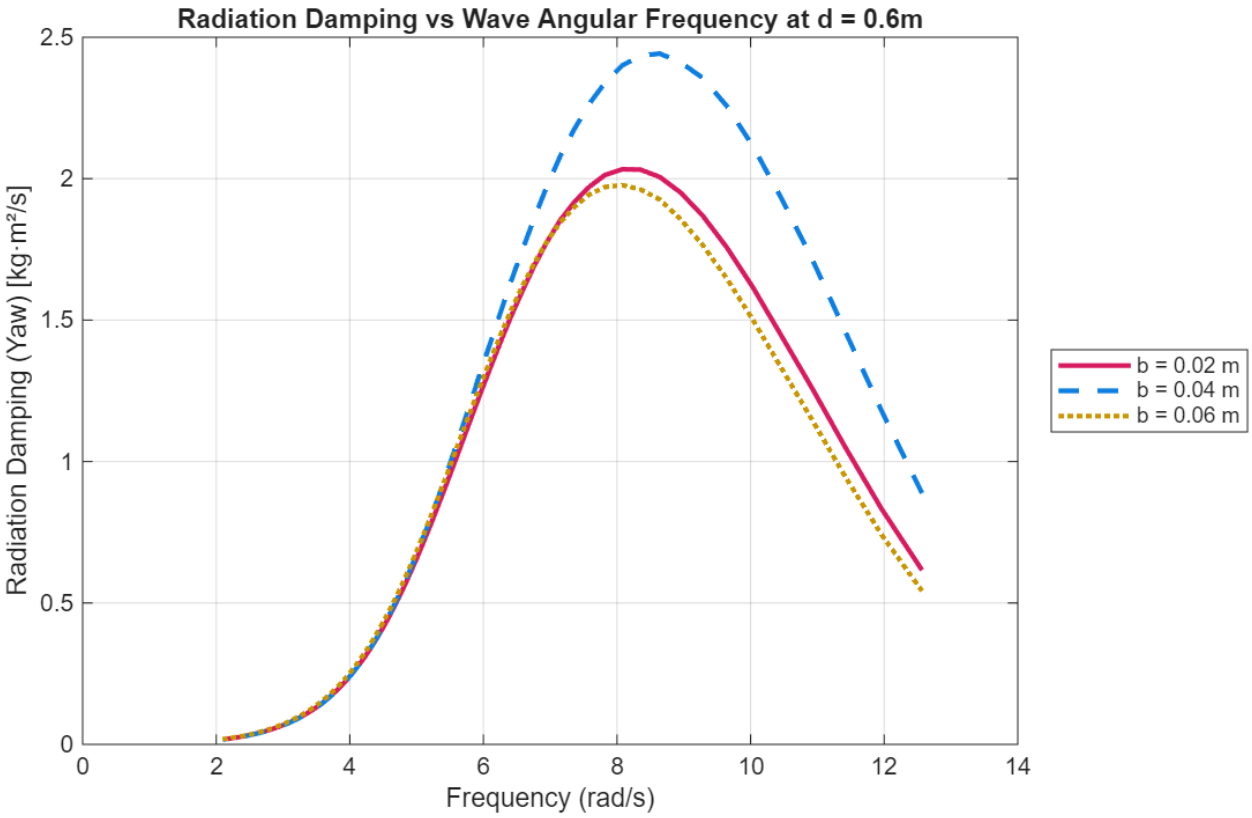

Figure 30. Case A: Radiation Damping comparison of three WEC plate thicknesses (b = 0.02 m (-), 0.04 m (--), and 0.06 m (:)) at draught condition d = 0.6 m and plate length L = 0.3 m.

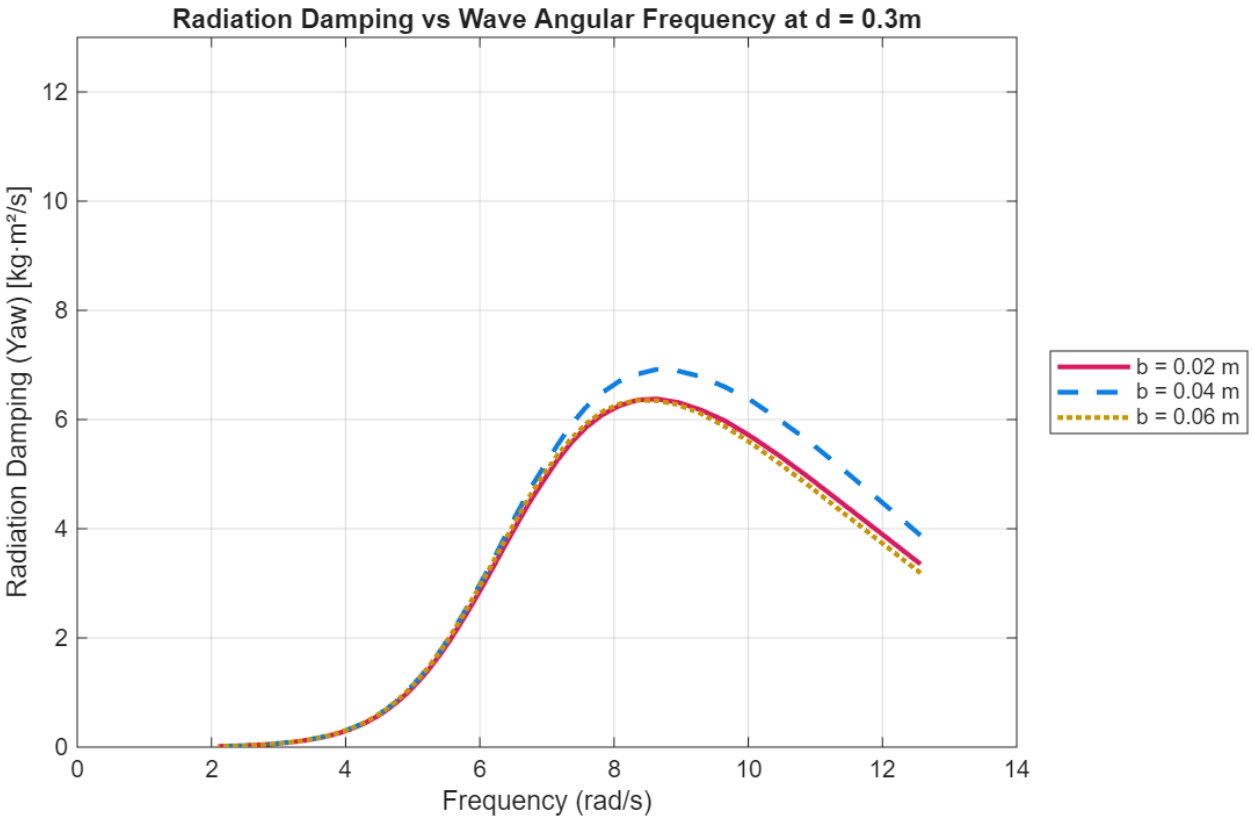

Figure 31. Case B: Radiation Damping comparison of three WEC plate thicknesses (b = 0.02 m (-), 0.04 m (--), and 0.06 m (:)) at draught condition d = 0.3 m and plate length L = 0.4 m.

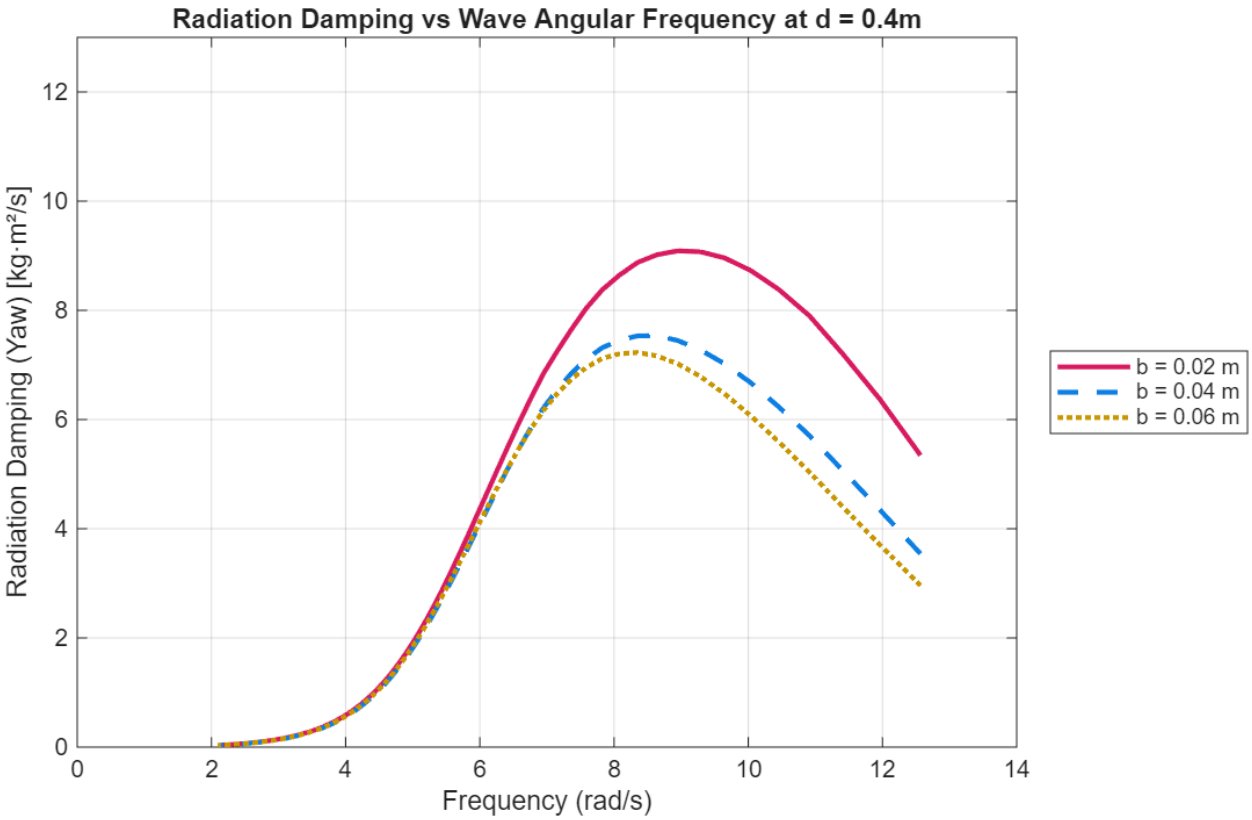

Figure 32. Case B: Radiation Damping comparison of three WEC plate thicknesses (b = 0.02 m (-), 0.04 m (--), and 0.06 m (:)) at draught condition d = 0.4 m and plate length L = 0.4 m.

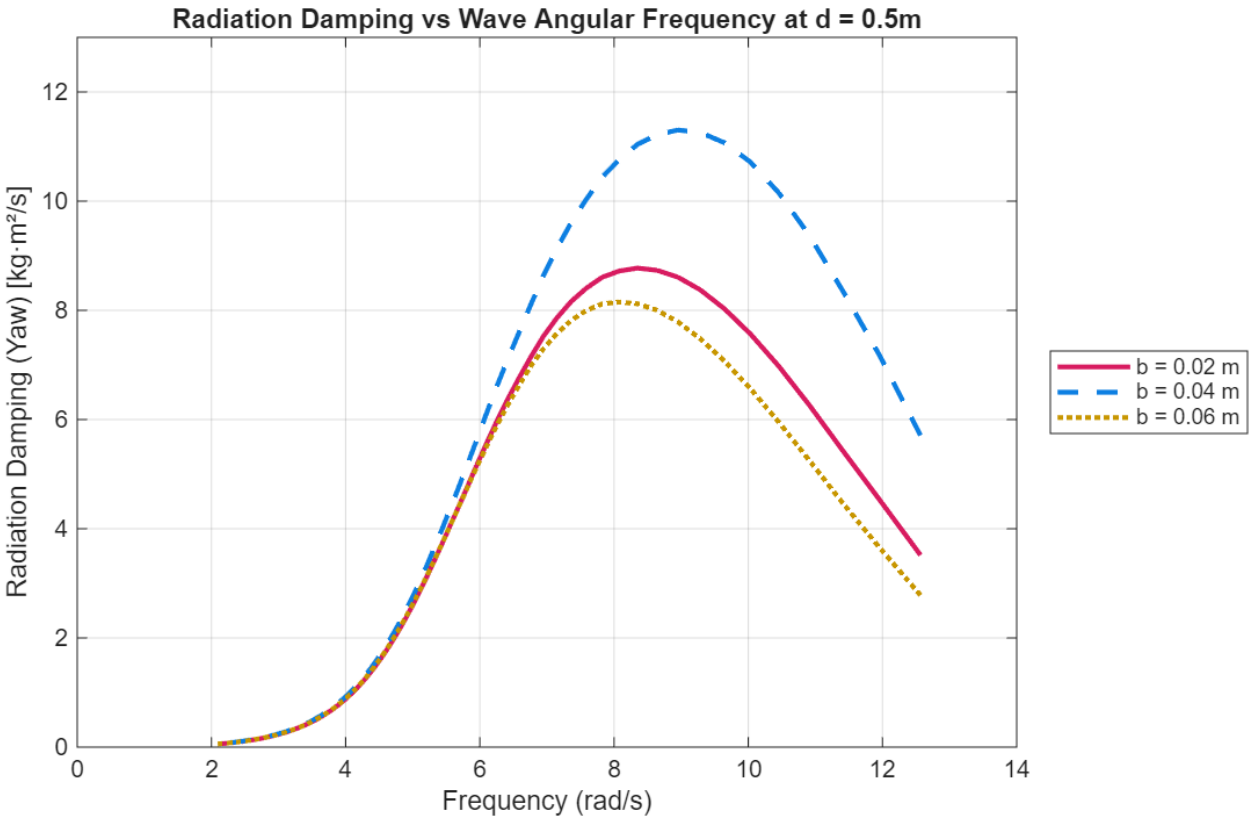

Figure 33. Case B: Radiation Damping comparison of three WEC plate thicknesses (b = 0.02 m (-), 0.04 m (--), and 0.06 m (:)) at draught condition d = 0.5 m and plate length L = 0.4 m.

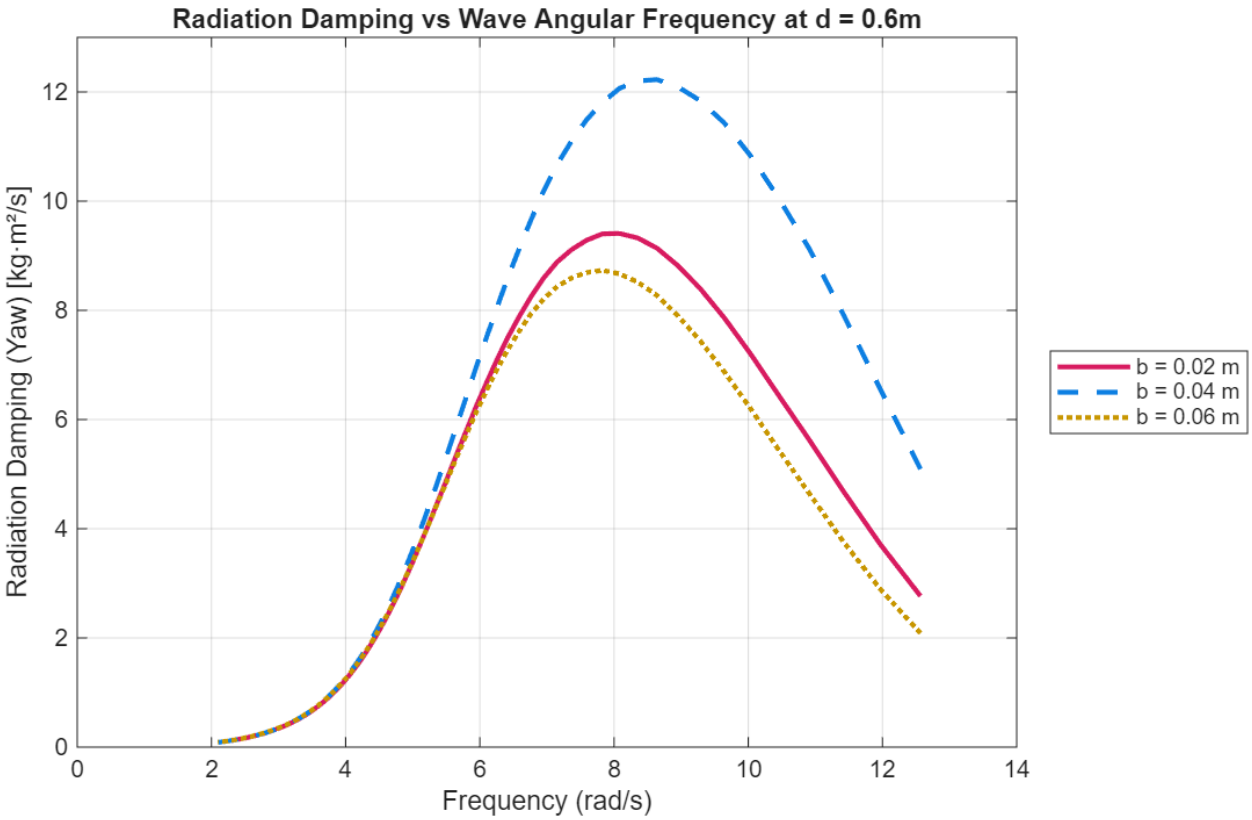

Figure 34. Case B: Radiation Damping comparison of three WEC plate thicknesses (b = 0.02 m (-), 0.04 m (--), and 0.06 m (:)) at draught condition d = 0.6 m and plate length L = 0.4 m.

5.4 MTU Tank Test Preliminary Results

A series of scaled laboratory experiments was conducted at the Michigan Technological University (MTU) Wave Facility, as detailed in the *Methods* section. Initial diffraction tests, in which incident waves were forced against a locked VOSWEC device, revealed the complex hydrodynamic interactions between the wave field and the converter structure. Test conditions included regular, irregular, and pink multisine wave inputs (Tables 3 and 4), although the present discussion focuses exclusively on selected results obtained under regular wave conditions. These

experiments provide an early characterization of wave–structure interactions under controlled laboratory conditions, forming the foundation for subsequent performance and validation studies.

Table 3. Experimental test matrix for regular waves.

		Wave Height, H (m)				
Wave Period, T (sec)	**Wave Frequency, f (Hz)**	**0.012**	**0.022**	**0.03**	**0.06**	**0.07**
1.06	0.94	E1	E2	E3	E4	E5
1.43	0.70	D1	D2	D3	D4	D5
2.02	0.50	C1	C2	C3	C4	C5

Table 4. Experimental test matrix for pink multisine waves.

	Pink Noise Wave (0.3-1.2Hz) – 3min	
Naming	**RMS Value**	**Significant Wave Height (m)**
P1	0.0125	0.05
P2	0.008	0.032
P3	0.003	0.012

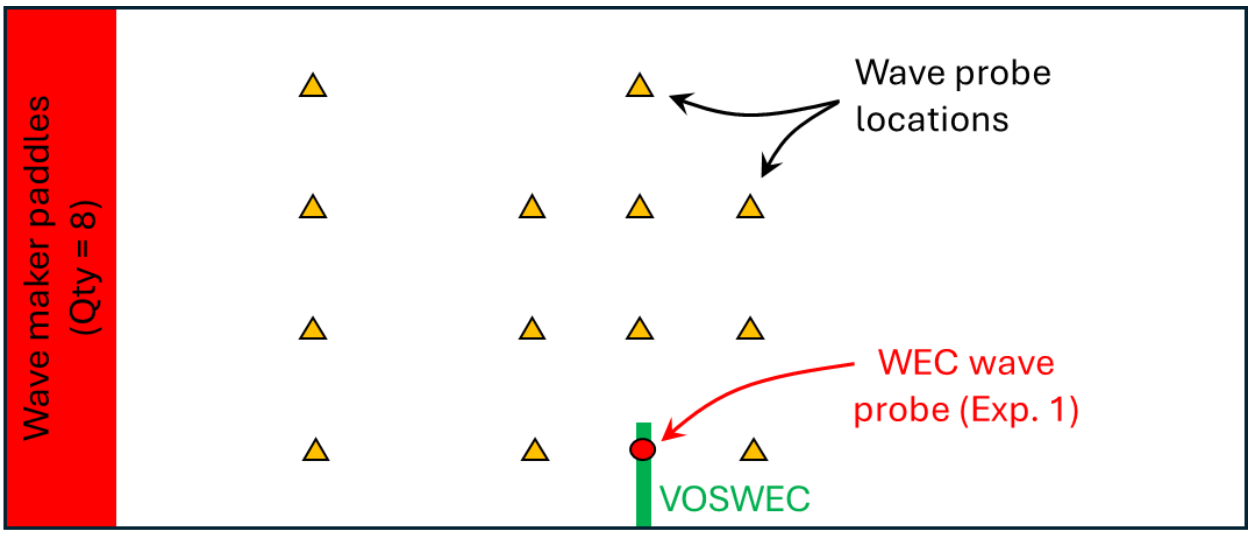

Figure 35. Schematic of the wave tank layout showing locations of the resistance wave probes and the location of the VOSWEC.

Each experiment was conducted for a minimum duration of one minute. The initial 20 seconds of each run were excluded from analysis to account for the tare phase of data acquisition and the ramp-up period during which the wave paddles progressively increased sinusoidal motion until the target wave condition was achieved. This resulted in approximately 40 seconds of high-quality data for the preliminary analysis presented here.

Figure 36 illustrates a representative torque sensor signal, which exhibits a complex sinusoidal-like oscillation in yaw-axis torque as each wave passes the VOSWEC plate. The example shown corresponds to Experiment C5, with a wave frequency of $f = 0.5$ Hz and a significant wave height of $H_s = 0.07$ m. When magnifying a 5-second interval of this record, the non-linear nature of the response becomes more evident: the torque signal demonstrates asymmetric rising and falling limbs within each wave cycle, with multiple smaller oscillations superimposed on the dominant waveform (Figure 37).

The signal morphology varies between experiments. For instance, Figure 38 presents a comparable 5-second interval from Experiment E3 (f = 0.94 Hz, H_s = 0.03 m), where the shorter-period waves generate a distinctly different oscillatory signature. To quantify these variations, peak-finding algorithms in MATLAB were applied to the 40-second analysis window of torque and load measurements, identifying maximum and minimum values within each wave cycle (shown as cyan and red markers at the signal peaks and troughs in Figures 35-37).

These extrema were compiled to calculate the mean and standard deviation across the 15 regular wave experiments listed in Table 3. Results for torque, total tension force, and total compression force are presented in Figures 38, 39, and 40, respectively. Total tension was computed as the sum of Load Cells 1 (above water) and 2 (submerged) positioned on the up-wave side of the apparatus. Total compression was computed as the sum of Load Cells 4 (above water) and 3 (submerged) located on the down-wave side. Across all test cases, both torque and force increased linearly with wave height. Furthermore, lower-frequency conditions (e.g., f = 0.5 Hz) consistently produced smaller mean torque and force values than higher-frequency conditions (e.g., f = 0.94 Hz), where shorter-period waves generated the largest observed mean responses.

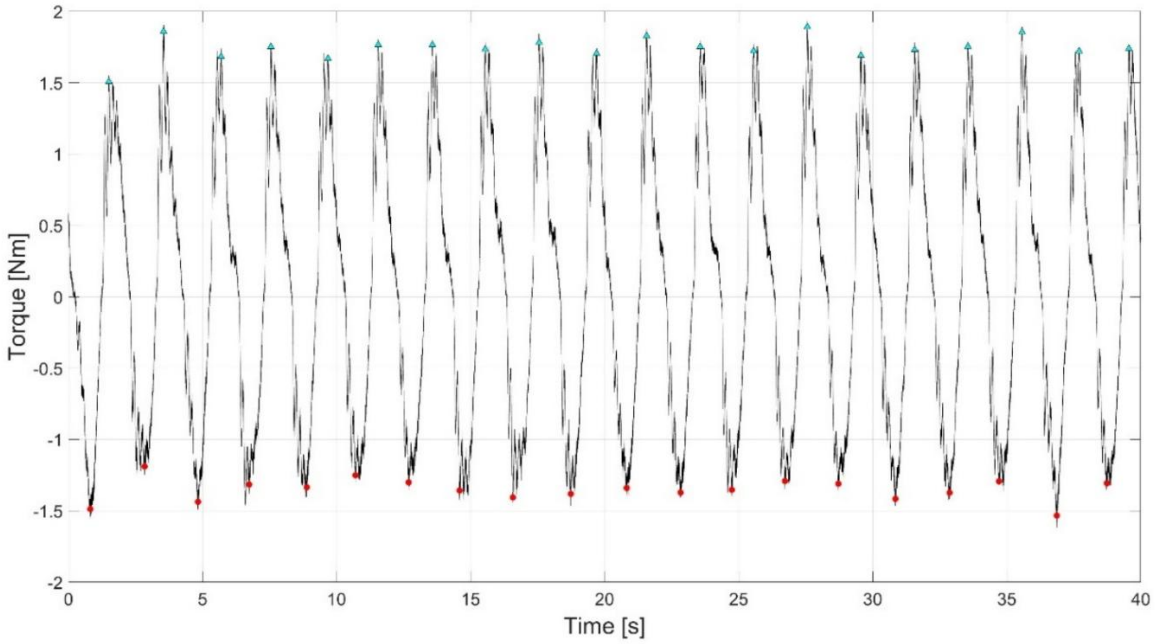

Figure 36. Torque measurements from Experiment C5, when the wave frequency was $f = 0.5$ Hz and the significant wave height was $H_s = 0.07$ m.

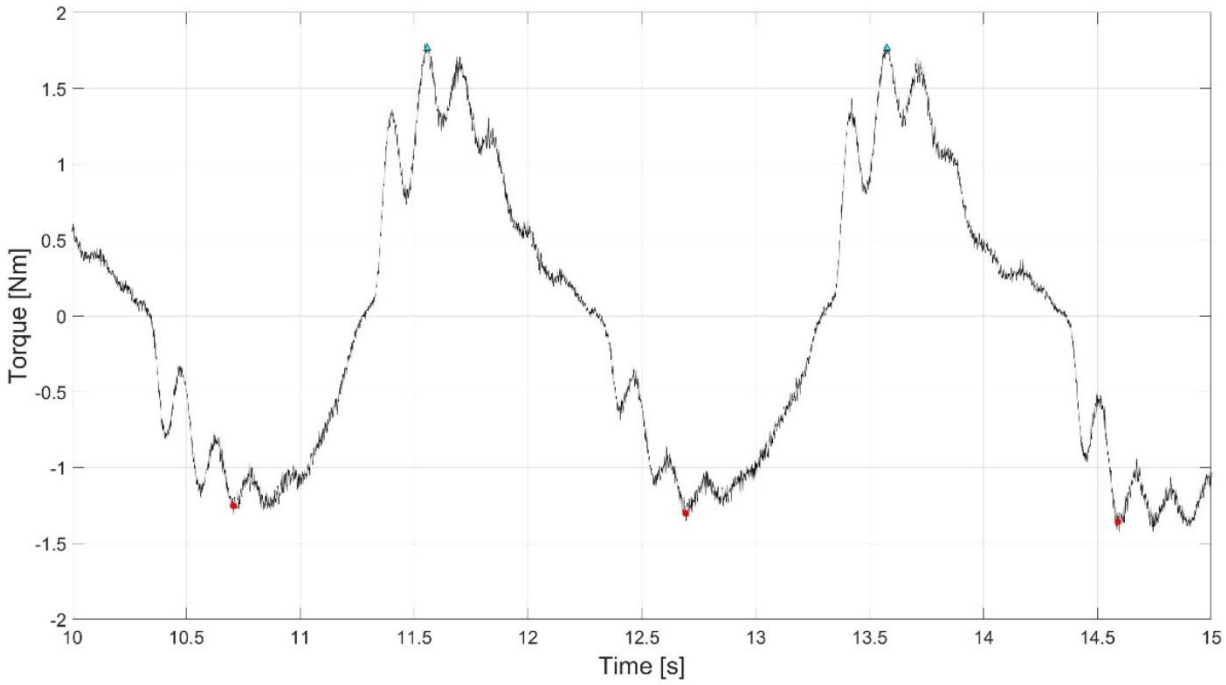

Figure 37. Zoomed in 5-second segment of torque measurements from Experiment C5, when the wave frequency was $f = 0.5$ Hz and the significant wave height was $H_s = 0.07$ m.

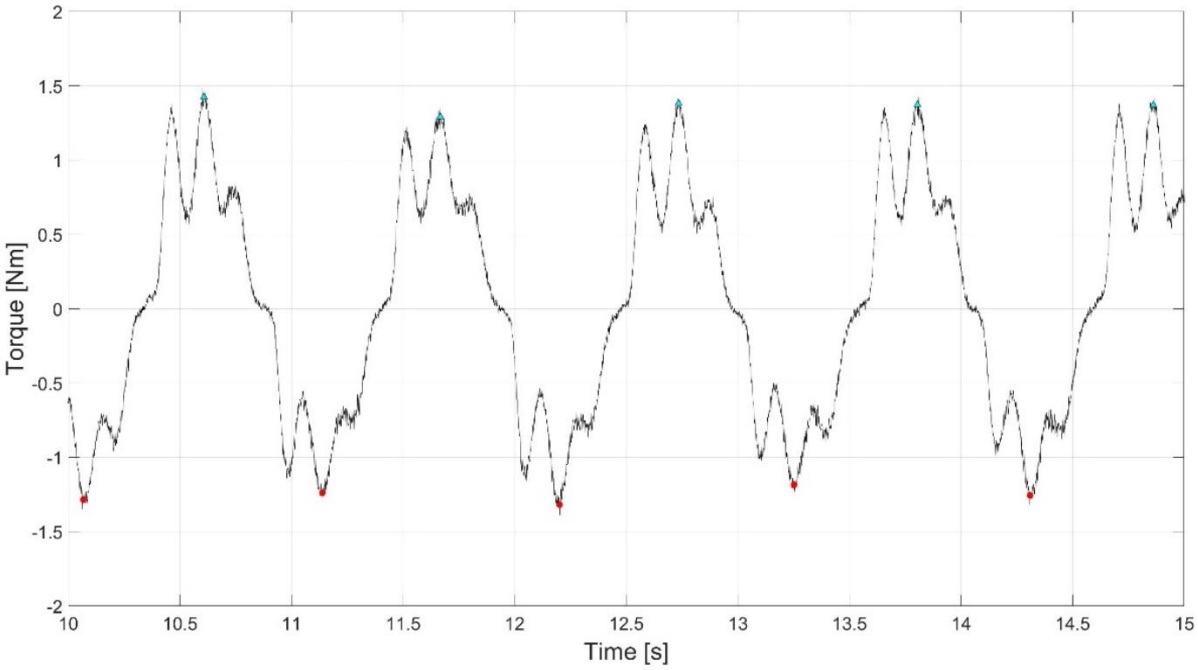

Figure 38. Zoomed in 5-second segment of torque measurements from Experiment E3, when the wave frequency was $f = 0.94$ Hz and the significant wave height was $H_s = 0.03$ m.

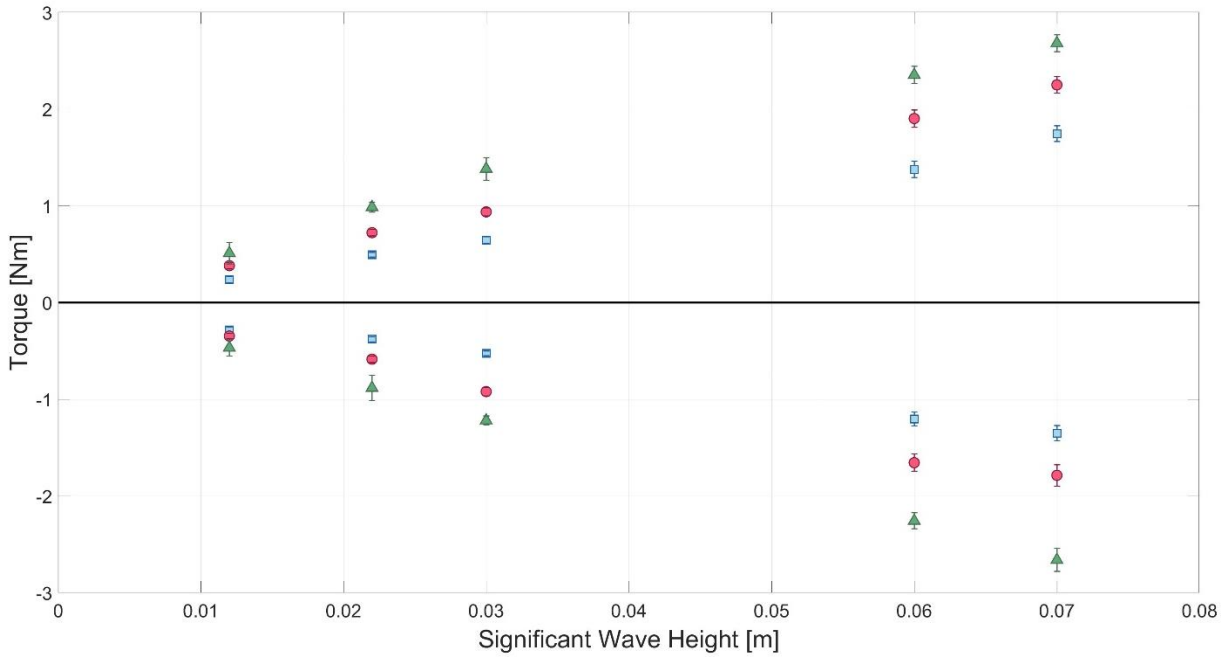

Figure 39. Average maximum torque values (above zero line) and average minimum torque values (below zero line) for all 15 regular wave experiments from Table 3. The green triangle symbols correspond to Experiments E1-E5, the red circle symbols correspond to Experiments D1-D5, and the blue square symbols correspond to Experiments C1-C5. Vertical error bar lines illustrate +/- one standard deviation from the mean value.

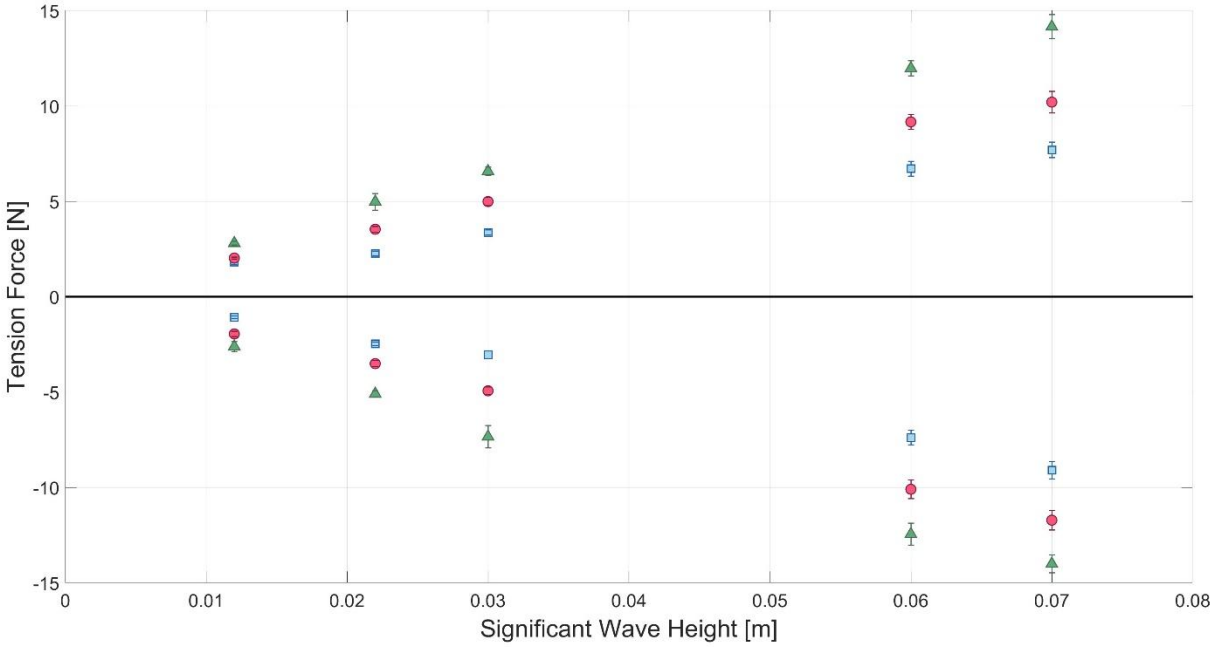

Figure 40. Average maximum tension values (above zero line) and average minimum tensions values (below zero line) for all 15 regular wave experiments from Table 3. The green triangle symbols correspond to Experiments E1-E5, the red circle symbols correspond to Experiments D1-D5, and the blue square symbols correspond to Experiments C1-C5. Vertical error bar lines illustrate +/- one standard deviation from the mean value.

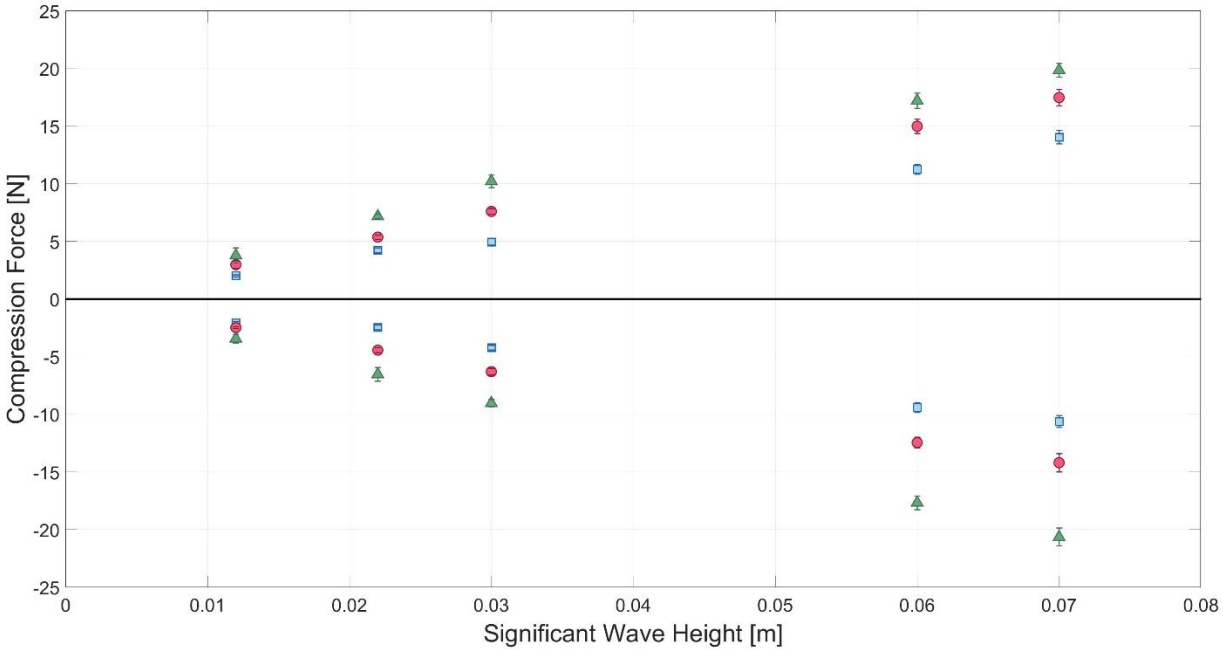

Figure 41. Average maximum compression values (above zero line) and average minimum compression values (below zero line) for all 15 regular wave experiments from Table 3. The green triangle symbols correspond to Experiments E1-E5, the red circle symbols correspond to Experiments D1-D5, and the blue square symbols correspond to Experiments C1-C5. Vertical error bar lines illustrate +/- one standard deviation from the mean value.

6. Discussion

The results of the BEM simulations reveal critical trends in the hydrodynamic performance of the VOSWEC under systematic variations in plate geometry. The hydrodynamic coefficients observed (excitation torque**,** added mass, and radiation damping) exhibited a dependence on both plate thickness and draught across the frequency spectrum analyzed. These variabilities have important implications for the design and optimization of wave energy converters intended for deployment in real ocean conditions.

Derived from the BEM simulations, these hydrodynamic variables provide information on each plate's capacity for wave energy absorption under varying sea state conditions. The study encompassed two case conditions: Case A (L = 0.3 m) and Case B (L = 0.4 m), each having three plate geometries tested at four draught conditions, for a total of 24 plate configurations. Hydrodynamic efficiency was primarily evaluated based on how well each configuration aligned the frequency response characteristics of excitation torque and radiation damping with expected peak wave energy periods.

6.1 Influence of Plate Geometry on Hydrodynamic Performance

Across both Case A and Case B, a consistent trend was observed: increasing either the plate thickness or the draught led to an increase in excitation torque. This outcome is driven by the increased wetted surface, amplifying pressure differentials across the plate due to incoming wave fields. As the plate width increased from b = 0.02 m to b = 0.06 m, greater pressure differentials and stronger torque responses were produced. Similarly, greater submergence increased the wetted surface area and enhanced wave-body interaction, further amplifying the

torque imparted by the waves, consistent with theoretical expectations that larger hydrodynamic cross-sectional areas promote greater excitation forces.

The highest excitation torque in Case A was observed for Plate 12a, reaching 145.42 Nm at a frequency of 5.68 rad/s, while the minimum occurred for Plate 7a at 28.30 Nm at 12.57 rad/s (Figures 13 and 12, respectively). In Case B, these effects were more pronounced with the greater plate length, with Plate 8b yielding a peak excitation torque of 335.40 Nm at 5.55 rad/s (Figure 18). This behavior could be attributed to the role of increased moment arm in rotational WECs, which enhances torque response without a proportional increase in damping.

Radiation damping followed a similarly depth-dominant trend, increasing consistently with draught. The largest damping coefficients were associated with deep plates, where the oscillatory motion radiates substantial wave energy compared to more shallow conditions. However, peak damping did not scale linearly with thickness; intermediate plate thicknesses often demonstrated the highest radiation damping characteristics across the same submergence. For example, in Case A, Plate 7a achieved the highest radiation damping value of 2.45 $kg \cdot m^2/s$ at 9.28 rad/s, despite its intermediate plate thickness (Figure 13). In Case B, Plate 8b exhibited the overall maximum damping of 12.23 $kg \cdot m^2/s$ at 8.64 rad/s (Figure 18).

Radiation damping also displayed a nuanced relationship with plate width. The highest values occurred at the intermediate plate width (b = 0.04 m), while the smallest occurred with the narrowest plate (b = 0.02 m). This suggests that the intermediate geometry may produce more favorable hydrodynamic coupling for wave generation, whereas narrow plates lack sufficient area to generate strong radiated wave fields.

Added mass, which governs the inertial response of the system, showed a more complex relationship with geometry. Added mass generally increased with depth, reflecting the increased fluid volume accelerated during motion. However, the effect of plate thickness was not monotonic. Across all depths, the added mass was largest for the intermediate plate width (b = 0.04 m) and smallest for the thinnest plate (b = 0.02 m). This counterintuitive trend may reflect complex interference effects in the fluid-structure interaction arising from geometry-specific flow patterns, potentially due to more coherent or resonant flow coupling for intermediate widths.

One of the primary considerations was how changes in added mass shifted the natural frequency of the system. A higher added mass generally lowers the natural frequency, which can be advantageous in wave climates dominated by long-period (low-frequency) swells. However, excessively high added mass may cause the WEC to respond more slowly to wave forcing, diminishing the relative motion between the structure and the PTO. This can lead to a decrease in power absorption, especially if the system becomes overdamped or inertially constrained. Identifying a balanced added mass value that aligns the system's natural frequency with peak wave energy periods is therefore crucial.

The maximum added mass across all cases was observed for Plate 8b, with 5.39 kg·m² at 4.8 rad/s (Figure 18). Conversely, the thickest plate in shallow draughts often produced the smallest added mass values, suggesting suppression of fluid entrainment in these configurations.

6.2 Design Implications for VOSWEC Optimization

The combined analysis of excitation torque, added mass, and radiation damping demonstrates the strong dependence of hydrodynamic coefficients on plate thickness, draught,

and length, as well as the importance of tuning geometry to match the frequency content of the wave environment. Increasing plate length and depth enhances the magnitude of wave-induced forces and torques; however, designs must balance this with the implications of excessive added mass, which can depress the natural frequency of the system below the dominant wave frequencies, reducing dynamic responsiveness.

Similarly, while radiation damping is critical for efficient wave interaction, overdamping may suppress motion and reduce the relative displacement needed for an effective PTO. The highest-performing configurations in Case B aligned the peaks of excitation torque, added mass, and radiation damping within a narrow frequency range (approximately 5.5 to 9 rad/s), supporting the importance of spectral matching in geometry selection.

These findings highlight that design optimization is not strictly monotonic with respect to size. The observation that intermediate-width plates resulted in both the highest added mass and radiation damping, while thicker plates reduced these coefficients despite increased frontal area, underscores the role of nonlinear geometry-fluid interactions. Additionally, the consistent increase in all three hydrodynamic coefficients with draught suggests that submergence depth is a critical lever for tuning device dynamics to match target wave climates.

By systematically quantifying these relationships through BEM simulations before physical testing, the design space can be significantly narrowed, reducing the risk of costly design iterations during experimental campaigns. In the context of the VOSWEC, these numerical insights provided a foundation for selecting geometry candidates for MTU wave tank testing, ensuring that physical experiments could focus on validating and refining the most promising configurations rather than broadly screening less optimal designs.

6.3 MTU Wave Tank Preliminary Tests

The scaled wave tank tests faced complications during the initial attempts at radiation tests when the WEC plate oscillates in a calm tank. The control method used was based on sinusoidal analog position control. While the premise of the control method works well, the servo motor needed custom tuning and filtering applied to damping out small-scale corrections during the slower, larger oscillatory movements of the WEC. Only one test was attempted for this phase of the experiments, and it was quickly observed that the VOSWEC plate would "wiggle" and slosh around while attempt to make larger sinusoidal movements. This caused the formation of very high frequency vibrations and surface waves to radiate away from the WEC, an unrealistic condition for what is expected for this WEC operation. Moving forward, the servo motor needs to be properly tuned, the WEC plate net buoyancy and stability needs closer investigation, and adaptive filtering will likely be required to smooth out WEC motion in the tank and at larger scales.

6.4 Nearshore Wave Energy Assessments

Following analysis on a brief four-day period of data from a buoy deployment (Figure 42), the Spotter Buoy data (Figure 43) highlighted the consistent presence of meaningful wave energy, even in less than the average person's wingspan, in Lake Superior's nearshore. These results suggest that freshwater environments, often overlooked in marine renewable energy discussions, can provide sufficient resources to support small-scale applications in areas such as autonomous monitoring systems or coastal infrastructure power supply (Figure 44). These findings highlight the renewable energy resources available even in freshwater environments and during relatively short monitoring periods. Such energy availability could support a range of

applications, from small-scale autonomous systems to coastal infrastructure power supply, and underscores the importance of continued high-resolution wave monitoring to inform the design and deployment of wave energy technologies in the Great Lakes.

Figure 42. Park Point Spotter Buoy location GPS: 46.7359, -92.0427 located in 13m water depth approximately, located approximately 0.75km straight out from the Park Point Beach House in Duluth, MN.

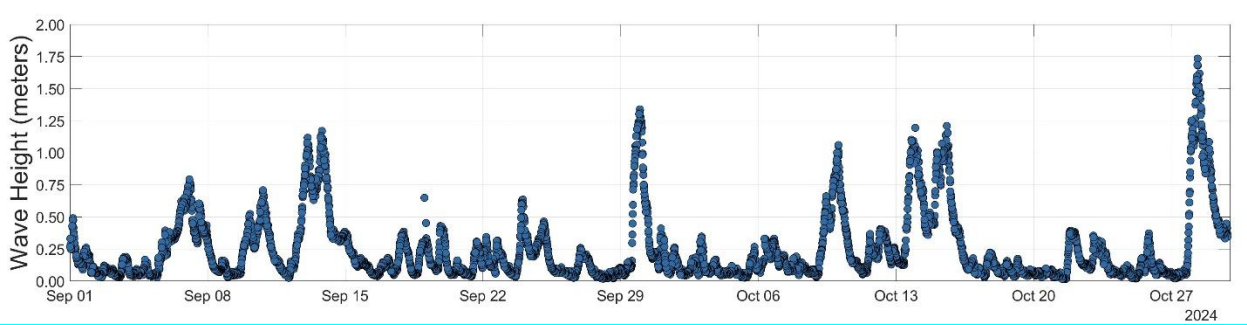

Figure 43. Spotter Buoy, September-October 2024 deployment. The buoy was deployed during the ice-free periods and assists with rip current risk level identification due to wave activity.

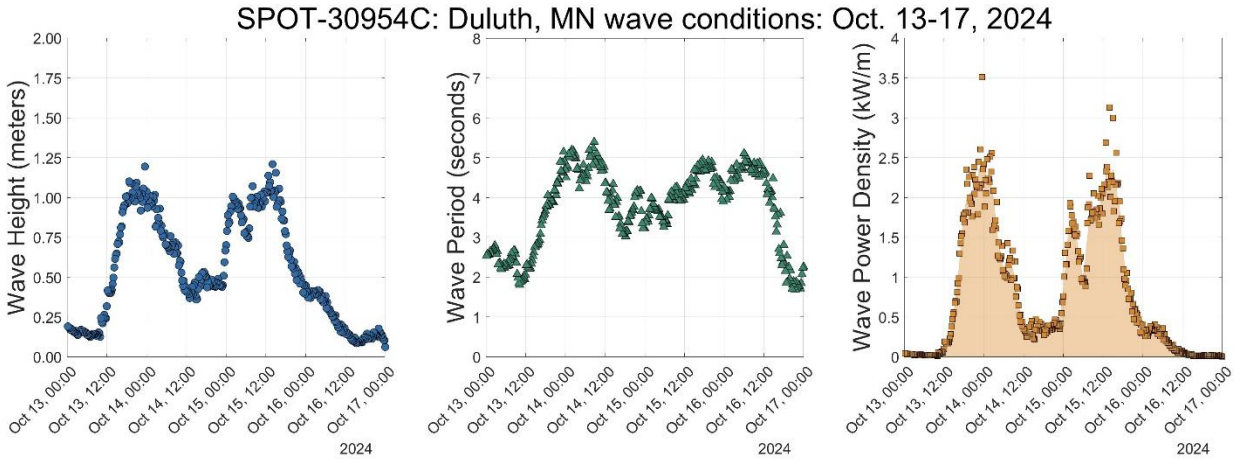

Figure 44. Spotter Buoy GPS: 46.7359, -92.0427, targeted data range from October 13-17, 2024 storm period.

6.5 Froude Scaling

Froude scaling provides a critical framework for translating device performance from the Great Lakes to ocean environments, enabling meaningful comparisons and predictions between testing sites. By maintaining dynamic similarity in gravitational and inertial forces, this method allows Lake Superior to serve as a valuable testing ground for WECs while preserving the ability

to accurately scale results to more energetic ocean conditions. For example, when comparing Lake Superior to the Oregon coast, home to PACWave, the first planned grid-connected wave energy test site in the United States, the average Froude scale factor is approximately 4 (Figure 45). This means that performance metrics such as power output can be scaled according to $\lambda^{3.5}$, where λ is the scale factor.

Applying this relationship, a 100 W device tested in Lake Superior could be expected to produce roughly 12.8 kW at PACWave, illustrating the substantial scaling potential. This approach allows engineers to test realistically manufactured, fully functional devices in the Great Lakes while maintaining direct relevance to ocean-scale deployment. In addition to predicting performance, scaled results can inform critical design refinements, such as reinforcing structural elements to withstand higher loads, adjusting springs or dampers in power take-off systems for optimal control, and selecting appropriate mooring lines or foundation systems for larger-scale installations. In this way, Froude scaling not only bridges the gap between freshwater and oceanic testing but also accelerates the path from concept validation to commercial-ready designs.

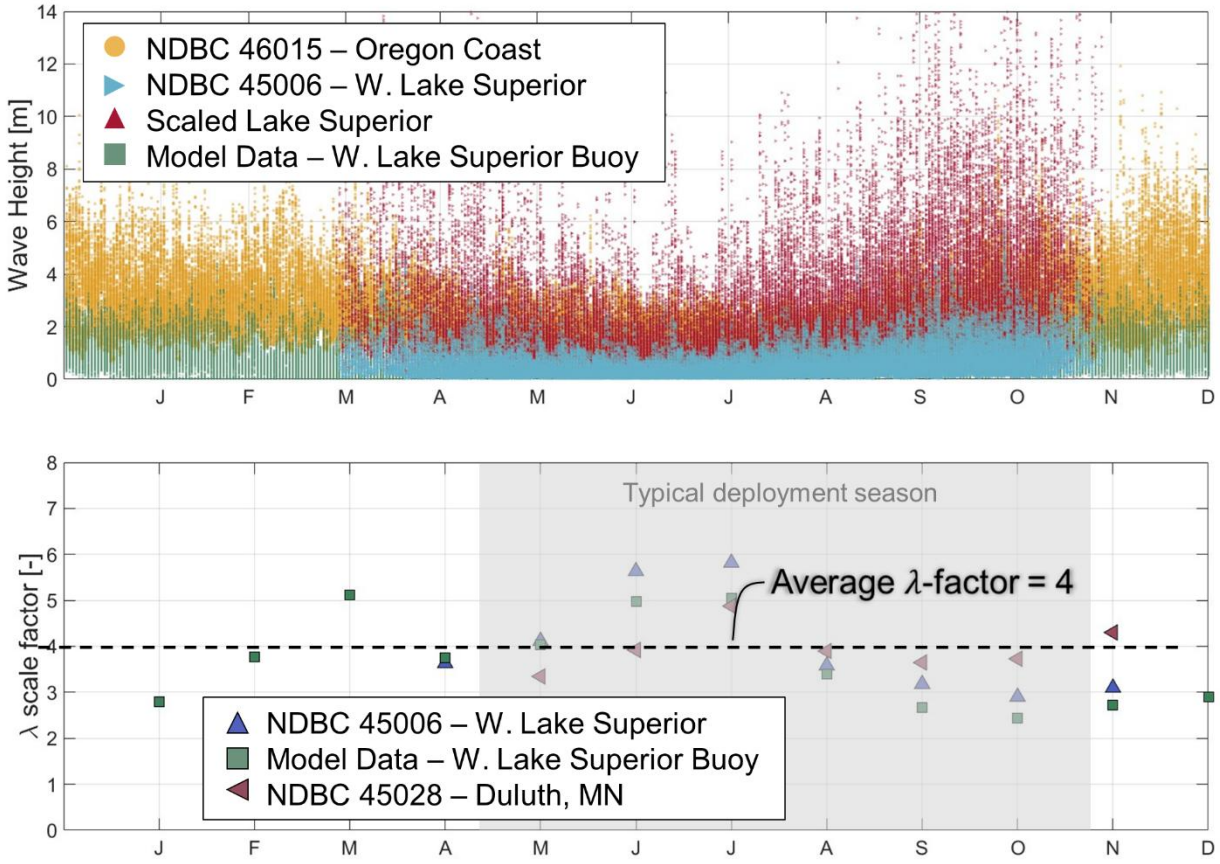

Figure 45. Froude scaling example comparing the Great Lake Superior to the Oregon Coast, USA.

6.6 Future Efforts

Future work should integrate these findings into time-domain models that include PTO system dynamics and nonlinearity and validate them against physical testing to refine design recommendations. This study provides the beginning of a hydrodynamic basis for geometry based optimization in vertically oriented OSWECs. Despite growing interest in deploying wave energy converters in inland and nearshore environments, there remains a significant gap in the understanding of wave climate characteristics, particularly within the Great Lakes. While preliminary investigations have identified the presence of usable wave energy, the temporal and spatial variability of wave conditions across the region is limited. Nearshore environments in the Great Lakes are influenced by complex bathymetry, seasonal ice cover, wind fetch limitations, and coastal geomorphology, all of which contribute to wave behavior that diverges from typical oceanic conditions. Publicly available, high resolution wave data in these zones is sparse, and long-term spectral datasets are largely absent. This lack of data presents a barrier to a fully comprehensive resource assessment, hydrodynamic modeling, and device tuning. Future research should prioritize the collection and analysis of detailed wave climate data in the nearshore Great Lakes to inform site selection, optimize wave energy converter geometries, and support the development of tailored control strategies. Designing a VOSWEC style device that integrates into coastal infrastructure ultimately needs to account for local sea states to model, account for, and optimize the WEC across a range of common sea states experienced at that site. Advancing this regional understanding is essential to realizing the full potential of wave energy in non-tidal inland “seas”.

7. Conclusion

As the global energy sector transitions toward renewable and distributed generation, wave energy remains a largely untapped yet promising resource, particularly in nearshore and coastal zones. These environments offer several unique advantages compared to open ocean deployment including reduced transmission distances to shore-based loads, simplified access for installation and maintenance, and the opportunity to integrate with existing or future coastal infrastructure. Coastal and structure-integrated WECs also offer dual benefits, potentially combining energy harvesting with shoreline stabilization or storm protection functions. These synergistic deployments are especially attractive for communities where space is limited, energy access is costly, and shoreline resilience is increasingly critical.

This study focused on a novel WEC design tailored for such environments: the VOSWEC. The intent is for this geometry to be well suited for fixed mounting to piers, breakwaters, or other shoreline structures and offers several unique design advantages. The vertical orientation allows the power (PTO) system to remain above water, protecting it from biofouling and corrosion. Additionally, the plate-style configuration enables control over structural simplicity and wetted surface area, which directly influences hydrodynamic performance. Despite these advantages, there is limited research on VOSWECs, especially in the context of non-tidal inland seas like the Great Lakes. This study aimed to close that gap through a methodical and practical approach that includes theoretical modeling, BEM simulations, physical testing, and scaling considerations.

One challenge in WEC development lies in understanding how the device interacts with waves over a range of frequencies. System identification provides a basis for understanding this

and allowing for the tuning of these technologies appropriately, characterizing the frequency-domain response of a device to wave forcing through its hydrodynamic coefficients including excitation torque, added mass, and radiation damping. Unlike many mechanical systems where the goal is to suppress motion, WECs benefit from amplification, ideally being driven by strong wave excitation near the natural frequency of the WECs. As a result, the SID process is intentionally designed to probe these dynamics through broad frequency sweeps in both simulations and physical experiments. SID also significantly informs in control design, time-domain simulation, and eventually energy performance estimation in real-world sea states.

The BEM simulations served as a critical foundation for the entire testing campaign. As a linear potential flow-based approach, BEM efficiently calculates frequency-dependent hydrodynamic coefficients by solving boundary-integral equations across a defined geometry. While BEM relies on the assumptions of LWT and inviscid, irrotational flow, it remains one of the most powerful and accessible tools to understand the baseline dynamic response for these WEC technologies. BEM results inform the experimental parameters before costly and time-consuming prototyping and physical testing begins providing a better space for what conditions these should be tailored to. By simulating a wide range of plate configurations, the most ideal geometries from the simulations can be selected for testing and the expected response behavior anticipated in the wave tank to compare the simulated with the actual results.

In this study, BEM simulations were conducted using Capytaine across 24 VOSWEC configurations. These configurations were divided into two main cases, Case A with a plate length of 0.3 m and Case B with a length of 0.4 m, each containing three plate widths (b =

0.02 m, 0.04 m, 0.06 m) at four submergence depths (d = 0.3 m, 0.4 m, 0.5 m, 0.6 m). Results demonstrated several important trends:

- **Excitation torque** increased consistently with both plate width and submergence depth. The largest values occurred in Case B, with Plate 8b reaching a peak torque of 335.40 Nm at 5.55 rad/s. These results are consistent with theory, as larger wetted areas and deeper immersion increase wave-body pressure differentials and lengthen the moment arm of the rotating plate.
- **Radiation damping** also increased with depth but peaked for intermediate plate widths (b = 0.04 m), suggesting a more efficient radiation of wave energy at these geometries. For example, Plate 8b exhibited a maximum damping value of 12.23 kg·m²/s at 8.64 rad/s.
- **Added mass** showed a more nuanced relationship, increasing with draught but not strictly with plate width. Intermediate widths again yielded the largest added mass, with Plate 8b reaching 5.39 kg·m² at 4.8 rad/s. This highlights complex fluid-structure interaction effects such as flow detachment and local interference, which do not scale linearly with geometry.

These hydrodynamic coefficients, when considered collectively, revealed that optimal energy capture is not solely achieved by maximizing size or surface area. Rather configurations that align peak excitation torque and radiation damping within the dominant frequency bands of expected sea states are likely to yield more ideal (or greater) energy performance. The results also emphasized that overdamping or excessive added mass can hinder relative motion and reduce net energy transfer to the PTO.

These insights directly informed the experimental setup at the MTU Wave Tank, where forced oscillation and diffraction tests are being conducted on a 1:20 scale wall-mounted VOSWEC prototype. The ideal plate configurations from the BEM simulations were selected for tank testing. The wave tank testing incorporates a precision actuation system, a torque transducer, multiple submersible load cells, and high-speed motion capture for full six-degree-of-freedom tracking. The facility also enables real-time data acquisition synchronized across all subsystems. The tank test sequence includes wave field calibration, forced oscillation (radiation) tests, locked-body (diffraction) tests, and multisine excitation to produce broadband frequency response estimates. The MTU wave tank testing contributed the first experimental SID dataset for this configuration, comparing the numerical predictions, identifying nonlinear response features, and yielding model-ready parameters for future control and performance simulations. The hydrodynamic sensitivity analysis offers guidance for geometric optimization, the MTU testing provides essential calibration data for dynamic simulation and control development, and the resource assessment establishes a realistic operational envelope for Great Lakes deployments.

To ensure scalability, Froude scaling principles were applied to allow the translation of measured tank-scale results to eventual full-scale prototypes operating in the nearshore environment in regions such as the Great Lakes, like Lake Superior. This inland sea, despite its wave energy potential, suffers from a lack of high-resolution, long-duration spectral data, especially in the nearshore zones where WECs are most likely to be deployed. As such, part of the future direction for this research involves collecting more detailed observational data, potentially using ADCP deployments and nearshore buoy networks to build a more robust wave climate database.

These real-world conditions can ultimately be modeled using WEC-Sim, which incorporates hydrodynamic coefficients from BEM and enables time-domain simulations of the WEC under irregular, site-specific sea states. Combined with the SID-informed parameters from the tank campaign, WEC-Sim will allow for a more refined estimate of power capture, PTO control strategy effectiveness, and survivability under extreme wave events.

Overall, this study explored a holistic methodology for assessing coastal VOSWEC designs, spanning from analytical theory to numerical simulation to physical testing. It demonstrates that early-stage modeling, such as BEM, can drastically improve the focus and efficiency of experimental campaigns. It also reinforces the relevance and potential of nearshore wave energy applications in underutilized regions such as the Great Lakes.

Ultimately, the integration of BEM simulations, physical tank testing, and scaled WEC-Sim modeling suggests further development of the VOSWEC concept is worthy of greater exploration and could be beneficial to the MRE field and greater energy complex as a whole. Continued refinement of the design, informed by both experimental and observational data, will support future control strategy development, full-scale prototyping, and real-world deployment assessments. In doing so, this research contributes meaningfully to the broader wave energy industry by advancing a new, structurally efficient, and regionally adaptable class of WECs designed for coastal and infrastructure-integrated applications.

8. Future Directions

This work has established a hydrodynamic foundation for the VOSWEC, demonstrating the potential for deployment in nearshore environments such as the Great Lakes and other low-resource coastal locations. There are several ways to move forward in exploring the possibilities surrounding these types of MRE technologies in small-scale sea state regions.

- **Expanded Scaled Model Development and Tank Testing**

  The BEM-derived hydrodynamic coefficients and geometry-performance trends identified in this study can be used to directly inform a scaled physical model of a VOSWEC based on these findings. A handful of iterations could be tested based on the optimal configurations from the outcomes of this study to be used in the MTU Wave Tank, with an emphasis on aligning the device's natural frequency and radiation damping peaks with the dominant wave periods of target deployment sites. Future campaigns should incorporate a broader range of irregular wave conditions and directional spectra to replicate realistic sea states. In addition, advanced SID techniques, including multisine and random wave excitation, should be included to further refine frequency-domain models and to enable control co-design in the laboratory before moving to field trials.

- **Detailed Design and Controls Development for Field Deployments**

  Following scaled validation, mechanical and PTO systems should be optimized for durability, efficiency, and maintainability in real-world conditions. This includes integrating robust mechanical transmission systems, corrosion-resistant materials, and out of water PTO housing for reduced biofouling.

- **Froude Scaling and Field-Scale Performance Projections**

  Froude scaling will remain the primary tool for extrapolating from tank-scale performance to full-scale operation. However, future work could integrate viscous corrections, such as for low-Reynolds-number effects in smaller-scale models, and elasticity scaling for mooring and structural elements. Applying this methodology will allow reliable projection of VOSWEC performance in the Great Lakes and other inland seas, as well as in coastal ocean environments.

- **Extended Wave Resource Characterization**

  A critical step toward deployment is the expansion of wave climate data for nearshore Great Lakes sites. Long-term, high-resolution measurements from ADCPs, coastal buoys, or shore-mounted radar should be collected to build a robust spectral database. These datasets will feed into extended modeling tools, such as WAVEWATCH III (WW3) hindcasts, improving the characterization of annual, seasonal, and extreme condition variability. Such information is vital for optimizing geometry, control strategy, and PTO sizing to maximize performance across the full employment of a fully encompassing WEC device.

- **Application to Global Low-Resource Coastal Environments**

  The VOSWEC's compact geometry and suitability for short-period seas make it an attractive candidate for wave energy development in other low-to-moderate-energy regions, such as islands, semi-enclosed seas, and sheltered coastal zones in developing countries. Future research should include a full comparative global wave resource

assessment to identify similar locations, followed by regional design optimization informed by local bathymetry, wave spectra, deployment constraints, etc.

- **WEC-Sim Integration for Site-Specific Design**

  The validated hydrodynamic parameters from tank testing will allow high-fidelity time-domain modeling in WEC-Sim for specific deployment environments. These models should incorporate site-specific wave spectra, mooring dynamics, and PTO control logic to assess not only annual energy production but also survivability under extreme events. WEC-Sim will serve as a critical design tool, enabling optimization of geometry and controls prior to costly prototype development and deployment.

Overall, the integration of rigorous hydrodynamic modeling, iterative scaled experimentation, site-specific resource assessment, and control co-design will be essential to unlocking the full potential of this adaptable wave energy converter in both inland and oceanic environments. By continuing to explore the advancement of the VOSWEC, this technology could transition from laboratory validation to a viable field-deployed technology, capable of enhancing regional renewable energy portfolios.

9. References

[1] Ahn, S., Neary, V. S., Allahdadi, M. N., & He, R. (2022). A framework for feasibility-level validation of high-resolution wave hindcast models. *Ocean Engineering*, *263*, 112193.

[2] Bergstrom, R. D., Johnson, L. B., Sterner, R. W., Bullerjahn, G. S., Fergen, J. T., Lenters, J. D., Norris, P.E., & Steinman, A. D. (2022). Building a research network to better understand climate governance in the Great Lakes. *Journal of Great Lakes Research*, *48*(6), 1329-1336.

[3] "Coastal Structure Integrated Wave Energy Converters." *NREL*, www.nrel.gov/water/coastal-structure-integrated-wave-energy-converters?utm_source.com (accessed on 13 August 2025).

[4] Forbush, Dominic, et al. "Theory Manual." *WEC*, National Renewable Energy Laboratory and National Technology & Engineering Solutions of Sandia, LLC (NTESS), 2022, wec-sim.github.io/WEC-Sim/main/theory/index.html.

[5] Golbaz, D., Asadi, R., Amini, E., Mehdipour, H., Nasiri, M., Nezhad, M. M., Naeeni, S.T.O., & Neshat, M. (2021). Ocean wave energy converters optimization: A comprehensive review on research directions. *arXiv preprint arXiv:2105.07180*.

[6] Hall, S., Peterson, K., Gjestvang, K., & McGilton, B. (2024). *GIS Supported Optimal Site Selection for Coastal Structure Integrated Wave Energy Converters* (No. NREL/CP-5700-90299). National Renewable Energy Laboratory (NREL), Golden, CO (United States).

[7] Holthuijsen, L., Booij, N., Ris, R. C., & Holthuijsen, L. H. (1999). A third-generation wave model for coastal regions, Part I, Model description and validation A third-generation wave

model for coastal regions 1. Model description and validation. *Article in Journal of Geophysical Research Atmospheres*, *778*.

[8] Iglesias, G., & Abanades, J. (2017). Wave power: Climate change mitigation and adaptation. In *Handbook of Climate Change Mitigation and Adaptation* (pp. 2007-2055). Springer, Cham.

[9] Jabbari, A., Ackerman, J. D., Boegman, L., & Zhao, Y. (2021). Increases in Great Lake winds and extreme events facilitate interbasin coupling and reduce water quality in Lake Erie. *Scientific Reports*, *11*(1), 5733.

[10] Karageorgis, P. (2012). Dispersion relation for water waves with non-constant vorticity. *European Journal of Mechanics-B/Fluids*, *34*, 7-12.

[11] Kelley Ruehl, Adam Keester, Dominic Forbush, Jeff Grasberger, Salman Husain, Jorge Leon, David Ogden, and Mohamed Shabara, "WEC-Sim v6.1". Zenodo, September 16, 2024.

[12] Le Roux, J. P. (2008). An extension of the Airy theory for linear waves into shallow water. *Coastal Engineering*, *55*(4), 295-301.

[13] *Li, L., Fujisaki-Manome, A., Miller, R., Titze, D., & Henderson, H. (2024). Evaluation of ICESat-2 significant wave height data with buoy observations in the Great Lakes and application in examination of wave model predictions. Remote Sensing, 16(4), 679.*

[14] Liu, Y., Cho, Y. H., Mizutani, N., & Nakamura, T. (2021). Study on the resonant behaviors of a bottom-hinged oscillating wave surge converter. *Journal of Marine Science and Engineering*, *10*(1), 2.

[15] Magkouris, A., Bonovas, M., & Belibassakis, K. (2020). Hydrodynamic analysis of surge-type wave energy devices in variable bathymetry by means of BEM. *Fluids*, *5*(2), 99.

[16] Mi, J., Huang, J., Li, X., Ahmed, A., Yang, L., Chung, U., ... & Zuo, L. (2024). Oscillating surge wave energy converter using a novel above-water power takeoff with belt-arc speed amplification. *Ocean Engineering*, *310*, 118503.

[17] Mi, J., Huang, J., Li, X., Ahmed, A., Yang, L., Chung, U., ... & Zuo, L. (2024). Oscillating surge wave energy converter using a novel above-water power takeoff with belt-arc speed amplification. *Ocean Engineering*, *310*, 118503.

[18] Moretti, G., Fontana, M., & Vertechy, R. (2015). Model-based design and optimization of a dielectric elastomer power take-off for oscillating wave surge energy converters. *Meccanica*, *50*(11), 2797-2813.

[19] Penalba, M., Giorgi, G., & Ringwood, J. V. (2017). Mathematical modelling of wave energy converters: A review of nonlinear approaches. *Renewable and Sustainable Energy Reviews*, *78*, 1188-1207.

[20] Pheifer, C., & Hill, C. (2024). Great Lakes wave energy resource classification and Blue Economy opportunities. Renewable Energy, 235, 121213.

[21] Ruehl, K., Forbush, D. D., Yu, Y. H., & Tom, N. (2020). Experimental and numerical comparisons of a dual-flap floating oscillating surge wave energy converter in regular waves. *Ocean Engineering*, *196*, 106575.

[22] Rusu, E. (2024). Marine Renewable Energy and the Transition to a Low-Carbon Future. *Journal of Marine Science and Engineering*, *12*(4), 568.

[23] Sarkar, D., Renzi, E., & Dias, F. (2013, June). Wave power extraction by an oscillating wave surge converter in random seas. In *International Conference on Offshore Mechanics and Arctic Engineering* (Vol. 55423, p. V008T09A008). American Society of Mechanical Engineers.

[24] Schmitt, P., & Elsäßer, B. (2017). The application of Froude scaling to model tests of Oscillating Wave Surge Converters. *Ocean Engineering*, *141*, 108-115.

[25] *Shields, M. A. (2014). An introduction to marine renewable energy. In Marine Renewable Energy Technology and Environmental Interactions (pp. 1-3). Dordrecht: Springer Netherlands.*

[26] Shields, M. A., Woolf, D. K., Grist, E. P., Kerr, S. A., Jackson, A. C., Harris, R. E., ... & Side, J. (2011). Marine renewable energy: The ecological implications of altering the hydrodynamics of the marine environment. *Ocean & coastal management*, *54*(1), 2-9.

[27] Sogut, D. V., Farhadzadeh, A., & Jensen, R. E. (2018). Characterizing the Great Lakes marine renewable energy resources: Lake Michigan surge and wave characteristics. *Energy*, *150*, 781-796.

[28] *Unlocking Ocean Power: $3.6m for Community-Centric Wave Energy Converters - Naval Architecture and Marine Engineering*, name.engin.umich.edu/2024/10/01/unlocking-ocean-power-3-6m-for-community-centric-wave-energy-converters/.

[29] Velioglu Sogut, D., Jensen, R. E., & Farhadzadeh, A. (2019). Characterizing lake ontario marine renewable energy resources. *Marine Technology Society Journal*, *53*(2), 21-37.

[30] Wang, L., Kolios, A., Cui, L., & Sheng, Q. (2018). Flexible multibody dynamics modelling of point-absorber wave energy converters. *Renewable energy*, *127*, 790-801.

[31] *Weiss, C. V., Guanche, R., Ondiviela, B., Castellanos, O. F., & Juanes, J. (2018). Marine renewable energy potential: A global perspective for offshore wind and wave exploitation. Energy conversion and management, 177, 43-54.*

[32] Yu, Y. H., Li, Y., Hallett, K., & Hotimsky, C. (2014, June). Design and analysis for a floating oscillating surge wave energy converter. In *International Conference on Offshore Mechanics and Arctic Engineering* (Vol. 45547, p. V09BT09A048). American Society of Mechanical Engineers.

[33] Zhang, H., Ding, X., Zhou, B., Zhang, L., & Yuan, Z. (2019). Hydrodynamic performance study of wave energy–type floating breakwaters. *Journal of marine science and application*, *18*(1), 64-71.

10. Appendices

A. Capytaine Script Written using in Spyder Case 1a

The following code implements a Capytaine boundary element method (BEM) solver to compute the hydrodynamic coefficients (excitation torque, added mass, and radiation damping) for the six VOSWEC plate configurations tested. The script loads individual STL meshes exported from SolidWorks, positions them in the desired draught, and runs frequency-domain simulations to generate the hydrodynamic data. To switch between plate geometries, update the mesh file name in the # LOAD OR CREATE MESH section so it points to the STL file for the desired plate length and thickness. To change the draught, modify the z-coordinate inside the voswec_mesh.translate() call in the # TRANSLATE/ROTATE MESH section. The z-translation should equal the plate height minus the intended draught, which positions the plate further into or out of the water. If the plate dimensions change significantly, the center of mass can be adjusted in the # DEFINE FLOATING BODY section to maintain correct physical representation in the solver. Finally, to ensure outputs are saved to the correct files for later analysis in MATLAB, update the file names in the # Export to CSV and # Export to Excel in Google Drive sections to match the plate configuration specified in the load step. This structure allows a single script to be reused for multiple geometry–draught combinations, streamlining the generation of hydrodynamic coefficients for systematic geometry variation studies. More information on the uses of Capytaine can be found at (https://capytaine.org/stable/).

```python
# -*- coding: utf-8 -*-
"""
Created on Wed June 02 16:38:26 2025
@author: gbahr

The following code is an implementation of the BEM code Capytaine, used to determine
hydrodynamic coefficients for floating/fixed bodies in marine environments
"""
#_____________________________________________________________________________
# IMPORT NECESSARY LIBRARIES/DEPENDENCIES
import capytaine as cpt
import numpy as np
import time
import vtk
import xarray as xr
import matplotlib.pyplot as plt

# from capytaine.bem.airy_waves import airy_waves_free_surface_elevation
# from capytaine.ui.vtk.animation import Animation

#_____________________________________________________________________________
# SET DEBUGGING LEVEL ('INFO', 'DEBUG', 'WARNING')
cpt.set_logging('INFO')
# Control whether or not to run the animation section of code
vtk_view = 0 # shows mesh in normal VTK viewer
play_anim = 0  # 1 means yes, 0 means no

#_____________________________________________________________________________
# LOAD OR CREATE A MESH
# To load an existing mesh file, use the following syntax:
# If creating a geometry in Solidworks, export as an *.stl file format, but
# be sure to change export units to meters and do not flip to positive space
# if your design is oriented in Solidworks to have some portion of the geometry below
# the water surface elevation.
# NOTE: Might need to force smaller resolution of mesh, either here or in Solidworks
mesh_flap = cpt.load_mesh('G:/My Drive/Masters Thesis and Related/Thesis/Research/Solidworks Parts/
voswec_mesh = mesh_flap

#_____________________________________________________________________________
# TRANSLATE/ROTATE MESH
# TRANSLATIONS
# voswec_mesh.translate_x(0.0)
# voswec_mesh.translate_y(0.0)
# voswec_mesh.translate_z(-0.3)
voswec_mesh.translate([0.0, 0.0, 0.3])
# ROTATIONS
# voswec_mesh.rotate_x(0.0)  # Rotation of pi/5 around the Ox axis
# voswec_mesh.rotate_y(0.0)  # Rotation of pi/5 around the Oy axis
# voswec_mesh.rotate_z(np.pi/-6)  # Rotation of pi/5 around the Oz axis

# voswec_mesh.show()

#_____________________________________________________________________________
# TRIM MESH AT DESIRED DEPTH OF PLATE
xOy_Plane = cpt.Plane(point=(0, 0, 0), normal=(0, 0, 1))
clipped_mesh = voswec_mesh.clipped(xOy_Plane)
lid_mesh=clipped_mesh.generate_lid(z=-0.01)
```

```python
if vtk_view:
    clipped_mesh.show()

#_____________________________________________________________________________
# DEFINE FLOATING BODY
# Define the center of mass (important for hydrostatics)
com = np.array([0, 0.15, 0.15]) # Center of Mass location (see Solidworks)
rotation_center = np.array([0.0, 0.0, 0.0])  # hinge location at seabed

body = cpt.FloatingBody(mesh=clipped_mesh, lid_mesh=lid_mesh, center_of_mass=com, name='VOSWEC')
body.rotation_center = rotation_center  # Set the rotation center
body.add_rotation_dof(name='Yaw')

# print("DOFs:", body.dofs)
# END DEFINE FLOATING BODY
# ------------------------

if play_anim:

    # ANIMATE BODY
    # The following animation code what developed using ChatGPT as help
    # === Step 1: Define mesh vertices and faces from the clipped mesh
    vertices = clipped_mesh.vertices
    faces = clipped_mesh.faces

    # === Step 2: Create VTK points and faces (Visualization Toolkit)
    points = vtk.vtkPoints()
    for v in vertices:
        points.InsertNextPoint(*v)

    polygons = vtk.vtkCellArray()
    for face in faces:
        polygon = vtk.vtkPolygon()
        polygon.GetPointIds().SetNumberOfIds(len(face))
        for j, idx in enumerate(face):
            polygon.GetPointIds().SetId(j, idx)
        polygons.InsertNextCell(polygon)

    # === Step 3: VTK PolyData and Mapper ===
    polydata = vtk.vtkPolyData()
    polydata.SetPoints(points)
    polydata.SetPolys(polygons)

    mapper = vtk.vtkPolyDataMapper()
    mapper.SetInputData(polydata)

    actor = vtk.vtkActor()
    actor.SetMapper(mapper)
    actor.GetProperty().SetColor(0.2, 0.5, 1.0)
    actor.GetProperty().SetOpacity(0.95)

    # === Step 4: Renderer and Window ===
    renderer = vtk.vtkRenderer()
    renderer.AddActor(actor)
    renderer.SetBackground(1, 1, 1)

    # === Set up camera ===
```

```
camera = renderer.GetActiveCamera()
camera.SetPosition(2, 1, 0.5)      # Where the camera is placed (X, Y, Z)
camera.SetFocalPoint(0, 0, -0.2)      # What the camera looks at
camera.SetViewUp(0, 0, 1)          # Defines the "up" direction
renderer.ResetCameraClippingRange()

render_window = vtk.vtkRenderWindow()
render_window.AddRenderer(renderer)
render_window.SetSize(800, 600)

interactor = vtk.vtkRenderWindowInteractor()
interactor.SetRenderWindow(render_window)

# === Create a fixed plane at y = 0 ===
plane = vtk.vtkPlaneSource()
plane.SetOrigin(-1, 0, -1)      # bottom-left corner of the plane
plane.SetPoint1(1, 0, -1)       # move in +x
plane.SetPoint2(-1, 0, 0.1)       # move in +z
plane.SetResolution(1, 1)
plane.Update()

# Create mapper and actor
plane_mapper = vtk.vtkPolyDataMapper()
plane_mapper.SetInputConnection(plane.GetOutputPort())
plane_actor = vtk.vtkActor()
plane_actor.SetMapper(plane_mapper)
plane_actor.GetProperty().SetColor(0.9, 0.9, 0.9)  # light gray
plane_actor.GetProperty().SetOpacity(0.5)          # semi-transparent

# Add to the renderer
renderer.AddActor(plane_actor)

# === Step 5: Sinusoidal Yaw Motion ===
pivot_origin = np.array([0.0, 0.0, 0.0])# base of flap
rotation_axis = np.array([0, 0, 1]) # yaw about z-axis
amplitude = 0.4  # rad (10 degrees = 0.174533 radians)
frequency = 0.5  # Hz
fps = 30
dt = 1.0 / fps
t = 0

def update_mesh():
    global t
    angle = amplitude * np.sin(2 * np.pi * frequency * t)
    Rz = np.array([
        [np.cos(angle), -np.sin(angle), 0],
        [np.sin(angle),  np.cos(angle), 0],
        [0, 0, 1]
    ])
    new_vertices = (vertices - pivot_origin) @ Rz.T + pivot_origin
    for i in range(len(new_vertices)):
        points.SetPoint(i, *new_vertices[i])
    points.Modified()
    render_window.Render()
    t += dt # increments time-step here

def timer_callback(obj, event):
```

```
        update_mesh()
        # interactor.CreateTimerEvent(vtk.vtkCommand.TimerEvent)

    # Set up a repeating timer event
    interactor.AddObserver("TimerEvent", timer_callback)
    interactor.Initialize()
    interactor.CreateRepeatingTimer(int(dt * 1000))
    interactor.Start()
    # END ANIMATE BODY SECTION
    # ------------------------

#_____________________________________________________________________________
# HYDROSTATICS
density = 1000
gravity = 9.81
hydrostatics = body.compute_hydrostatics(rho=density, g=gravity)

print("----------------")
print("Hydrostatics computed successfully.")
print("----------------")
# print("Keys:", hydrostatics.keys())
print("Displaced volume:", hydrostatics["disp_volume"])
print("Center of buoyancy:", hydrostatics["center_of_buoyancy"])

#_____________________________________________________________________________
# DEFINE TEST MATRIX PARAMETERS
# frequencies = np.linspace(0.5, 3.0, 10)  # 10 frequency points between 0.1 and 2.0 rad/s
# wave_directions = 0.0  # head-on waves
# solver = cpt.BEMSolver()
print("----------------")
print("Solving Test Matrix Calculations.")
test_matrix = xr.Dataset(coords={
    'period': np.linspace(0.5, 3.0, num=100),
    'wave_direction': [0,np.pi/4],
    'radiating_dof': list(body.dofs),
    'water_depth': [1.0],
})
dataset = cpt.BEMSolver().fill_dataset(test_matrix, body)
# TM_Result = dataset.solve(dataset, keep_details=True)
print("...Done Solving Test Matrix...")
print("----------------")

#_____________________________________________________________________________
# RUN VARIOUS BEM SOLVERS AND PROBLEMS
# NOTE: The Capytaine Tutorial documentation (which is not great), states this...
# The wave height is implicitly assumed to be 1m. Since all computations are
# linear, any wave height or motion amplitude can be retrieved by multiplying
# the result by the desired value.

# Part 1: Diffraction Problem (and Results) - Ex: The WEC is fixed and waves approach WEC body.
# How are waves scattered and distorted due to the body
# Key output is the Excitation Force that waves exert on the WEC body
# Complex-valued, depends on wave frequency and direction
DiffProb = cpt.DiffractionProblem(
    body=body,
    water_depth=1.0,
    rho=1000.0,
```

```
    omega=1.0,
    wave_direction=0.0)
Diff_Solver = cpt.BEMSolver()
Diff_Result = Diff_Solver.solve(DiffProb, keep_details=True)
print("----------------")
print("Diffraction Problem computed successfully.")
print("----------------")

# Part 2: Radiation Problem (and Results) - Added Mass, Radiation Damping.
# This is the wave field generated by oscillating the WEC body with no waves
# No incoming waves and VOSWEC just Yaws
# Key outputs include the Added mass (A) and radiation damping (B) (energy lost to wave radiations)
# Both A and B are functions of omega (wave frequency)
# QUESTION: How am I defining WEC motion here?

# # Original Radiation
# RadProb = cpt.RadiationProblem(
#     body=body,
#     water_depth=1.0,
#     rho=1000.0,
#     omega=1.0,
#     wave_direction=0.0,
#     radiating_dof="Yaw")
# Rad_Solver = cpt.BEMSolver()
# Rad_Result = Rad_Solver.solve(RadProb, keep_details=True)
# print("----------------")
# print("Radiation Problem computed successfully.")
print("----------------")


# Updated Radiation Problem to solve across multiple wave periods for Yaw
# Solve radiation problems across all wave periods for the 'Yaw' DOF
print("----------------")
print("Solving Radiation Problem Dataset.")
radiation_test_matrix = xr.Dataset(coords={
    'omega': 2 * np.pi / test_matrix.coords['period'].values,
    'radiating_dof': ['Yaw'],
    'influenced_dof': ['Yaw'],
    'water_depth': [1.0],
})

# Solve radiation problems and store in separate dataset
# rad_dataset = cpt.BEMSolver().fill_dataset(radiation_test_matrix, body)
rad_dataset = cpt.BEMSolver().fill_dataset(radiation_test_matrix, body)

# Merge with previous dataset
dataset = xr.merge([dataset, rad_dataset], compat='override')
print("...Done Solving Radiation Problems and Merging Dataset...")
print("----------------")


#_____________________________________________________________________________
# RUN VARIOUS POST PROCESSING MODULES
# Pressure, Velocity, and Free Surface Elevations
print("----------------")
print("Solving Potential, Pressure, Velocity, and Free Surface.")
Diff_Solver.compute_potential(body, Diff_Result)
```

```
Diff_Solver.compute_pressure(body, Diff_Result)
Diff_Solver.compute_velocity(Diff_Result.body.mesh, Diff_Result)
Diff_Solver.compute_free_surface_elevation(body, Diff_Result)
print("Done with Post-Processing solvers")
print("----------------")

# Computation of the impendance matrix
# Impedence
# capytaine.post_pro.impedance.impedance(dataset, dissipation=None, stiffness=None)
# RAO Transfer Function
# capytaine.post_pro.impedance.rao_transfer_function(dataset, dissipation=None, stiffness=None)
# RAO - Experimental function to compute the Response Amplitude Operator
# capytaine.post_pro.rao.rao(dataset, wave_direction=None, dissipation=None, stiffness=None)

# ------------------------
# PLOT PRESSURE PROFILE ON THE GEOMETRY
# body.show_matplotlib(
#         color_field=np.real(dataset.pressure),
#         cmap=plt.get_cmap("viridis"),  # Colormap
#         )

# # ------------------------
# # EXPORT RESULTS TO NETCDF FOR BEMIO AND WEC-SIM
# dataset = assemble_dataset([result])  # or list of results at many frequencies
# write_dataset_to_netcdf(dataset, "VOSWEC_results.nc")


#_____________________________________________________________________________
#PLOT VARIABLES

# PLOT EXCITATION FORCE VS WAVE PERIOD
import matplotlib.pyplot as plt
import numpy as np

# Extract wave periods and convert to omega
periods = dataset.coords['period'].values
omega = 2 * np.pi / periods
frequency = 1 / periods # Frequency in Hz

# Extract excitation force for yaw (complex-valued)
excitation = dataset['excitation_force'].sel(wave_direction=0.0)
excitation_real = np.real(excitation)
excitation_imag = np.imag(excitation)
excitation_mag = np.abs(excitation)

# Plot
plt.figure()
plt.plot(periods, excitation_mag, label='|Excitation|')
plt.plot(periods, excitation_real, '--', label='Real part')
plt.plot(periods, excitation_imag, ':', label='Imaginary part')
plt.xlabel('Wave Period [s]')
plt.ylabel('Excitation Torque [Nm]')
plt.title('Excitation Torque (Yaw)')
plt.grid(True)
plt.legend()
plt.tight_layout()
plt.show()
```

```
# PLOT EXCITATION FORCE VS FREQUENCY
import numpy as np

excitation_force = dataset.excitation_force.sel(influenced_dof='Yaw', wave_direction=0).values

amplitude = np.abs(excitation_force)
phase = np.angle(excitation_force, deg=True)

plt.figure()
plt.subplot(2,1,1)
plt.plot(frequency, amplitude, label='Amplitude', marker='^', color='orange')
plt.ylabel("Excitation Force Amplitude [N·m]")
plt.title("Excitation Force Amplitude vs Frequency")
plt.grid(True)

plt.subplot(2,1,2)
plt.plot(frequency, phase, label='Phase', marker='v', color='red')
plt.xlabel("Wave Frequency [rad/s]")
plt.ylabel("Phase [°]")
plt.title("Excitation Force Phase vs Frequency")
plt.grid(True)

plt.tight_layout()
plt.show()




#_____________________________________________
# PLOT ADDED MASS VS WAVE PERIOD
added_mass = dataset['added_mass'].sel(
    radiating_dof='Yaw',
    influenced_dof='Yaw',
    # wave_direction=0.0
)

periods = dataset.coords['period'].values
omega = 2 * np.pi / periods

plt.figure()
plt.plot(periods, added_mass, label='Added Mass (Yaw)', color='green')
plt.xlabel('Wave Period [s]')
plt.ylabel('Added Mass [kg·m²]')
plt.title('Added Mass (Yaw)')
plt.grid(True)
plt.tight_layout()
plt.show()

# PLOT ADDED MASS VS FREQUENCY

frequencies = 2 * np.pi / dataset.period.values  # Convert period to frequency (rad/s)
added_mass = dataset.added_mass.sel(radiating_dof='Yaw', influenced_dof='Yaw').values

plt.figure()
plt.plot(frequencies, added_mass, label='Added Mass (Yaw)', marker='o')
```

```
plt.xlabel("Wave Frequency [rad/s]")
plt.ylabel("Added Mass [kg·m²]")
plt.title("Added Mass vs Frequency")
plt.grid(True)
plt.legend()
plt.show()

#_____________________________________________________
# PLOT ADDED RATIATION DAMPING VS WAVE PERIOD

# Extract radiation damping for yaw
# Extract wave periods and convert to omega
periods = dataset.coords['period'].values
omega = 2 * np.pi / periods

# Select radiation damping from dataset
radiation_damping = dataset['radiation_damping'].sel(
    radiating_dof='Yaw',
    influenced_dof='Yaw',
    # wave_direction=0.0
)

# Plot
plt.figure()
plt.plot(periods, radiation_damping, label='Radiation Damping (Yaw)', color='orange')
plt.xlabel('Wave Period [s]')
plt.ylabel('Radiation Damping [kg·m²/s]')
plt.title('Radiation Damping (Yaw)')
plt.grid(True)
plt.tight_layout()
plt.show()

# PLOT ADDED RATIATION DAMPING VS FREQUENCY
radiation_damping = dataset.radiation_damping.sel(radiating_dof='Yaw', influenced_dof='Yaw').values

plt.figure()
plt.plot(frequencies, radiation_damping, label='Radiation Damping (Yaw)', marker='s', color='green'
plt.xlabel("Wave Frequency [rad/s]")
plt.ylabel("Radiation Damping [kg·m²/s]")
plt.title("Radiation Damping vs Frequency")
plt.grid(True)
plt.legend()
plt.show()

#_____________________________________________________
# # PLOT RESPONSE AMPLITUDE OPERATOR VS FREQUENCY
# solver = cpt.BEMSolver()
# result = solver.solve(
#     body=body,
#     wave_directions=[0.0],
#     omega=np.linspace(0.2, 2.0, 25)
# )


# # Get radiation impedance components for yaw (Z_ROTATION)
# A = result.get_radiation_impedance('z', 'z').real  # Added mass
# B = result.get_radiation_impedance('z', 'z').imag  # Added damping
```

```
# # Get complex excitation torque in yaw
# F = result.get_excitation('z')

# # Compute yaw RAO
# RAO_yaw = np.abs(F / (-omega**2 * A + 1j * omega * B))

# # Plot RAO
# plt.figure(figsize=(8, 5))
# plt.plot(frequencies, RAO_yaw, label='Yaw RAO')
# plt.xlabel('Frequency (Hz)')
# plt.ylabel('Response Amplitude Operator [rad/m]')
# plt.title("Yaw RAO vs Frequency")
# plt.grid(True)
# plt.legend()
# plt.tight_layout()
# plt.show()

#_____________________________________________________________________________________
#SAVE RESULTS INTO .CSV FILE
import pandas as pd
import os


# Recalculate omega (angular frequency) from period
periods = dataset["period"].values  # shape: (N,)
omega = 2 * np.pi / periods         # angular frequency ω = 2π / T


#_____________________________________________
# Radiation Damping (Yaw)

try:
    radiation_damping = dataset["radiation_damping"].sel(
    radiating_dof='Yaw',
    influenced_dof='Yaw'
).values
except KeyError:
    radiation_damping = np.full_like(omega, np.nan)

#_____________________________________________
# Added Mass (Yaw)

try:
    added_mass = dataset["added_mass"].sel(
    radiating_dof='Yaw',
    influenced_dof='Yaw'
).values
except KeyError:
    added_mass = np.full_like(omega, np.nan)

#_____________________________________________
# Excitation Torque (Yaw)

try:
    excitation = dataset["excitation_force"].sel(
    influenced_dof='Yaw',
```